Repository Istituzionale dei Prodotti della Ricerca del Politecnico di Bari

# Stress analysis and buckling stability of imperfect pressure vessel heads with geometric variations

This is a PhD Thesis

*Original Citation:*
Stress analysis and buckling stability of imperfect pressure vessel heads with geometric variations / Malik, Muhammad Shoaib. - ELETTRONICO. - (2025). [10.60576/poliba/iris/malik-muhammad-shoaib_phd2025]

*Availability:*
This version is available at http://hdl.handle.net/11589/284040 since: 2025-02-14

*Published version*
DOI:10.60576/poliba/iris/malik-muhammad-shoaib_phd2025

Publisher: Politecnico di Bari

*Terms of use:*

(Article begins on next page)

25 June 2026

UNIONE EUROPEA
Fondo Sociale Europeo

Ministero dell'Università e della Ricerca

PON RICERCA E INNOVAZIONE

REACT EU

Politecnico di Bari

**D**epartment of **M**echanics, **M**athematics and **M**anagement
MECHANICAL AND MANAGEMENT ENGINEERING
Ph.D. program
SSD: IIND-03/A – Mechanical Design And Machine Construction

*Final Dissertation*

# Stress Analysis and Buckling Stability of Imperfect Pressure Vessel Heads with Geometric Variations

by

**Muhammad Shoaib Malik**

**Referees:**

Prof.ssa Gilda Renna

Prof.ssa Rosa De Finis

**Supervisors:**

Prof.ssa Katia Casavola

Prof.ssa Claudia Barile

Dr. Vincenzo Moramarco

**Coordinator of Ph.D. Program:**
Prof. Giuseppe Casalino

Course n° 37, 01/01/2022 – 31/12/2024


**La borsa di dottorato è stata cofinanziata con risorse del Programma Operativo Nazionale Ricerca e Innovazione 2014-2020, risorse FSE REACT-EU**

**Azione IV.4 "Dottorati e contratti di ricerca su tematiche dell'innovazione"**

**e**

**Azione IV.5 "Dottorati su tematiche Green"**

# Acknowledgment

First and foremost, I am profoundly grateful to **Allah Almighty** for granting me strength, guidance, and perseverance to complete this thesis. Without His countless blessings, this accomplishment would not have been possible.

I would like to express my deepest gratitude to my supervisors, **Prof.ssa Katia Casavola**, **Prof.ssa Claudia Barile**, and **Dr. Vincenzo Moramarco**, for their invaluable guidance, encouragement, and insightful feedback throughout this journey. Their expertise and support have been instrumental in shaping this thesis and my academic growth.

I am also sincerely grateful to **Michele Attolico** and **Daniyal Altaf Baloch**, whose unwavering support, constructive advice, and encouragement have been a cornerstone of this work. Your assistance and dedication have truly made a difference.

Lastly, I would like to extend my heartfelt thanks to my family, friends, and colleagues who have been a constant source of motivation and strength during this challenging yet rewarding journey.

This thesis is a reflection of the collaborative effort, trust, and dedication of everyone who contributed to its completion. Thank you all for making this endeavor possible.

# *Dedication*

*This thesis is dedicated to the memory of my beloved father,* ***Malik Muhammad Sharif****, whose wisdom, love, and unwavering belief in me continue to inspire and guide me every day. Though he is no longer with us, his presence is deeply felt in every step of this journey.*

*I also dedicate this work to my wife,* ***Saboora****, whose patience, understanding, and sacrifices have been my greatest source of strength during this journey.*

# Table of Contents

# List of Figures

# List of Tables

# Chapter 1

# Introduction

## 1.1 Preface

Pressure vessels are important components in various industrial sectors, including chemical processing, energy production, and oil & gas storage. It is due to their ability to store and transport fluids or gases at pressures higher than atmospheric levels [1]. The structural integrity of these vessels is important to prevent failures which can result in leakage, environmental hazards, or catastrophic accidents. Metals like steel and aluminum have been the standard materials for manufacturing pressure vessels historically, but the use of alternative materials is increasing continuously to meet the growing demands for efficiency, portability, and cost-effectiveness [2]. High-Density Polyethylene (HDPE) has gained importance as a suitable material due to its advantageous properties, including lighter weight, excellent corrosion resistance, and lower cost in comparison to conventional metals [3]. These good properties make HDPE particularly attractive for applications that require durable and portable solutions, especially in applications where weight and resistance to corrosion are essential requirements.

As industries like oil refining, gas processing and vacuum truck manufacturing industry continue to expand, the need for safe, reliable, and efficient pressure vessels increases [4,5]. Therefore, precise stress distribution analysis during the design phase of pressure vessels is critical to ensure both safety and performance. This research is especially important for manufacturers of lightweight tanks, such as those used in wastewater treatment systems operating under vacuum pressure, which are increasingly made from HDPE [5]. The understanding of stress

distribution within these vessels is especially important in regions where the vessel's geometry changes abruptly, such as the transition from the cylindrical body to the head. These transitions are subject to increased wall bending stresses due to the combined effects of internal pressure, edge forces, and edge moments [6], all of which contribute to higher stress concentrations and a greater risk of structural failure.

The design of pressure vessels depends on accurately predicting the effects of these stress concentrations. The membrane theory of shells is essential for understanding the mechanical behavior of pressure vessels, particularly in regions of regular geometry where stresses are predominantly in-plane. This theory is particularly useful for assessing cylindrical and spherical sections of a vessel far from any structural discontinuities. However, it does not fully account for areas near junctions or reinforcements, where additional bending stresses develop to maintain compatibility in displacement and rotation. These bending stresses, often referred to as discontinuity loads, can significantly change the stress field near geometric transitions. Though localized, these stresses can create stress concentrations much higher than those predicted by only membrane theory. Therefore, for accurate design of HDPE pressure vessels, it is essential to incorporate these local bending effects to determine the minimum thickness and strength needed to safely withstand internal pressure.

Under internal pressure, the cylindrical body and head of a pressure vessel are subjected to membrane stress, leading to membrane deformation. This deformation can be analyzed by evaluating the radial displacement of circular sections and the meridian angle at various points along the vessel. The analysis is typically based on the non-moment theory, which assumes smooth deformation of the shell's mid-plane without abrupt changes in curvature, transverse shear forces, or bending moments at the boundaries [6]. However, real-world pressure vessels are generally composed of multiple components with differing curvatures, such as the cylindrical body and the head, which often have varying radii of curvature. When analyzed

separately, each section shows unique radial displacements and meridian angles at its boundaries. Because these sections are interconnected, their displacements and angles must align at the junctions, which introduces transverse shear forces and bending moments. These effects deviate from the assumptions of the non-moment theory, thereby making the use of moment theory important for a more accurate and realistic analysis of pressure vessel behavior.

The design becomes more complex when thin-walled pressure vessels are considered, particularly those with tori spherical and elliptical heads. These head shapes are commonly used in industries such as chemical processing, civil and marine engineering, and power generation due to their efficient geometric properties [7–11]. The risk of buckling is very high in these vessels when they are subjected to internal pressure. This buckling failure mode, if not effectively managed, can lead to catastrophic consequences [12,13]. The cause of buckling in these vessels is influenced by various factors, including geometric imperfections, wall thickness, material properties, and overall shape [14–16].

Geometric imperfections are a substantial challenge in the manufacturing of pressure vessels [17–20]. These deviations from an ideal geometry arise due to manufacturing limitations, material inconsistencies, and operational wear over time. Imperfections can take various forms, such as localized dimples, cutouts for access or instrumentation, flat patches resulting from uneven forming processes, and deviations induced by eigenmode-shaped imperfections during manufacturing. Even small irregularities in the structure can act as stress concentrators, amplifying local deformation and triggering premature buckling [21]. Research shows that the buckling load of a pressure vessel with imperfections can be substantially lower than that of a perfectly idealized structure, highlighting the importance of understanding and accounting for these flaws during the design and analysis phases [22,23].

In practical scenarios, imperfections are not only theoretical considerations, but they are often unavoidable. For example, in the chemical industry, vessels may

feature cutouts for inspection ports or nozzles that interrupt the continuity of the shell. During fabrication, welding and forming processes may introduce uneven surface areas or residual stresses, resulting in flat spots or slight dimpling. In addition, operational factors such as thermal cycles, corrosion, and mechanical impacts can increase the impact of existing imperfections or introduce new ones. These real-world factors make it vital for engineers to adopt advanced analytical techniques capable of capturing the influence of imperfections on the structural stability of pressure vessels.

In the design of pressure vessel heads, the wall thickness is typically assumed to be uniform across the structure, especially for ellipsoidal heads. However, this uniformity may not be optimal for all applications, as certain areas of the vessel may experience different levels of stress or strain. For example, regions of the pressure vessel that face higher internal pressure or external loading may require thicker material for enhanced strength, while other areas may benefit from reduced thickness to save on material costs and weight. To address this, the concept of variable wall thickness has been explored to optimize the design of pressure vessel heads. By applying principles like the *iso-strength* method [24], which ensures constant strength across the structure, researchers aim to adjust the wall thickness distribution in a way that improves load-bearing capacity and minimizes the risk of structural failure. This approach also considers factors such as the ellipticity of the head, which can significantly influence buckling behavior. Overall, the integration of variable wall thickness into pressure vessel design holds the potential to enhance both performance and cost-effectiveness.

This study employs a mixed methodology, combining analytical and numerical approaches to evaluate the structural performance of HDPE pressure tanks. Chapter 3 focuses on stress analysis, using moment theory for analytical evaluation and finite element analysis (FEA) for numerical simulations, with particular attention to high-stress regions such as the junctions between the cylindrical shell and elliptical heads. Chapter 4 conducts detailed buckling analysis using numerical

simulations to assess the impact of geometric imperfections on the tank's stability under pressure. Although the two chapters address different aspects of structural behavior, namely stress distribution and buckling resistance, they collectively provide a comprehensive understanding of the tank's performance.

## 1.2 Aims and Objectives

This research aims to improve the understanding of stress distribution and buckling behavior in High density polyethylene (HDPE) pressure tanks, particularly those with elliptical, tori spherical, and hemispherical heads. The complex shapes of these geometries create significant challenges, especially as they lead to stress concentration when subjected to pressure. The study uses both linear and nonlinear buckling analyses to assess the structural stability of these vessels. Linear buckling analysis provides a preliminary estimate of the critical buckling load and mode shapes within the elastic range, while nonlinear buckling analysis offers a more realistic evaluation by incorporating geometric imperfections and nonlinear material behavior, which is essential for HDPE’s unique properties.

The primary objective of this work is to assess the sensitivity of HDPE pressure vessels to geometric imperfections, including geometric dimples, circular cutouts, flat patches, and eigenmode-affine shapes. This study explores the impact of amplitude variation of these geometric imperfections on the buckling strength of these different head shapes. By systematically varying imperfection amplitudes, the research aims to establish a more comprehensive understanding of the limits within which these imperfections can be tolerated without significantly compromising the tank’s structural integrity.

Another major goal is to apply the moment theory approach to improve the accuracy of stress analysis in HDPE vessels. This theory considers both membrane and bending forces, providing a more detailed understanding of stress distribution, particularly in regions where the geometry changes abruptly, such as at the junctions of cylindrical shells and elliptical heads. The moment theory will be used

to offer a more thorough assessment of stress behavior in HDPE pressure vessels, ensuring that the analysis accounts for these critical areas that traditional methods may overlook.

In addition, the research investigates the optimization of vessel geometry and wall thickness to enhance the vessel's resistance to buckling. Main importance is given to variable wall thickness designs applied to the two best-performing head geometries identified through stress and buckling analyses. These geometries demonstrate superior structural performance, and the study aims to determine the effects of varying wall thickness in improving material efficiency, reducing stress concentrations, and optimizing overall stability. The research will also explore different wall thickness profiles designed for specific geometrical features to improve the buckling resistance of HDPE pressure vessels, contributing to their overall performance in real-world applications.

## 1.3 List of Conferences and scientific publications

- Date: October 28-29, 2024, Title: "Evaluation of the effects of geometric imperfections and wall thickness variation on the buckling behaviour of HDPE domes" at the International Conference on Mechanical & Production Engineering (ICMPE-24), Split, Croatia.

- Date: May 15-17, 2024, Title: "Integrating Membrane and Bending Theory with HDPE Material for Optimized Pressure Vessel Design" at the 19th International Conference on New Trends in Fatigue and Fracture (NT2F24), Politecnico di Bari – Bari, Italy.

- M.A. Attolico, C. Barile, C. Casavola, **M.S. Malik**, V. Moramarco, "Effects of geometric imperfections and wall thickness variation on the buckling behavior of HDPE domes," *International Journal of Pressure Vessels and Piping*, under review (Manuscript No: IPVP-D-24-00873).

- C. Barile, C. Casavola, **M.S. Malik**, V. Moramarco, "Integrating membrane and bending theory with HDPE material for optimized pressure vessel design," *Journal of the Brazilian Society of Mechanical Sciences and Engineering*, under review (Manuscript No: BMSE-D-24-01720).

# Chapter 2

# Literature review

This chapter presents a comprehensive review of the existing literature on the utilization of High-Density Polyethylene (HDPE) in pressure-bearing applications, (such as piping systems and pressure vessels) focusing on key aspects relevant to structural analysis and design. It begins by discussing foundational studies that evaluate HDPE's potential for pressure bearing applications, emphasizing its mechanical properties and advantages over other materials. Subsequent sections highlight specific challenges, such as stress concentration and edge effects at the junction between the cylindrical body and the tank head. The review further explores buckling phenomena, highlighting the sensitivity of cylindrical and spherical shells to imperfections and the methodologies used to optimize buckling resistance. Lastly, the chapter examines innovative designs with variable wall thickness, demonstrating their impact on stress distribution and buckling resistance.

The chapter concludes by identifying research gaps and limitations in the reviewed studies, particularly the lack of comprehensive stress analyses that integrate both membrane and bending forces, limited investigations into imperfection sensitivity specific to HDPE, and underexplored optimization strategies for wall thickness. Addressing these gaps, the subsequent research focuses on using moment theory and novel geometric considerations to advance the design of HDPE pressure vessels, offering improved structural performance and practical insights for industrial applications.

## 2.1. High-Density Polyethylene (HDPE) in Pressure Vessel Design

In recent years, the use of thermoplastic polymers like High-Density Polyethylene (HDPE) has grown significantly. These materials are increasingly becoming cost-effective alternatives to traditional materials such as metals, concrete, and timber [25]. They are popular because of their affordability, ease of manufacturing, significant weight reduction, resistance to corrosion, versatility in design, non-conductive properties (both thermal and electrical), and their low density while maintaining high strength [26–28]. Additionally, thermoplastics can be customized to meet specific requirements and are recyclable, with many types of processing methods available to transform raw material into finished products [29–31]. In the context of pressure tanks, HDPE's ductile behavior, resistance to chemical degradation, and ability to withstand significant mechanical loads make it particularly appealing. However, challenges such as stress concentration and sensitivity to geometric imperfections remain critical considerations [31].

### 2.1.1. Thermo-Mechanical Behavior of HDPE

Recent studies have discussed the thermo-mechanical behavior of HDPE under high temperatures and pressures to support its use in high-pressure hydrogen storage liners [32]. Experimental and numerical analyses evaluated HDPE under tensile and compressive loads across a temperature range of 223K to 373K. Key properties, such as Young's modulus and tensile strength, were found to vary significantly with temperature. For example, the Young's modulus increased over 25 times from 83 N/mm² at 373K to 2381 N/mm² at 223K, and tensile strength showed eight times increase in the same range. Compressive properties followed similar trends, while non-isosensitive behavior between tensile and compressive loads was observed, with stress ratios showing nonlinear variations across strain ranges.

Numerical simulations were conducted using elastic-plastic and hyper elastic material models to verify the experimental results. Both models showed strong agreement with tensile stress-strain data, with relative errors of about 1-3%, though slightly higher errors were observed under compressive loads at higher strains.

### 2.1.2. Burst Behavior of HDPE and CPVC

High-Density Polyethylene (HDPE) and Chlorinated Polyvinyl Chloride (CPVC) are widely used in water piping systems due to their unique mechanical and thermal properties [33]. This study compares the behavior of these two thermoplastic materials under increasing internal pressure, focusing on evaluation of their performance and failure mechanisms. The experimental tests, conducted according to ASTM 1599 standards, analyzed the burst pressure and failure time of pipe specimens. The investigation included both plain and grooved specimens to assess the impact of defects on material performance.

HDPE and CPVC showed distinct mechanical responses after analyzing the results. Pure HDPE pipes displayed ductile failure behavior, supporting pressures up to 70 bars, whereas CPVC pipes have shown brittle failure under pressures as high as 160 bars. When groove notches were introduced, the burst pressure and time for failure significantly decreased for both materials. The shift from ductile to brittle behavior in HDPE pipes under grooved conditions have shown the influence of defects on mechanical performance. In contrast, CPVC pipes were consistent with a brittle failure mode across all test conditions.

The study also evaluated the damage evolution in HDPE and CPVC using a non-dimensional analysis of burst pressures. The comparison revealed a divergence in damage behavior near critical life fractions. For HDPE, the static damage closely followed Miner's linear damage theory until reaching a critical life fraction of 52%, after which the damage accelerated. In CPVC, the rate of damage was slow until surpassing a critical life fraction of 60%, where rapid progression took place. These differences were linked to the natural characteristics of the materials. Moreover,

CPVC was found to withstand internal pressure in a better way but was more prone to accumulating damage over time. The findings of this study have shown that CPVC demonstrates superior pressure resistance, its brittle nature poses challenges under certain conditions. HDPE, with its ductile behavior, may be more suitable for applications where toughness is critical.

### 2.1.3. Failure Mechanisms in HDPE Liners

A study by Rondinella et al. [34] focused on the failure mechanisms of HDPE liners in Type IV high-pressure gas storage cylinders. These liners which are encased in a composite shell play a crucial role in ensuring gas impermeability and mechanical integrity. The failure, observed in the hemispherical head region during cyclic pressure tests, was a result of significant plastic deformation that caused thickness reduction and eventual cracking. Morphological and chemical analyses (SEM/EDXS, FTIR, DSC, and XRD) confirmed that the failure was not due to material degradation during manufacturing but rather a design-related issue. Stress concentration and cyclic plastic deformation, aggravated by poor adhesion between the HDPE liner and composite shell, were identified as the primary causes.

The findings emphasized the importance of improving the interface between the liner and shell, such as adopting better adhesives or modifying geometries, to mitigate stress concentrations and enhance the durability of HDPE liners in pressure vessels. The study further highlighted that while HDPE demonstrates excellent mechanical properties and ductility, design considerations and manufacturing integration are crucial to optimizing its performance under high-pressure conditions.

The reviewed studies show HDPE's potential in pressure tank applications, owing to its mechanical robustness, ductility, and resistance to chemical degradation. However, challenges such as sensitivity to defects, stress concentrations, and the influence of geometric imperfections require further investigation. These insights highlight the importance of adopting advanced design

methodologies, such as detailed nonlinear buckling analyses and geometry optimization, to maximize the potential of HDPE in pressure tank applications.

## 2.2. Mitigation of Edge Effects in Pressure Tanks

The design and analysis of cylindrical pressure vessels with non-standard dished heads have been widely studied to tackle challenges like stress concentration, edge effects, and ensuring structural reliability. This review highlights advancements in head geometry, stress reduction methods, and theoretical modeling while identifying limitations that this study aims to overcome.

### 2.2.1. Super-Ellipsoidal Dished Heads and Stress Reduction

Jasion et al. [35] studied sandwich cylindrical pressure vessels but examined the role of super ellipsoidal dished heads in reducing the stress concentrations, especially edge effects. Their finite element analysis demonstrated that super ellipsoidal heads effectively minimized edge effects, which typically induce shear stress disturbances in the core. These disturbances, prominent in vessels with hemispherical heads, were notably absent in the super ellipsoidal designs. The study also revealed that symmetrical cross-sections yielded the highest buckling resistance. Moreover, the proposed design reduced von Mises stress concentrations, making it suitable for practical applications such as storage and transportation tanks for gases and liquids. As shown in figure 1, the distribution of von Mises stress for a tank with a super ellipsoidal head (with aspect ratio of $k$=0.3) is illustrated, covering the outer face, inner face, and core. However, challenges related to the manufacturing of precise geometries and adherence to existing pressure vessel standards were acknowledged. The authors suggested further investigations into post-buckling behavior, risks of layer separation, and the influence of varied boundary conditions to validate these findings for real-world applications.

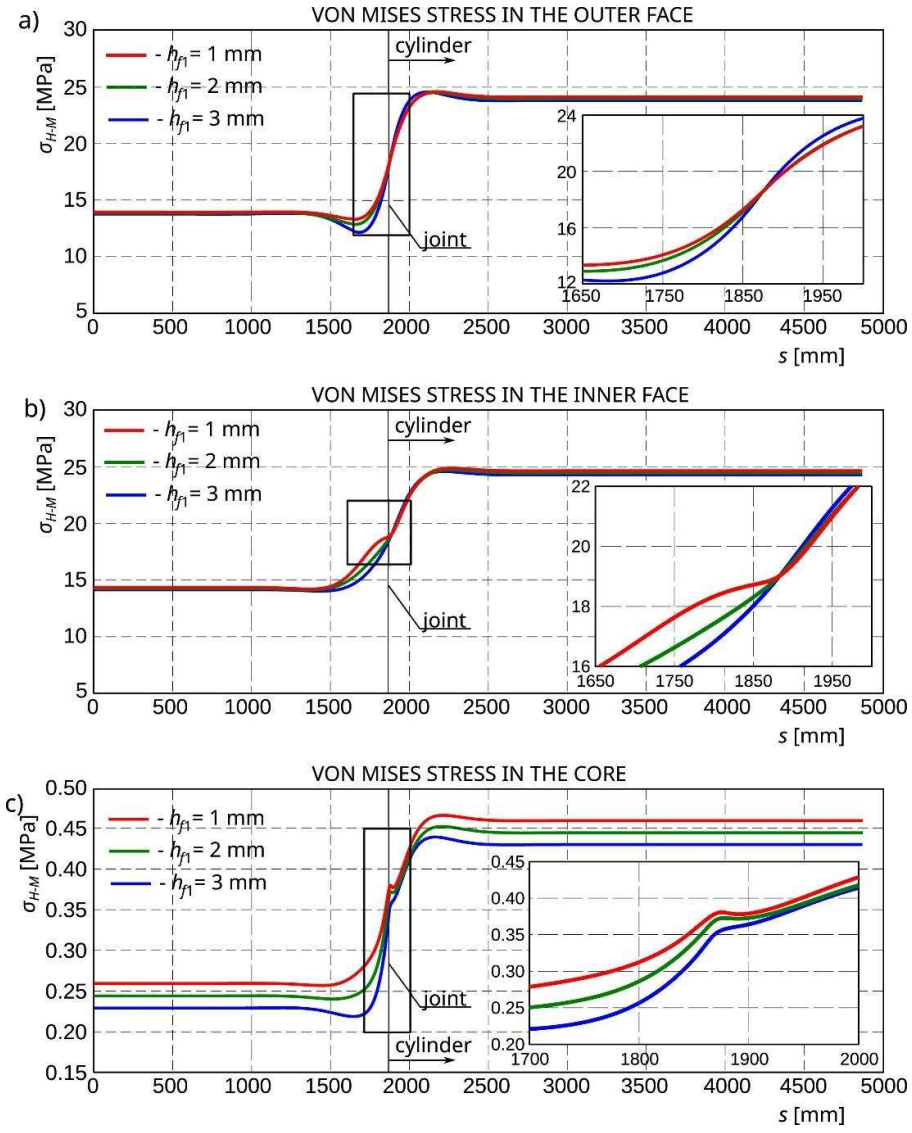


**Figure 1: Distribution of von Mises stress for tank with super ellipsoidal head with $k = 0.3$: (a) outer face; (b) inner face; (c) core** [35]

Magnucki et al. [36] expanded the work by examining the static stress behavior in cylindrical tanks with non-standard dished heads. These heads have a super-ellipsoidal shape, which is described mathematically using two parameters that control their depth and curvature. The researchers used both analytical calculations

and finite element methods to evaluate the distribution of stress along the meridian of the dished head.

The study shows that replacing classical ellipsoidal heads with super-ellipsoidal pressure vessel heads can reduce the edge effect. The intensity of this edge effect, which is a concentration of stress where the vessel head meets the cylindrical shell, reduces when the depth of the head is increased as shown in figure 2. The authors explain that this improvement occurs because the super-ellipsoidal shape helps to distribute stresses more uniformly.

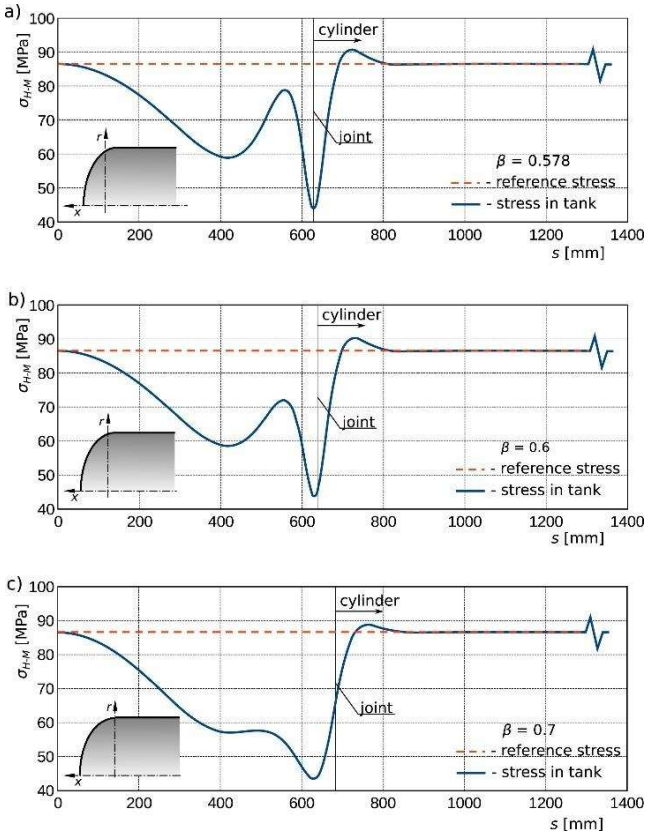


**Figure 2: Comparison of Stress distribution in pressure vessels with different dish head shapes** [36]

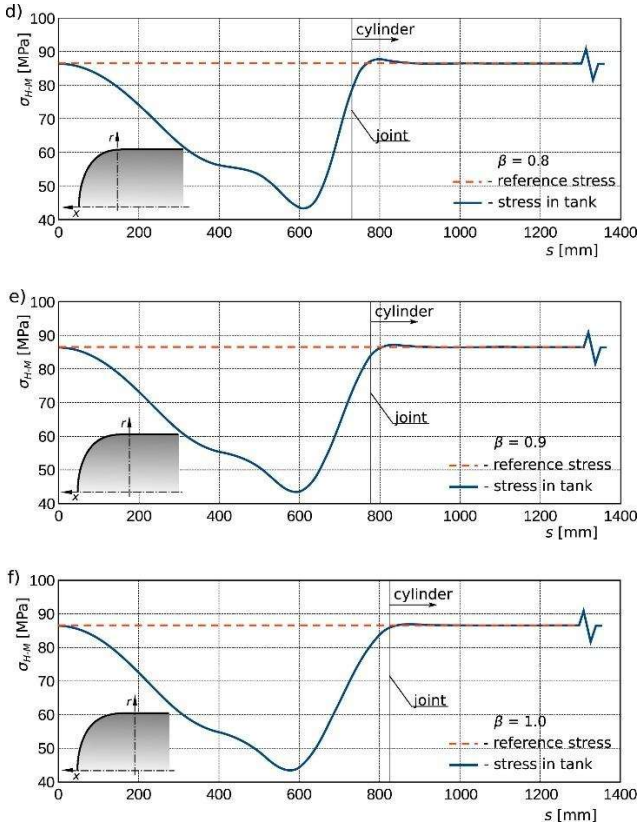


**Figure 2 (continued)** [36]

An advantage of this approach is that the analytical description allows designers to easily adjust the shape of the dished head. By modifying the two dimensionless parameters, the geometry can be tailored to suit specific design needs. This flexibility is particularly useful for analyzing and developing new types of tank structures.

Despite these benefits, the study also points out challenges with manufacturing deeper dished heads. While a deeper head reduces stress concentration and closely matches the numerical results, it can be more difficult to produce. Shallower heads, on the other hand, satisfy analytical conditions but may cause stress peaks to extend into the cylindrical section, as observed in the finite element analysis and potentially in real-world applications.

### 2.2.2. Non-standard Dished Heads

Sowiński et al. [37] conducted a detailed study on reducing the edge effect in three nonstandard dished heads of cylindrical pressure vessels subjected to uniform internal pressure. The research explored the behavior of the edge effect at the joint between the dished head and the cylindrical shell. The dished heads analyzed were based on Cassini oval, Booth lemniscate, and clothoid geometries (shown in figure 3), with their meridians described as plane curves. The stress states of these dished heads were studied both analytically and using finite element methods (FEM) in Ansys.

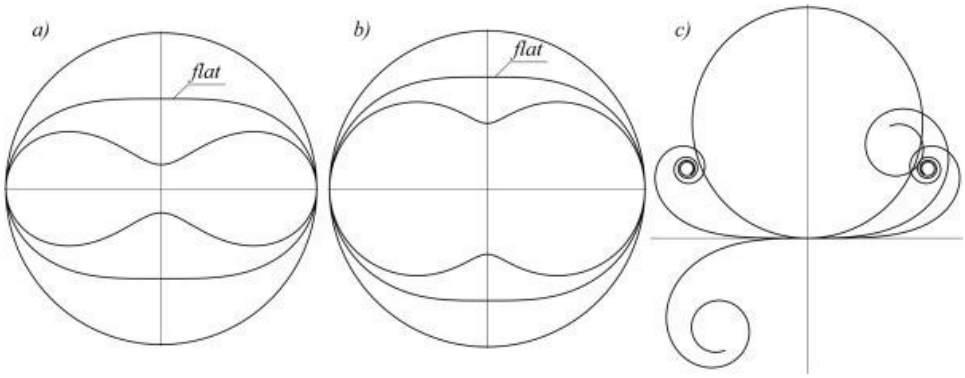


**Figure 3: Visual representation of: a) Cassini ovals, b) Booth ovals, c) generalized clothoids** [37]

The study focused on achieving a membrane stress state, which is characterized by the elimination of the edge effect. This effect arises from bending moments and shearing forces in the meridional plane of the shell and is a critical consideration in the design of pressure vessels. The authors observed that the edge effect decreases as the relative depth parameter, $\beta$ (figure 4), increases, eventually achieving a membrane stress state.

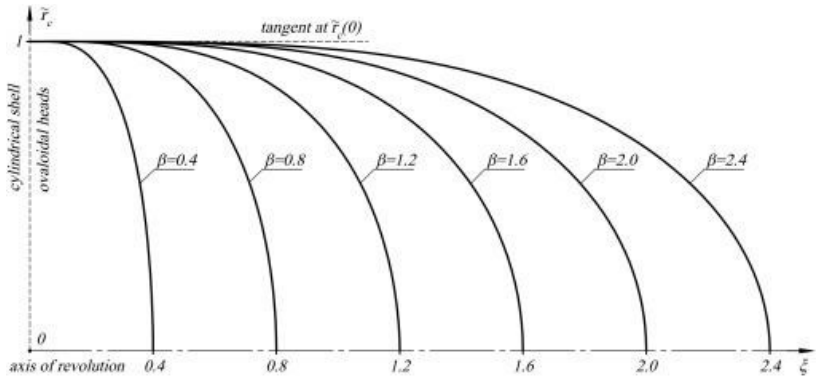


**Figure 4: Dished heads with different relative depth β** [37]

However, this reduction in the edge effect introduces challenges related to stress concentration, especially in the joint area of certain geometries, such as clothoidal heads. For these geometries, achieving the membrane stress state requires a $\beta$ value greater than 1, but stress concentrations in the joint remain significant.

The study further highlighted that ovaloidal dished heads, based on Cassini oval and Booth lemniscate geometries, demonstrate improved stress characteristics in the joint area, achieving a membrane stress state at lower $\beta$ values compared to clothoidal heads (figure 5). However, these geometries exhibit greater stress levels beyond the joint area for smaller $\beta$ values due to abrupt changes in meridional curvature. This trade-off reflects a contradiction in simultaneously minimizing the edge effect and reducing the relative depth. The authors emphasized that while complete elimination of the edge effect is unattainable, shaping the dished heads allows for minimizing its intensity to negligible levels.

Collectively, these studies primarily focused on reducing edge effects and stress concentrations through innovative head geometries. However, they relied on membrane theory, which neglects bending moments and shear forces, both of which significantly influence the overall stress state. Building on these foundational works, our study addresses these limitations by introducing moment theory as a comprehensive approach to stress analysis. Unlike the previous studies, moment theory accounts for both membrane and bending forces, providing a detailed

understanding of stress distribution, particularly at abrupt geometric transitions like junctions in HDPE pressure vessels.

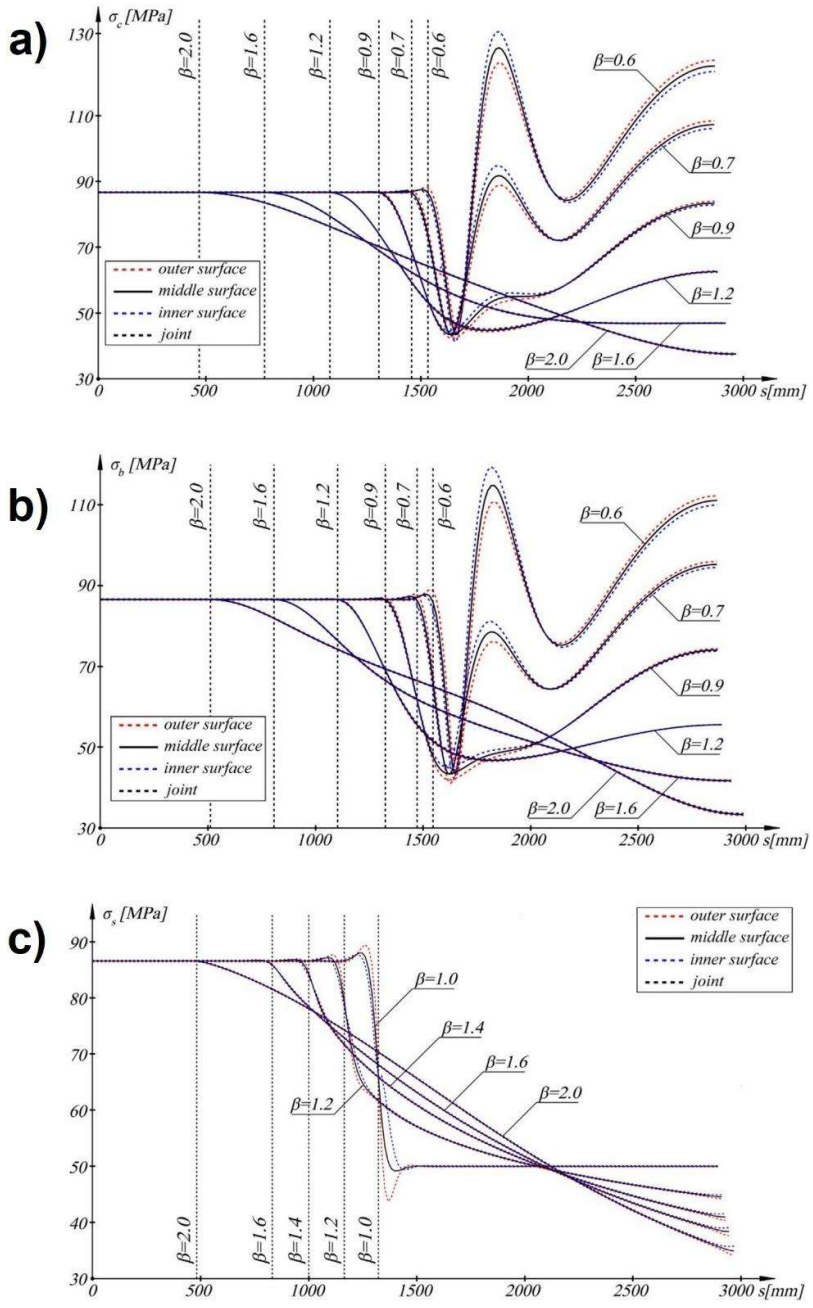


**Figure 5: Stress distribution along pressure vessel meridian with a) Cassini ovaloidal b) Booth ovaloidal c) clothoidal heads with variable parameter β.** [37]

### 2.2.3. Limitations of Membrane Theory in Pressure Vessel Stress Analysis

Pressure vessels are typically analyzed using membrane theory, a simplified approach that assumes uniform stress distribution and neglects the effects of bending. Many studies have relied on membrane theory to assess the behavior of pressure vessels. As described earlier, membrane theory is effective for many applications, but it ignores an increase in localized stress, especially in regions where the geometry transitions, such as at the junction between the cylindrical shell and the heads of the vessel. These areas, due to their curved geometry, experience bending effects that contribute significantly to the overall stress state and potential failure modes.

Belardi et al. [38] addressed these limitations by introducing bending theory to analyze composite pressure vessels and developed an analytical framework to evaluate the stress resultants at the junction between the cylindrical shell and elliptical heads in composite pressure vessels. This approach has shown that the geometric transition between these regions generates localized discontinuity loads, specifically in the form of a shear force ($Q_x^0$) and a bending moment ($M_x^0$). These discontinuity loads are critical as they create localized stress fields that are significantly higher than the membrane stresses predicted by classical membrane theory. The bending theory, therefore, gives a more accurate assessment of the stresses at the junction, which is essential for reliable structural design.

Belardi's model considered the composite cylindrical shell and elliptical heads as separate bodies subjected to internal pressure, leading to distinct deformation behaviors. As shown in Figure 6, the cylindrical shell undergoes uniform radial expansion along its length, resulting in a centrifugal radial displacement ($w_p^c$) with no rotation of the mid-surface normal. Also, the elliptical heads, under internal pressure, experience a different response characterized by inward radial displacement ($w_p^e$) at the equatorial plane, with no meridian displacement ($u$) or normal rotation ($\phi$). The inconsistency in these displacement patterns leads to the

generation of discontinuous loads at the junction, showing that a bending theory-based approach should be used for accurate stress evaluation.

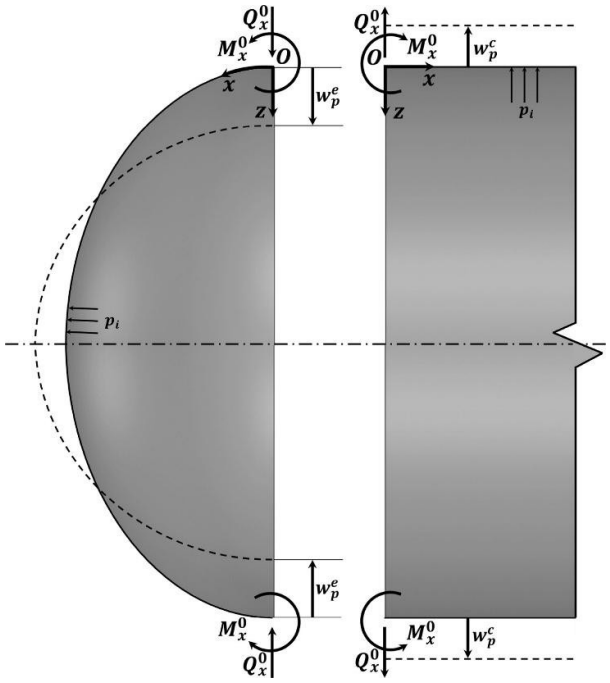


**Figure 6: Membrane displacements and localized shear force, bending moment components to ensure stress equilibrium** [38]

In short, their approach demonstrated the significance of discontinuity-induced stresses, such as localized shear forces and bending moments, at junctions. However, their work was confined to composite materials, leaving the stress behavior of HDPE pressure vessels unexplored. While the material and application differ, the concept of discontinuity-induced localized stresses at the junctions of cylindrical shells and heads remains same.

## 2.3. Shell Buckling behaviour and Imperfection sensitivity

The investigation of catastrophic behavior and the sensitivity of spherical shells to imperfections under external pressure can be traced back to the foundational work

of Karman et al. [39]. Building on this, researchers such as Thompson [40] and Sanders [41] highlighted the highly nonlinear nature of the buckling behavior in these structures. Over time, the use of Finite Element Methods (FEM) has become a standard approach for studying pressure vessels and domes, allowing for detailed analysis of their static and dynamic responses, stability, and material characteristics.

A comprehensive review provided in [42] surveys around 630 studies published between 1996 and 1998. This review examines a range of topics, including material and geometric nonlinearities, buckling phenomena, and failure mechanisms under both internal and external pressures. Additionally, it explores the application of FEM to pressure vessel heads with various geometries, such as spherical, ellipsoidal, and tori-spherical shapes, emphasizing the method's importance in assessing structural stability and ensuring integrity.

Modern analyses have integrated classical thin shell theory with advanced numerical methods and are carried out on materials such as steel, aluminum & polymers. Studies on shell stability [[43–47] focus on two main aspects, determining critical loads and load-bearing capacities using Euler's framework and investigating post-critical behavior with large deformations and deflections. The integration of FEM with traditional methods has enhanced the understanding of these complex behaviors, solidifying its role as an essential tool in structural stability analysis.

Di Pasqua et al. [48] contributed significantly to the understanding of imperfection sensitivity in thin-walled composite structures, particularly conical shells. Their study focused on the buckling behavior of conical shells with a 45° semi-vertical angle, using numerical approaches to account for initial geometric imperfections. Two strategies, Single Perturbation Load Approach (SPLA) and the Real Measured Mid-Surface Imperfections (MSI), were employed. SPLA simulates defects through localized lateral loads, while MSI incorporates imperfections measured directly from the shell surface.

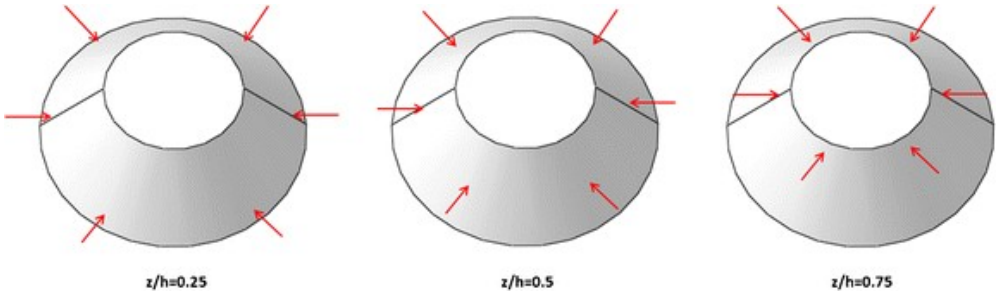


**Figure 7 : Different application points considered for perturbation** [48]

The investigation considered different application points for the perturbation loads as shown in Figure 7, characterized by the *z/h* ratio, where z is the position of the perturbation load along the shell height and h is the total shell height. The study examined specific *z/h* ratios, revealing positions where local snap through phenomena occurred, transitioning into global buckling in certain cases. SPLA was found to induce local snap through phenomena, preliminary stiffness losses that precede global buckling. This phenomenon was absent when MSI was applied independently but re-emerged when MSI and SPLA were combined for specific perturbation load positions. This approach helped to understand the progression from localized instability to overall structural buckling, highlighting the importance of accounting for imperfection sensitivity to achieve balanced and reliable designs without being excessively conservative.

### 2.3.1. Buckling Behavior and Stability of Shell Structures

Extensive research has addressed critical challenges, including imperfection sensitivity and optimization of design parameters, to improve the structural stability of these systems. Studies have explored toriconical shells, layered metallic domes, and reinforced torispheres to provide deeper understanding of their buckling behavior under external pressure.

Research on toriconical shells emphasizes the role of knuckle (toroidal) segments in stress diffusion at junctions [49]. Experimental results show that reducing the knuckle radius to diameter ratio can significantly lower buckling

pressure, with reductions reaching up to 50% in thin shells. Sensitivity analysis indicates that localized inward dimples caused by concentrated forces are more damaging than eigenmode affine imperfections. These findings highlight the need to avoid small knuckle sizes and to employ heat treatment to mitigate material anisotropy effects, which decrease the structural stability.

The stability of layered metallic domes, constructed from materials such as copper steel copper and titanium aluminum, demonstrates the potential of using laminate structures for enhanced pressure resistance. Experimental and numerical studies [50] show that copper outer layers plastically deform when supported by a steel core, emphasizing the importance of careful material selection. Buckling pressures ranging from 1.7 to 10 MPa underline the flexibility offered by varying material and thickness configurations. However, challenges in modeling laminate properties and boundary conditions necessitate meticulous analysis during design to ensure accurate predictions of structural behavior.

Reinforcement strategies such as the addition of stringers in tori spheres, also play a critical role in improving buckling performance. Figures 8 and 9 show the geometry details, shape prior to buckling, and buckling mode of a plain torisphere, as well as the corresponding behavior of a dome reinforced with a single stringer. Experimental results showed that adding a small number of stringers reduced buckling pressure by triggering eigenmodes with fewer hoop waves, contrary to expectations. Only when the number of stringers exceeded a threshold value did the buckling pressure increase. The research demonstrated that reinforcement models often overestimated load-carrying capacity, leading to potential design errors. The findings highlight the need for detailed eigenmode analysis to optimize stringer placement and quantity.

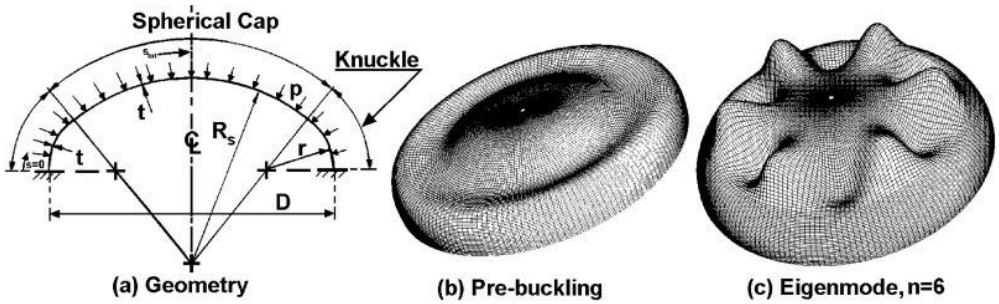


**Figure 8: Geometry details, shape just prior to buckling, and buckling mode of plain tori sphere** [51]

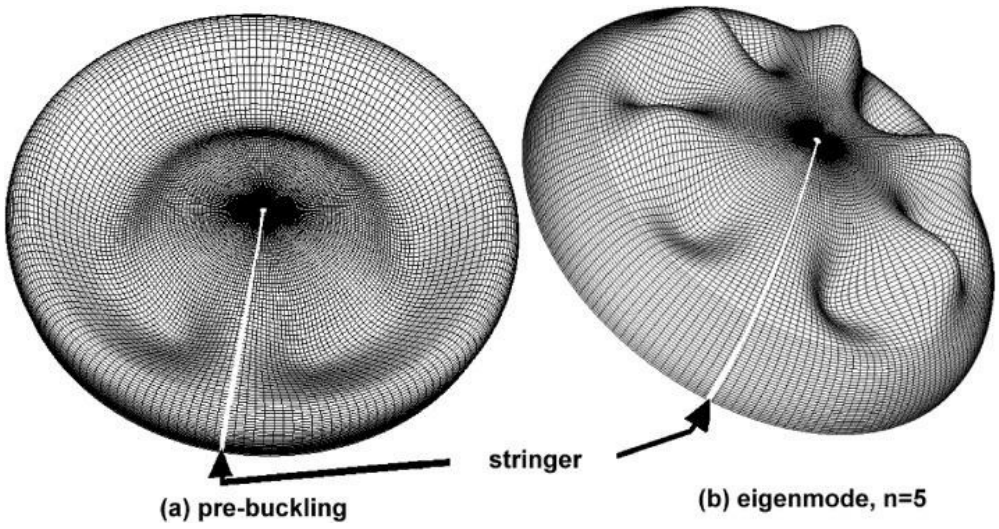


**Figure 9: Shape just prior to buckling (Fig. 9a), and buckling mode (Fig. 9b) of dome reinforced by a single external stringer** [51]

## 2.3.2. Buckling Behaviour in Cylindrical Shells

Evkin et al. [52] examined the influence of various boundary conditions on the local buckling behaviour of axially compressed cylindrical shells. The study emphasized the disparity between classical boundary conditions and real-world scenarios, particularly the impact of rigid plates and stiffened edges on post-buckling behaviour. A combination of numerical methods and Pogorelov's geometrical approach (which focuses on analysing localized buckling patterns and

the energy balance in shell deformation) was employed to explore the metastability and energy barriers associated with different loading schemes. The experimental setup, including possible end rotations, translational motion, and lateral perturbations, is schematically illustrated in the Figure 10, which provides a comprehensive depiction of the loading scheme used in the analysis.

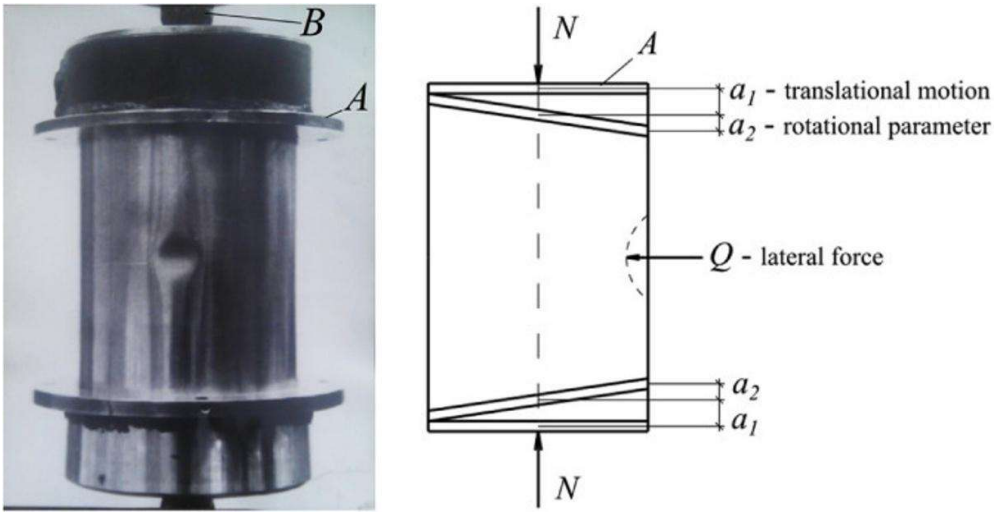


**Figure 10: a) Cylindrical shell in post-buckling equilibrium with a single buckle, depicting experimental loading conditions. b) Experimental loading scheme for a cylindrical shell, showing end rotation, translational motion, and lateral perturbations.** [52]

Building on this, Evkin [53] refined the analytical model of local buckling for axially compressed cylindrical shells by incorporating numerical insights. The updated model builds on Pogorelov's method and includes adjustments for moderate deflections, improving its accuracy in predicting buckling behavior. This was validated through comparisons between experimental data and numerical simulations. The results revealed that the enhanced model effectively captures both the qualitative trends and the quantitative characteristics of shell buckling under various perturbation conditions. Furthermore, the parametric analysis offered a practical method for calculating design buckling loads, making the model a valuable tool for engineering applications.

Among the various methods developed to address buckling and imperfection sensitivity of cylindrical shells, the Single Perturbation Load Approach (SPLA) has gained significant attention as a practical tool in these shapes as well. Proposed by multiple researchers, including Kriegesmann et al. [54], the SPLA is based on fundamental mechanical principles, with the goal of determining realistic design loads by introducing a single localized perturbation to the shell. This approach has been found to be effective in predicting the effects of imperfections, such as local boundary irregularities and single buckle deformations in cylindrical shells. However, Kriegesmann et al. identified a key limitation in the SPLA framework, stating that a single perturbation load doesn't always capture the worst-case imperfection. Their research demonstrated that applying multiple perturbations simultaneously could lead to a lower bound in load bearing capacity. However, this adjustment reduces realism, as real-world imperfections are rarely distributed in such a manner. As a result, the SPLA may overestimate the buckling strength in certain scenarios.

Further reinforcing their conclusions, this study conducted finite element modeling of cylindrical shells under axial compression, revealing postbuckling deformations that highlighted the complexities of imperfection sensitivity (Figure 11). These findings show the challenges in accurately capturing worst-case scenarios and demonstrate the limitations of simplified approaches like the SPLA in real-world applications.

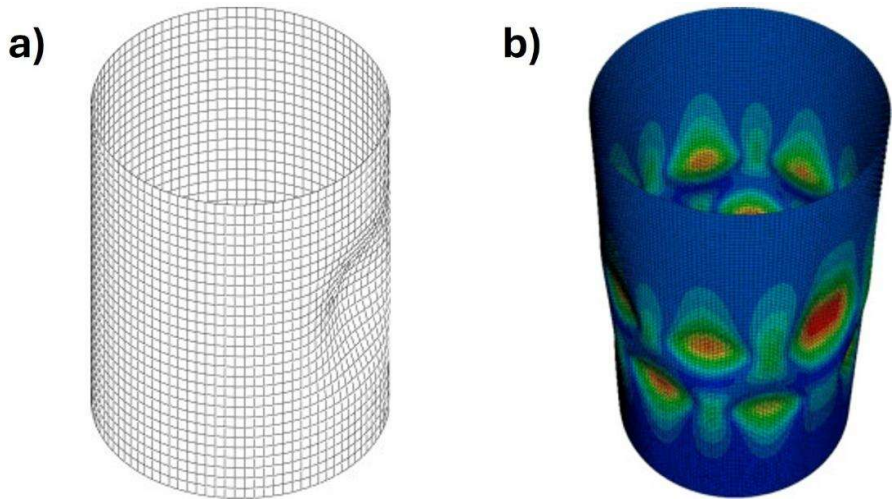


**Figure 11: (a) Cylindrical model featuring an initial single dimple imperfection; (b) Finite element model of the cylinder showing post buckling deformations under axial compression** [54]**.**

Building on this foundational work, our research applies eigenmode-affine geometric imperfections with the SPLA framework to assess the buckling behavior and imperfection sensitivity of HDPE structures. The eigenmode-affine approach allows for a more realistic representation of initial geometric deviations, facilitating a detailed evaluation of their impact on the buckling strength of HDPE pressure tank heads. By systematically varying the amplitude of imperfections, this present research identifies critical thresholds beyond which the structural integrity of these pressure tanks is significantly compromised.

### 2.3.3. Buckling behavior of spherical shells

In the context of spherical shells, Evkin's [55] study on spherical shell buckling under external pressure focused on the localization phenomenon that occurs in the post buckling stage. The research introduced an analytical model combining Rayleigh-Ritz and asymptotic methods, specifically addressing low-pressure conditions. A key aspect of this study was the examination of the energy barrier needed for the transition from pre-buckling to post-buckling states. This energy barrier is crucial for evaluating the shell's vulnerability to perturbations. By comparing spherical shells with cylindrical shells under axial compression, the

study highlighted both similarities and differences in their stability behaviors. The findings show the importance of energy considerations in understanding shell stability when subjected to localized disturbances.

Evkin [56] extended his previous work by applying an analytical model to examine the effects of imperfections and perturbations (such as probing radial forces and energy barriers) on the buckling load of spherical shells. The variability in buckling load predictions was quantified using the Monte Carlo method and error propagation techniques. This probabilistic approach revealed the role of uncertainty in predicting design buckling pressures, emphasizing the importance of considering randomness in perturbations during the design phase.

Expanding on these studies, Yang et al. [57] investigated the implosion behavior of deep-sea titanium alloy spherical pressure shells. Their work emphasized the influence of geometric imperfections on implosion dynamics. By introducing the first ten linear buckling modes as initial imperfections, they quantified their corresponding critical loads and analyzed their impact on failure behavior (Figure 12). They found that imperfections not only amplify peak implosion loads but also accelerate failure onset, with imperfection amplitude having a more significant effect than shape. Furthermore, they demonstrated the role of the implosion strength parameter in influencing load peaks and energy distributions, showing that higher values lead to behavior resembling ideal bubble collapse.

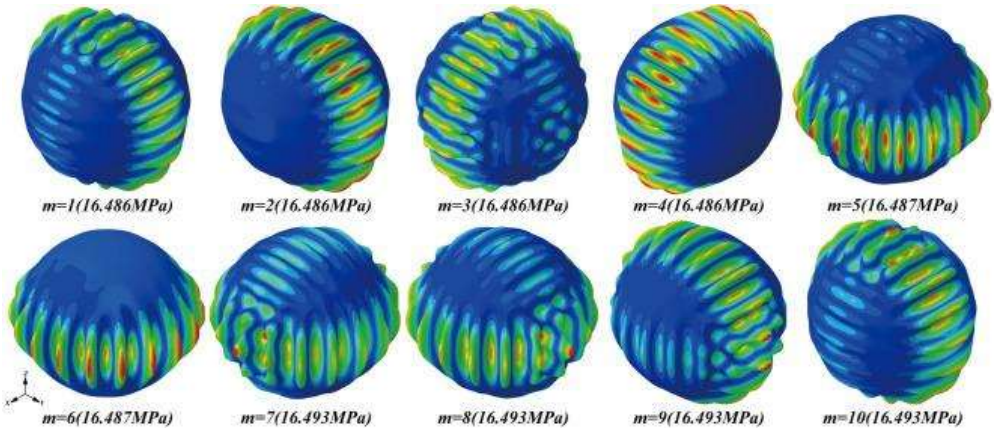


**Figure 12: Ten linear buckling modes with critical buckling pressures** [57]

The combined insights from these studies highlight the critical role of geometric imperfections, perturbations, and probabilistic approaches in understanding and designing spherical pressure shells for stability under extreme conditions. The integration of analytical, numerical, and probabilistic methods provides a comprehensive framework for assessing the vulnerability of these structures to implosion and buckling.

### 2.3.4. Buckling Behavior of toroidal shells

Enoma et al. [58] carried out a numerical study on the buckling resistance of toroidal shells with a doubly symmetric parabolic ogival cross-section under uniform external pressure. The research considered both perfect and imperfect geometries of elastic steel shells, using boundary conditions designed to reduce buckling pressure. It was found that non-axisymmetric buckling, marked by circumferential waves, began near the top and bottom edges of the vessel's outer face, while axisymmetric buckling occurred at higher pressures. The research identified that the critical buckling pressure is significantly influenced by the geometrical parameters of the cross-section and the shell's thickness relative to its overall dimensions.

Imperfection sensitivity was explored using eigenmode-shaped perturbations, revealing a sharp decline in buckling strength with increasing imperfection amplitude in shells with high diameter-to-thickness ratios. To optimize the buckling resistance, the study suggested increasing shell thickness or introducing stiffeners in the weak zones. The variation of buckling pressure with the aspect ratio *h/d* demonstrated a maximum resistance at *h/d=1.5* as shown in Figure 13, making it the most effective design for maximizing buckling strength under external pressure.

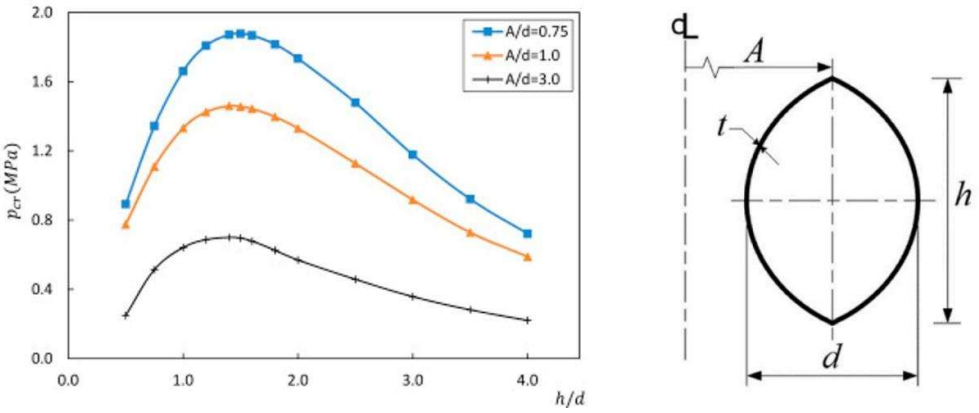


**Figure 13: Plot of critical buckling pressure versus *h/d* for three cases of *A/d*** [58]

## 2.3.5. Buckling Behavior of Sandwich Cylindrical Pressure Vessels

Jasion et al. [59] investigated the mechanical performance of sandwich cylindrical pressure vessels featuring hemispherical and super ellipsoidal dished heads subjected to external pressure. This study employed finite element methods within the linear elastic range to evaluate stress distribution and buckling resistance for vessels constructed with aluminum faces and a functionally graded aluminum foam core. Their findings indicated that super ellipsoidal dished heads provided more favorable stress distributions, especially for shear stresses, as they eliminated the peak stress values observed in hemispherical heads. The distribution of shear stress varied significantly along the thickness of the vessel and between different sections, with the highest values observed in the head region. Furthermore, buckling

resistance was found to decrease with increasing core softness, as represented by the $k_e$ parameter. This parameter, shown on the x-axis in Figure 14, reflects the mechanical properties of the core material. The y-axis represents the buckling load, which corresponds to the critical load a structure can withstand before buckling occurs.

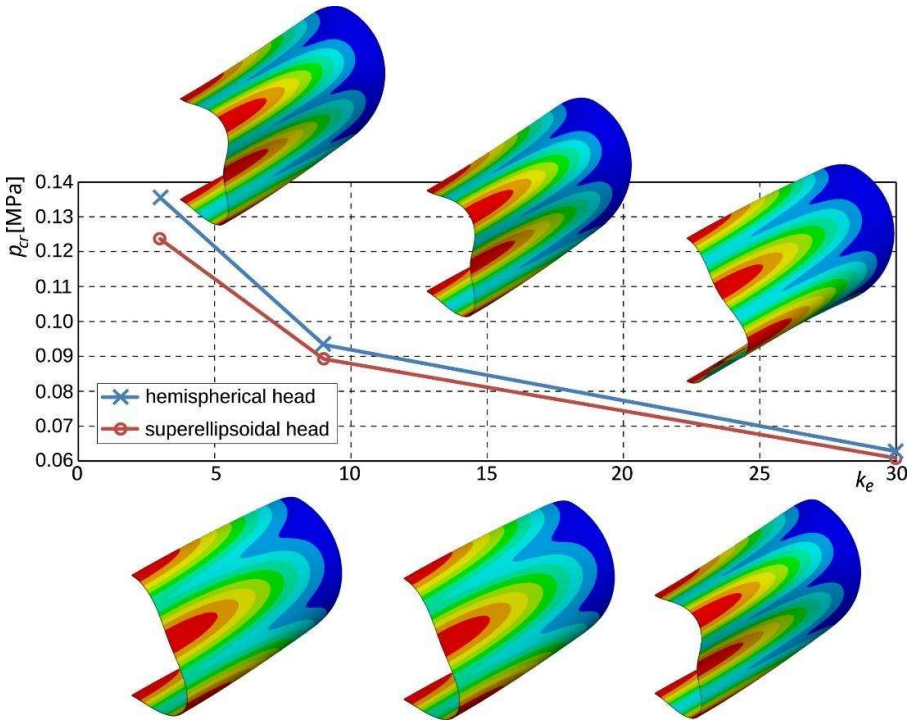


**Figure 14: Buckling load versus $k_e$ parameter for sandwich cylindrical pressure vessels with hemispherical and super ellipsoidal heads** [59]

As illustrated in the figure 14, three different values of the $k_e$ parameters 3, 9, and 30 were considered for both types of dished heads, allowing for a comparison of the performance of the two head designs and analysis of how core softness affects the buckling load. The results from above figure showed that the critical load for the model with a hemispherical dished head was about 9% higher than that for the super ellipsoidal head when $k_e$=3. However, for $k_e$=30, this difference decreased to 3%. As expected, smaller values of $k_e$ resulted in lower buckling resistance. At the

extremes, for $k_e$=30, the buckling load was only 46% of that for $k_e$=3 in the case of the hemispherical head, and 49% in the case of the super ellipsoidal head. The study emphasized the potential for modern manufacturing techniques such as 3D printing to facilitate the production of such advanced geometries. Limitations of the study, including its linear nature, were highlighted, with suggestions for future research to explore plastic deformation, post-buckling behavior, and practical non-linearities.

### 2.3.6. Stress and Buckling Analysis of Dished Heads

Magnucki et al. [60] explored an alternative design for a dished head in thin-walled shells, aiming to minimize the edge effect that occurs at the junction of the cylindrical shell and the head. The proposed head shape combines a circular arc and a fifth-degree polynomial as shown in figure 15, and its stress distribution and buckling behavior were studied through both analytical methods and finite element modeling (FEM).

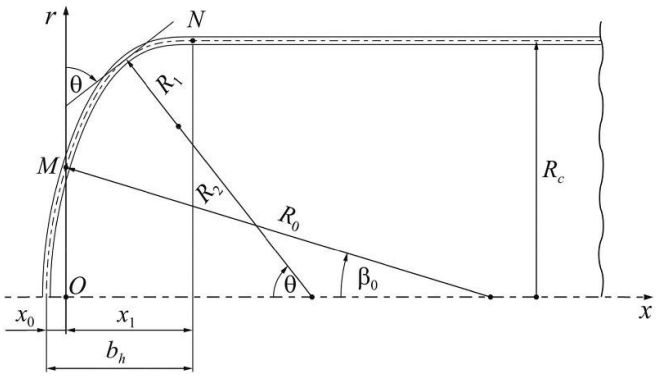


**Figure 15: Proposed geometry of dished head of a pressure vessel** [60]

The study revealed that the stress distribution for thinner shells (e.g 1 mm thickness) matches closely between analytical and numerical models, except at specific points near the transition zones. In contrast, for thicker shells, such as 4 mm, differences between the results of these models become more visible. The research emphasizes the necessity of buckling analysis due to the compressive stresses present in the dished head, considering both internal and external pressures. The study demonstrated that under external pressure, the cylindrical part of the tank

buckles in one longitudinal half-wave with multiple circumferential waves. For internal pressure, buckling occurred in regions of compressive stress in the head, forming short waves. It is to be noted that the internal buckling load was significantly higher than the external one due to the stiffness in the head's compressed regions.

A comparison of the buckling load and modes of the proposed head with traditional ellipsoidal and tori-spherical heads showed comparable results under both external and internal pressure conditions. However, under internal pressure, the ellipsoidal head gave a 57% higher buckling load than the other heads as shown in figure 16. These findings suggest that the proposed head's performance aligns with conventional designs in terms of buckling behavior, making it a good alternative.

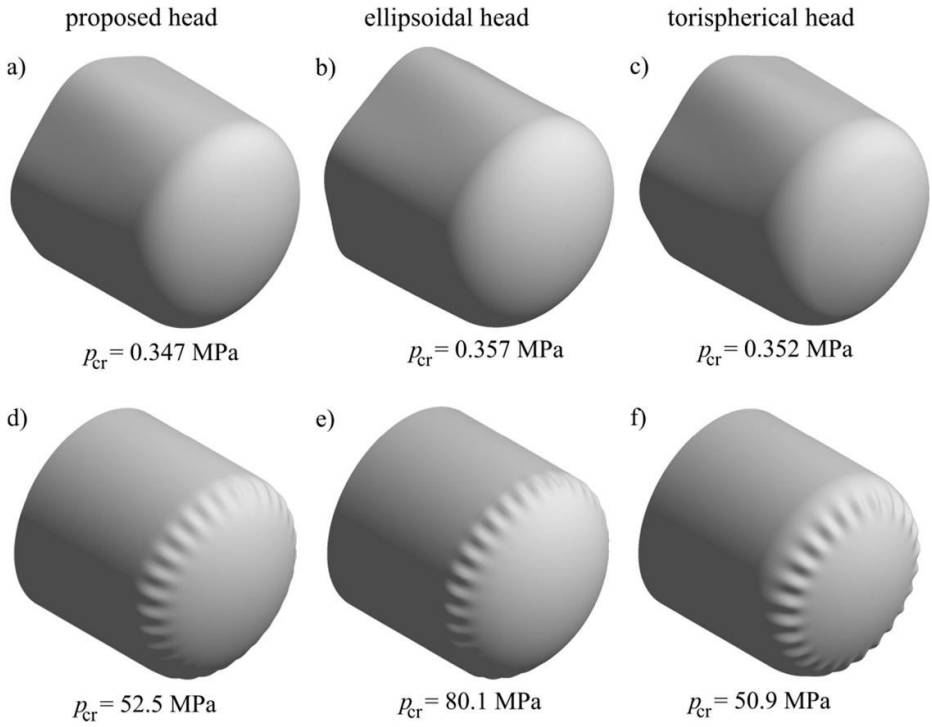


**Figure 16: Comparison of critical buckling pressure for different Head Designs Under a)-c) External and d)-f) Internal Pressure Conditions** [60]

The study concluded that while the proposed dished head achieves an equivalent stress level comparable to the cylindrical section of the tank, it cannot eliminate sudden changes in stress distribution near the junction. In addition, the curvature continuity at the connection points does not fully resolve the edge effect.

### 2.3.7. Buckling Behavior of Ellipsoidal Heads under Internal Pressure

Li et al. [61] studied the buckling behavior of ellipsoidal heads subjected to internal pressure and specifically analyzed their role in maintaining the structural strength of steel nuclear containment vessels. These ellipsoidal heads are widely used in nuclear pressure vessels. It plays a crucial role in withstanding internal pressures during potential accident scenarios. Buckling, as a key failure mode, poses a serious threat to the safety of these containment systems. Therefore, a thorough understanding of their buckling characteristics is vital for improving design standards and ensuring the reliability of pressure vessels.

The study involved designing a pressure vessel with an ellipsoidal head featuring a diameter of 4797 mm, having a radius-to-height ratio of 1.728, and a thickness of 5.5 mm. The primary objective was to determine the buckling pressure and analyze the deformation behavior of the ellipsoidal head under internal pressure. To accurately capture both the initial and deformed geometries of the head, the researchers utilized three-dimensional (3D) laser scanning technology, as illustrated in Figure 17. The experiments provided a detailed account of the buckling process, including deformation patterns, strain distributions, and critical buckling pressures. The buckling initiated progressively, with the first significant deformations occurring at the knuckle meridional weld seams.


**Figure 17: 3D Laser Scan Contour of Buckling Deformation** [61]

The results from the experiments show that initial geometrical imperfections played an important role in influencing the buckling pressure of the ellipsoidal head. The importance of accounting for such imperfections during the design and analysis stages of pressure vessel heads were highlighted. The researchers performed nonlinear FE analysis to predict the initial buckling pressures. The analysis was conducted for both the measured shape of the head, including imperfections, and an idealized perfect shape. The predictions considering the measured shapes were found to be in good agreement with the experimental results which highlights the importance of using actual imperfections in buckling analysis.

### 2.3.8. Numerical Investigation of Buckling Behavior of Dome Caps Under External Pressure

Ismail et al. [62] investigated the buckling behavior of steel dome caps under external pressure, using numerical methods in accordance with the European Standard EN 1993-1-6. FEA results showed good agreement when compared to experimental results, with an error of less than 7%. The study examined several approaches for introducing imperfections into the models, including single load indentation (SLI), axisymmetric outward bulge (AOB), and eigenmode-affine (EM), to assess their effects on the buckling performance. Among these,

eigenmode-affine imperfections were identified as the most critical, significantly reducing the buckling capacity as shown in Figure 18. The SLI approach, however, was favored for simulating realistic imperfections due to its practical representation of localized flaws.

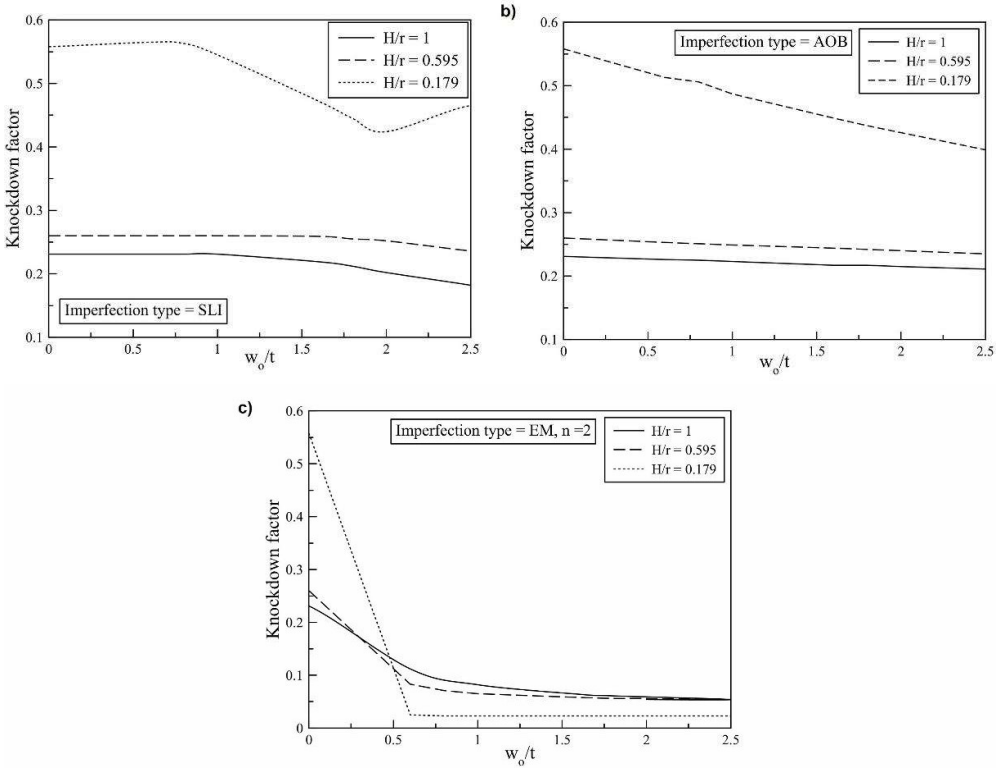


**Figure 18: Sensitivity analysis of the dome cap under external pressure, showing the impact of (a) Single Load Indentation (SLI), (b) Axisymmetric Outward Bulge (AOB), and (c) Eigenmode-Affine (EM) imperfections on buckling performance** [62]

A parametric study explored the influence of imperfection sensitivity and design configurations, providing upper and lower bound buckling curves as design recommendations similar to NASA SP-8032 guidelines. Regression analysis resulted in an empirical equation with a high reliability ($R^2 = 0.97$) for estimating the buckling load. The research also extended its scope to a case study involving stress assessment and buckling design of an oil storage tank's spherical partition under pressure. These findings contribute to valuable knowledge for designing and

evaluating dome caps in preliminary stages, emphasizing the importance of imperfection considerations in achieving structural reliability.

Zhang et al. [63] examined the buckling behavior of stainless-steel spherical caps with circular arc meridians under uniform external pressure. Their research included both laboratory-scale caps and numerically simulated models with varying geometric parameters. The main aim was to evaluate the load-carrying capacity of these caps and identify the most effective configurations for specific applications.

The experimental phase of the study involved six laboratory scale caps, each with a nominal base diameter of 146 mm, a wall thickness of 1 mm, and a height of 37 mm. These models were carefully fabricated and then subjected to gradual pressurization to observe their buckling behavior. Post-buckling models are illustrated in figure 19. Experimental results were compared to numerical simulations, revealing strong agreement between the two approaches. The buckling loads for caps with deterministic imperfections ranged from 5.255 MPa to 5.647 MPa, with post-buckling patterns resembling localized dimples, as shown in figure 20. The consistency in these findings, both in terms of load values and failure modes, confirmed the reliability of the experimental methodology.


**Figure 19: Tested models after buckling** [63]

Numerical analyses were conducted using both elastic plastic and elastic perfectly plastic models to simulate the buckling process. These simulations aligned well with the experimental data, although the elastic perfectly plastic model tended to produce more conservative predictions. This modeling approach was recommended as a useful tool for assessing the buckling behavior of spherical caps under external pressure. Post-buckling modes observed in the simulations also featured localized dimples, in accordance with the experimental findings.

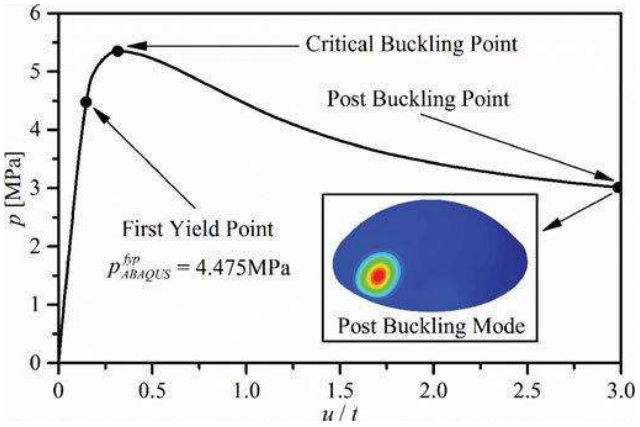


**Figure 20: Equilibrium Path of the SC1 Cap Highlighting Different Buckling Stages and Post-Buckling Mode** [63]

The study expanded to include a numerical analysis of 13 spherical caps with varying height to base diameter ratios but the same mass. It was found that the buckling load increased with the height ratio initially, peaking at a critical point before declining. The optimal configuration was determined to occur at a height to diameter ratio (h/d) of approximately 0.274, which provided the highest buckling load. This configuration was recommended for applications such as end closures in cylindrical pressure hulls or as manhole covers in deep sea vehicles.

Additionally, the authors highlighted that the shape of imperfections, such as eigenmode based variations, did not significantly affect the post-buckling mode, which consistently showed localized dimpling. This suggests that the overall structural design plays a more crucial role in buckling behavior than the specific characteristics of imperfections. Nonetheless, they acknowledged the importance

of further investigating other types of imperfections, such as increased radius patches or inward dimples, to fully understand the buckling phenomena of spherical caps.

Similarly, Zhu et al. [64] investigated the elastic plastic buckling behavior of hemispherical heads under external pressure using experimental, numerical and analytical methods. Their research involved fabricating and testing five stainless steel hemispherical head models (shown in Figure 21) with a nominal diameter of 120 mm and a wall thickness of 0.4 mm. Both geometrically perfect and imperfect heads were analyzed. Nonlinear buckling performance was studied numerically across a range of wall thicknesses t (0.24–0.6 mm), yield strengths $\sigma_y$ (180–230 MPa), and imperfection sizes $\delta$ (0.01–0.05 mm). Analytical formulae were proposed to predict buckling loads, and their accuracy was verified through experiments and numerical simulations.


**Figure 21: Collapsed hemispherical heads subjected to external hydrostatic pressure, exhibiting localized dimples as the characteristic failure pattern** [64]

The study demonstrated that linear elastic buckling loads for perfect heads, predicted using Zoelly's formula [65] (Eq.1), matched closely with numerical results.

$$P_{act} = k\frac{2}{\sqrt{3(1-\nu^2)}}\frac{Et^2}{r^2} \tag{1}$$

However, for nonlinear elastic-plastic buckling, significant discrepancies (18–26% error) were observed between numerical results and predictions using Koiter and Karman formulas. To address this, the authors introduced a combined reduction factor $k$ (Eq.2), which accounts for the geometric and material nonlinearities, as

well as imperfections. This factor was incorporated into a new analytical formula for predicting the nonlinear buckling load, which was validated experimentally. The results showed deviations between 3.9% and 6.7% compared to experimental findings, indicating good agreement.

$$k = \left(5.3357\left(\frac{\delta}{r}\right)^3 - 3.3004\left(\frac{\delta}{r}\right)^2 - 0.0142\frac{\delta}{r} + 6.8721 \times 10^{-5}\right)\sigma_y^{0.8508}\left(\frac{t}{r}\right)^{-0.7433} \quad (2)$$

The authors also studied the effects of wall thickness-to-radius ratios (ranging from 0.004 to 0.010), imperfection sizes, and yield strengths on buckling behavior. They extended an empirical model to derive formulae for predicting buckling loads during the design phase. These formulae can guide preliminary designs of hemispherical heads, and the study encourages further exploration of the influence of different imperfections and material properties on buckling performance.

### 2.3.9. Strength and Failure of Welded Hemispherical Shells

Cho et al. [66] investigated the ultimate strength and failure behavior of steel welded hemispherical shells under external hydrostatic pressure, using both experimental and numerical methods. Mild steel hemispheres were created through press forming and welding. The study focuses on the impacts of initial shape imperfections, shell thickness variations, and residual stresses from the fabrication process. Four hemisphere models with radius to thickness (R/t) ratios ranging from 50 to 130 were tested to failure which is illustrated in Figure 22. Detailed measurements of geometric imperfections and thickness were recorded prior to testing. Nonlinear FE simulations were conducted to explore ultimate load capacity and plastic deformation, considering variations in sphericity, thickness, and residual welding stresses.

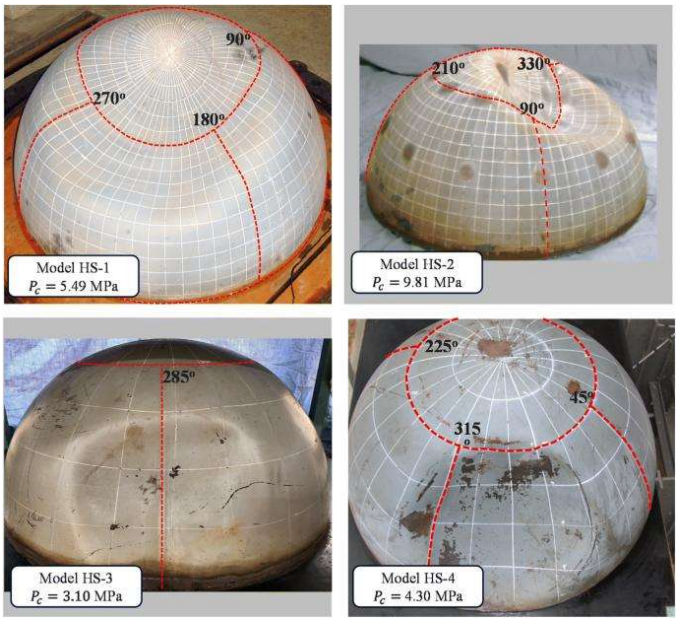


**Figure 22: Post-buckle geometry for all tested hemispherical models** [66]

The results showed that buckling pressures for the experimental models ranged from 3.10 to 9.81 MPa. Two distinct failure modes were observed which are crown-area failure in two models (HS-1 and HS-2) and shell-segment-side failure in the other two (HS-3 and HS-4). A near-perfect hemisphere model exhibited failure exclusively at the crown, which highlighted the role of imperfections and residual stresses in determining failure modes. Nonlinear FE analysis closely matched the experimental results, with predicted collapse pressures ranging from 3.04 to 9.25 MPa and a coefficient of variation (COV) of 6%. This correlation validated the numerical method for assessing the ultimate strength of structures such as submarine pressure hulls.

## 2.3.10. Imperfection Sensitivity and Deep Spherical Domes

In continuation of research on spherical shells, Wagner et al. [67] investigated deep spherical domes, commonly used in aerospace and ocean engineering. These structures were found to be highly sensitive to geometric imperfections, with small deviations from ideal geometries leading to significant reductions in buckling

pressure. Conventional design approaches, based on linear buckling analyses corrected by empirical knockdown factors, often proved overly conservative.

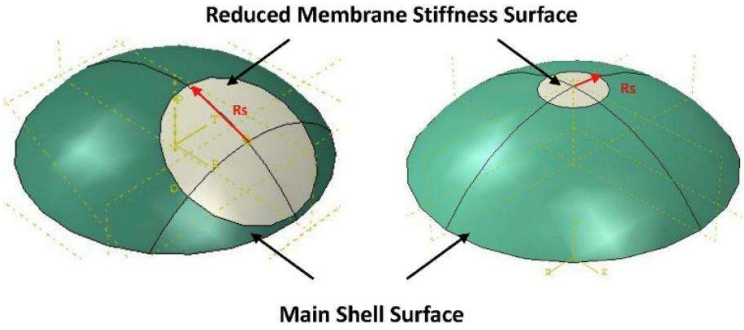


**Figure 23: Localized reduced stiffness method configuration for spherical domes in Abaqus (FEA): axisymmetric imperfection (right) asymmetric imperfection (left)** [67]

The Localized Reduced Stiffness Method (LRSM) was proposed as an efficient numerical technique to know the effects of imperfections without the need for extensive measurements. By local reducing the shell's stiffness, the method provided a practical means to estimate lower-bound buckling pressures. Finite element analysis of deep spherical domes validated the LRSM, which successfully predicted knockdown factors in both elastic and plastic buckling ranges. As shown in Figure 23, the LRSM was applied using a perfect-plastic material model. The results for both axisymmetric and non-axisymmetric buckling cases led to a consistent knockdown factor (KDF) of 0.19 which can be seen in figure 24. Furthermore, the LRSM's applicability extended to orthogrid-stiffened hemispheres, illustrating its versatility across various shell configurations and reinforcing its potential as a reliable design tool for complex shell structures.

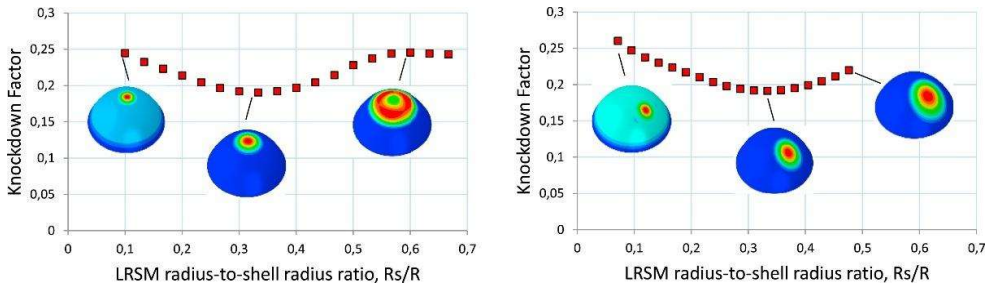


**Figure 24: Knockdown factor for buckling pressure (plastic) vs load increment in the numerical analysis: axisymmetric buckling with LRSM (left) and asymmetric buckling with LRSM (right)** [67]

## 2.3.11. Buckling Behavior of Tori-Spherical Shells

Wagner et al. [68] conducted a detailed investigation on the complex buckling behavior of tori spherical shells, which are commonly used in pressure vessel applications. The study highlighted the sensitivity of these structures to both geometric parameters, such as the knuckle radius, and material properties, particularly under external pressure. The researchers carried out an elastic plastic buckling analysis, incorporating several imperfection modeling techniques. These included measured geometric imperfections (MGI), geometric dimple imperfections (GDI), increased radius of curvature imperfections (IRCI), circular cutout imperfections (CCI), and localized stiffness reductions.

Among the methods analyzed, the Localized Reduced Stiffness Method (LRSM) proved to be particularly effective in providing conservative estimates for buckling pressures. This approach, which considered both perfectly plastic material behavior and geometric imperfections, produced results comparable to the IRCI and CCI methods. All approaches yield knockdown factors (KDF) close to 0.15. In contrast, the geometric dimple imperfection method (GDI) resulted in lower knockdown factors, approximately 0.1, offering limited improvement over traditional empirical guidelines.

The comparative analysis emphasized the LRSM's superiority as the most reliable approach for designing spherical and tori-spherical shells, especially in

predicting conservative lower-bound buckling pressures. Figure 25 demonstrates that accurately estimating the low experimental KDFs of test shells was only possible when both plasticity and real geometric imperfections were incorporated. The spherical portion of tori-spherical shells was also identified as particularly sensitive to imperfections, necessitating advanced numerical methods to enhance design accuracy.

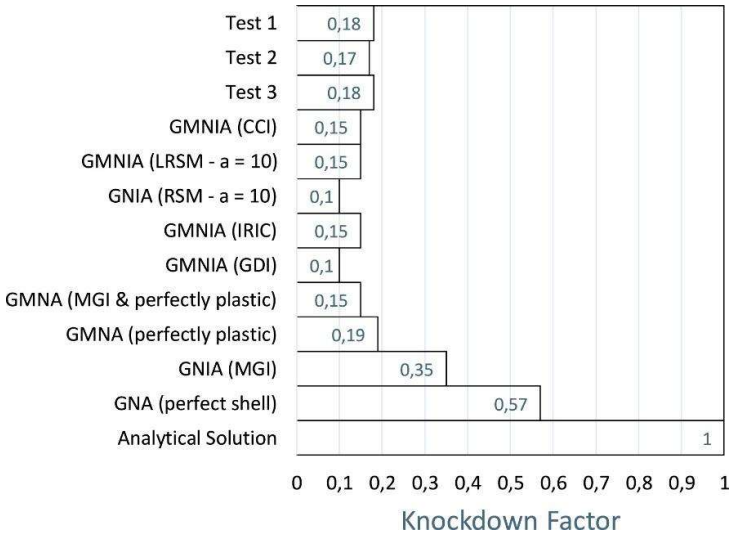


**Figure 25: Analysis of knockdown factors for tori-spherical domes subjected to external pressure using different simulation approaches.** [68]

## 2.3.12. Global–Local Buckling in CFRP Cylindrical Shells

Xin et al. [69] investigated the global and local buckling behavior in carbon fiber-reinforced polymer (CFRP) cylindrical shells using a multi-Digital Image Correlation (DIC) system for 360-degree full-field deformation measurement. Their study focused on the influence of imperfections which are both geometric and loading, on the buckling loads and deformation characteristics. Axial compression tests showed that imperfections caused deviations from theoretical behavior, where ideal shells would exhibit only global buckling. In practice, local buckling occurred due to manufacturing and loading imperfections. The authors highlighted that loading imperfections, such as hand-applied edge flattening, significantly

influenced local buckling loads and axial displacement, while geometric imperfections primarily affected global buckling loads.

Figure 26 illustrates the axial load versus displacement behavior for the W0-11 and W0-12 composite cylindrical shells, confirming the occurrence of both local and global buckling. Differences in buckling loads between the two shells were observed, attributed to the imperfections present during manufacturing and loading.

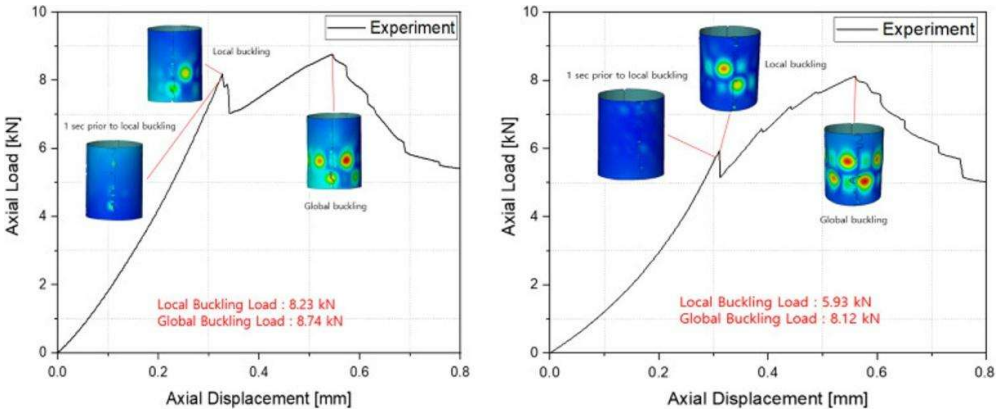


**Figure 26: Experimental results of W0-11 (left) and W0-12 (right) composite cylindrical shells**[69]

To further analyze the effects of imperfections, finite element analysis (FEA) results were compared with experimental data and linear buckling predictions. Figure 27 presents the comparisons, where the linear analysis assumes a geometrically perfect shell, and nonlinear analysis includes measured imperfections. The results demonstrated that geometric imperfections caused a reduction in buckling loads, while loading imperfections influenced both buckling loads and axial displacement. These comparisons highlighted the significant impact of imperfections on structural performance. The study overall emphasized the utility of the multi-DIC system for non-destructive monitoring of buckling behavior, offering a reliable means of evaluating global and local deformations. Although effective, the approach faced limitations related to calibration, scalability,

and equipment requirements, which the authors noted could be addressed in future developments.

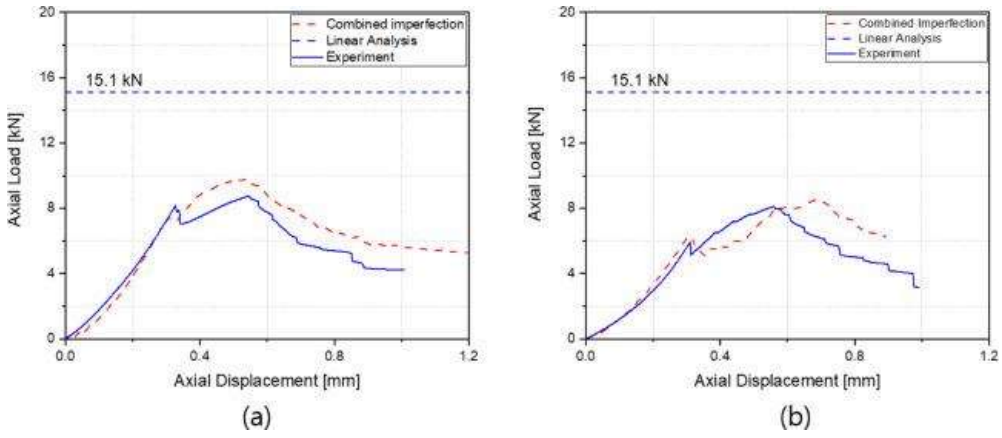


**Figure 27: Impact of geometric imperfections on buckling capacity by FEA simulations on W0-11 (left) and W0-12 (right) composite cylindrical shells.**[69]

## 2.4. Analysis of Pressure Components with Variable Wall Thickness

The structural performance of pressure tank components has been extensively studied to optimize their design for material efficiency and buckling resistance. Among these, the exploration of variable wall thickness designs stands out as a promising approach for enhancing load-carrying capacity and reducing material usage. While substantial progress has been made in this field, critical gaps remain, particularly in addressing the effects of geometrical imperfections, nonlinear buckling behavior, and advanced stress analyses for realistic operating conditions. This section reviews the current state of research in the analysis of pressure vessel components with variable wall thickness, identifying limitations in existing approaches.

### 2.4.1. Design of Externally Pressurized Ellipsoidal Heads with Variable Wall Thicknesses

Yang et al. [24] investigated the buckling and strength behavior of ellipsoidal heads under uniform external pressure, with a focus on the impact of variable wall thickness. The study utilized the isostrength principle to design the wall thickness distribution, exploring its effect on the strength of the ellipsoidal head. Both ellipsoidal heads with variable and constant wall thicknesses were evaluated numerically using the modified Riks method. The study also explored the effect of ellipticity on buckling performance, determining the optimal ellipticity for improved performance.

The theoretical formula for thin-shell strength was used to derive a distribution for the wall thickness of ellipsoidal heads, offering a basis for the structural design of these heads with variable wall thickness. In comparison with spherical heads, the study found that an ellipsoidal head with constant wall thickness had a 2.89% lower buckling load than a spherical head with constant volume, but its thickness was 21.36% larger. This indicated that, at equal volume, the spherical head was more efficient in material utilization. However, the simulation results showed that the ellipsoidal head with variable wall thickness has 13.41% higher buckling load as compared to a spherical head with constant volume, while also having a 21.34% smaller volume. These results suggest that ellipsoidal heads with variable wall thickness have distinct advantages, particularly in scenarios where material costs are high. The stress distribution for the ellipsoidal head with variable wall thickness is shown in Figure 28, where the maximum stress was found to be 661 MPa, meeting the material strength requirements for a titanium alloy head with a yield strength of 830 MPa.

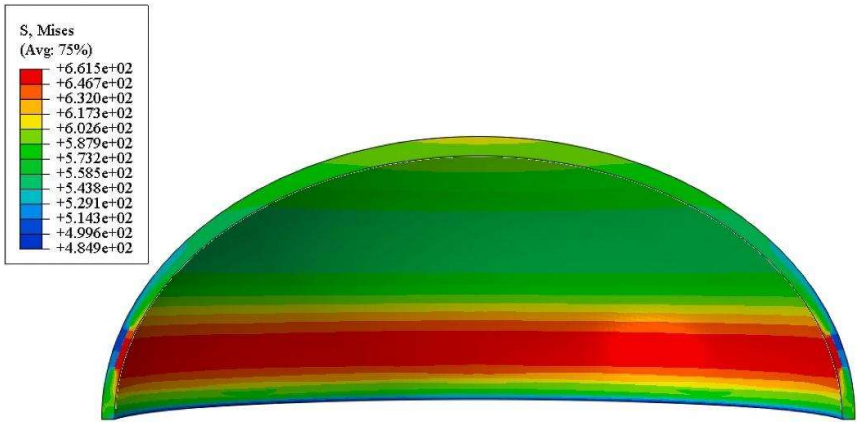


**Figure 28: Stress distribution in elliptical head with variable wall thickness** [24]

The buckling behavior of the ellipsoidal heads with different ellipticities was analyzed in more detail, with numerical results presented in Figure 29. $P_{lb}$, $P_{nlb}$ represent linear elastic buckling pressure and Nonlinear buckling pressure respectively. Knockdown factor (KDF) is the ratio of the nonlinear critical buckling load to the first order linear elastic buckling load ($P_{nlb}/P_{lb}$). The analysis showed that the nonlinear critical buckling load varied by a factor of 4.43, and the buckling load attenuation coefficient increased as ellipticity decreased. However, when the ellipticity dropped below 10/6, the effect on the buckling load became less pronounced, indicating less impact of ellipticity on buckling when it reaches a certain level.

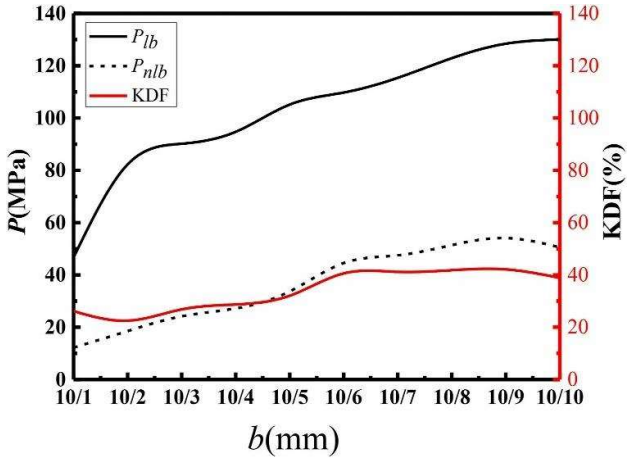


**Figure 29: Effect of different aspect ratio of elliptical heads on buckling pressure P and Knockdown factor** [24]

Figure 30 shows the final instability modes of ellipsoidal heads with different ellipticities, further illustrating the relationship between ellipticity and buckling behavior in these structures. The results further showed that when the ellipticity was set to $4\sqrt{3}$ ($\rho = 1.316$), the ellipsoidal head with variable thickness outperformed the spherical head in terms of load-carrying capacity. Moreover, the ellipsoidal head with variable thickness demonstrated a 16.79% higher buckling load at a depth of 4 km, while having a 4.83% smaller volume compared to the ellipsoidal head with constant thickness. These findings suggest that the ellipsoidal head with variable thickness offers significant improvements in load-bearing performance, material utilization, and structural stability. The influence of ellipticity on buckling characteristics was found to be considerable, with the best performance observed when the ellipticity was set at 1.316. For lower or higher ellipticities, the buckling load sharply decreased, especially in the case of constant wall thickness.

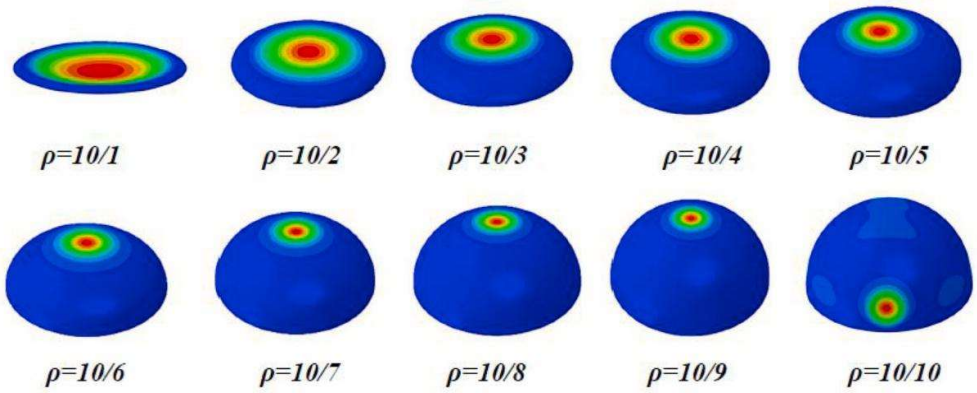


**Figure 30: Post buckling shape of elliptical heads with different aspect ratio** [24]

However, this study primarily focused on idealized geometries and did not focus on the geometrically nonlinear analyses (GNA) with different types of imperfections, such as geometrical dimples, flat patches, circular cutouts, and eigenmode-affine shapes. This limitation leaves a significant gap in understanding the interaction of imperfections with variable wall thickness to affect buckling performance, reducing the applicability of the findings to real-world designs where imperfections are inevitable.

### 2.4.2. Buckling Performance of Egg-Shaped Shells with Variable and Constant Thickness

Zhang et al. [70] conducted an experimental and numerical study to examine the nonlinear elastic buckling behavior of egg-shaped shells under uniform external pressure. The egg-shaped shells were fabricated from photosensitive resin, each with a nominal mass of 570 g, a major axis of 260.36 mm, and a minor axis of 181.32 mm. Four egg-shaped shells were produced using rapid prototyping, specifically stereolithography. Two shells were designed with a constant wall thickness, labelled ES1 and ES2, while the other two shells, ES3 and ES4, featured variable wall thickness along the meridian. Fabricated egg-shaped shells with constant (ES1 and ES2) and variable (ES3 and ES4) wall thicknesses are shown in Figure 31, providing a clear visual comparison of the two types of designs. The

geometry of each shell was precisely measured before subjecting them to controlled pressurization until failure. The experimental results demonstrated were consistent and alligned with FEA results from Abaqus.

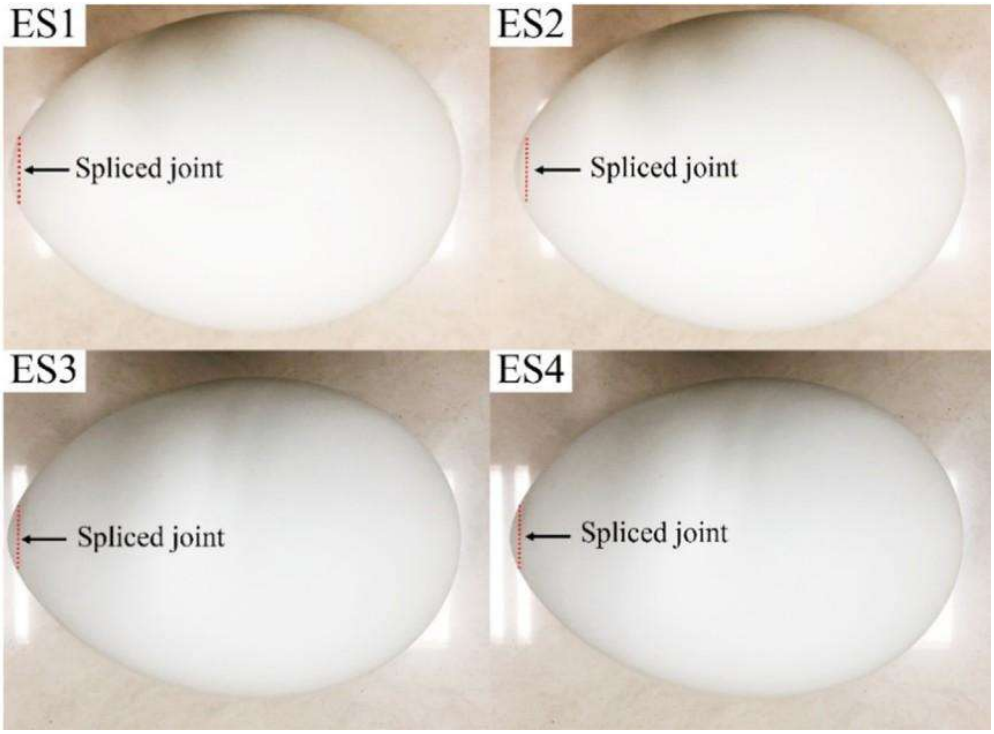


**Figure 31: Manufactured shells with constant (ES1, ES2) and variable wall thickness (ES3, ES4)** [70]

The key finding of the study was that the average collapse pressure of the egg-shaped shells with variable wall thickness was approximately 24% higher than that of the shells with constant thickness which can be seen in Figure 32. This improvement indicates a significant increase in the load-bearing capacity of the shells when a variable thickness design is used. During the tests, the shells consistently failed by forming local dents near the equator, which is typical behaviour for such shells when subjected to external pressure.

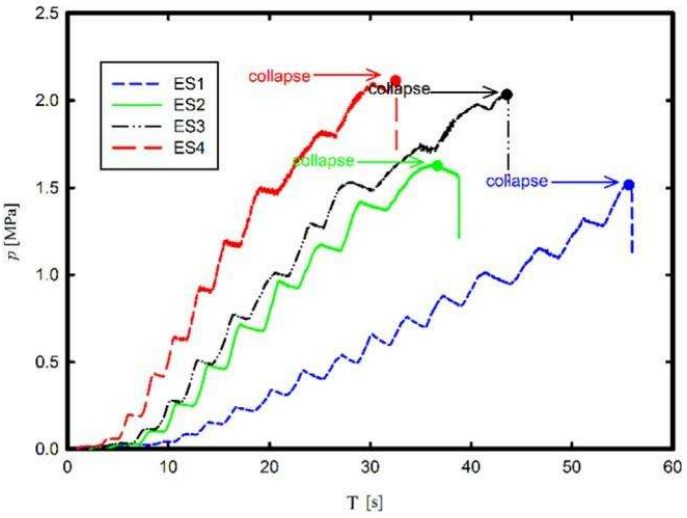


**Figure 32: Buckling pressure comparison for four fabricated egg-shaped shells with constant (ES1, ES2) and variable wall thickness (ES3, ES4)** [70]

Numerically, the results showed that the critical buckling pressure of the perfect egg-shaped shell with variable thickness was significantly higher than that of its constant thickness counterpart, confirming the advantages of a variable wall thickness design. Furthermore, the equilibrium paths after buckling revealed unstable behavior and local dent formation as shown in Figure 33, characteristic of revolution shells with positive Gaussian curvature under uniform external pressure. The location of maximum stress was found at the collapse region's center, further validating that buckling initiates at the weakest zone of the structure.

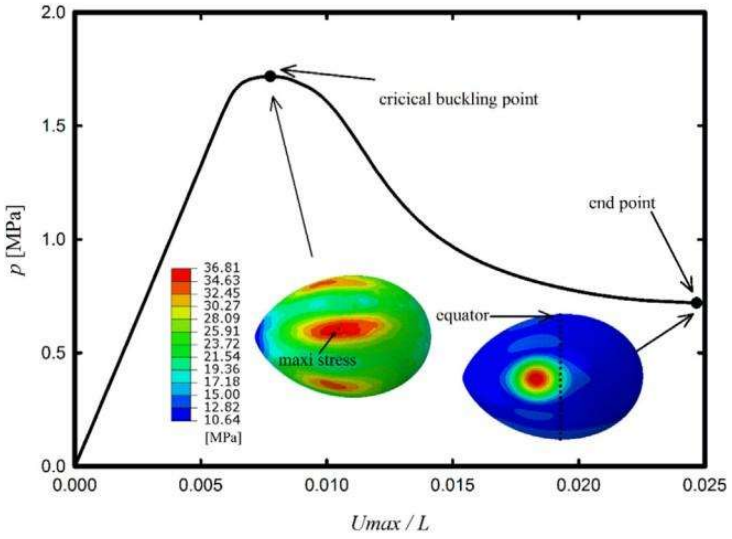


**Figure 33: Equilibrium curve of ES1 shell buckling** [70]

The study's findings suggest that egg-shaped shells with variable wall thickness can be applied in a variety of pressure-bearing components, including underwater pressure vessels, liquid storage tanks under negative pressure, and pressure hulls for submarines. The concept of utilizing variable wall thickness to enhance buckling performance could be extended to other shell structures with positive Gaussian curvature. However, this research has focused only on elastic buckling in weak resin-based materials, future work can examine the elastic–plastic buckling behavior in high-strength thermoplastic materials, like HDPE, and also metals with variable wall thickness to further explore their load-carrying potential.

### 2.4.3. Optimization Techniques for Pressure Vessels with Variable Wall Thickness

Another related study [71] investigates the optimization of pressure vessel shapes using an analytical method based on calculus of variations. The purpose is to target mass minimization or volume maximization under structural constraints. The resulting optimized geometries, characterized by variable wall thickness along the meridian, share similarities with my work in addressing stress distribution challenges. While the study applies these principles to metallic pressure vessels

manufactured through additive manufacturing (AM) techniques, these concepts of shape optimization are equally relevant to polymer-based materials like HDPE.

The study has shown the feasibility of producing optimized pressure vessel designs using selective laser melting (SLM), which is an additive manufacturing process. A metallic prototype was successfully fabricated as shown in figure 34, and optical scanning confirmed that the manufacturing tolerances were within acceptable ranges. Finite element (FE) analysis of the measured geometry revealed that the stress distribution met the theoretical expectations, achieving a nearly uniform hoop stress with minimal variation. These results validate the potential of variable thickness designs to improve structural performance, a principle directly applicable to HDPE vessels in my research.

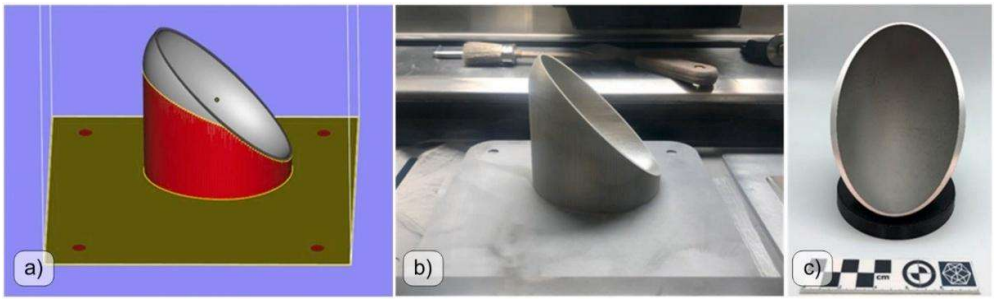


**Figure 34: (a) Model created using Magics RP. (b) After manufacturing view. (c) Semi vessel final visual** [71]

The study also highlights the limitations of traditional manufacturing processes for variable thickness structures, which are better suited to advanced techniques like AM. For HDPE, however, the material's inherent versatility and ease of processing could overcome some of these limitations, making it a promising candidate for implementing similar optimized designs. This study also aligns with my work on HDPE pressure vessel heads, emphasizing the potential of variable thickness designs to enhance structural performance.

## 2.5. Novelty and Research Gap

This research addresses critical gaps in the design and analysis of HDPE pressure tanks, particularly concerning imperfection sensitivity and variable wall thickness. Previous research often did not fully account for the influence of edge forces and bending moments in stress analysis. Many studies primarily focused on internal pressure, overlooking significant bending forces such as transverse shear and bending moments. To address these gaps, this study introduces moment theory as a comprehensive approach to stress analysis. Moment theory incorporates both membrane and bending forces, providing a more accurate assessment of stress, particularly near the boundaries of elliptical heads and cylinders, where internal bending forces are significant. By applying moment theory, this research aims to advance the understanding of stress distribution and failure mechanisms in HDPE pressure vessels, a material that has been relatively unexplored in this context.

One of the key novel contributions of this work is the detailed exploration of imperfection sensitivity in buckling analysis. While previous studies have investigated geometric imperfections in pressure vessels, limited attention has been given to their specific impact on HDPE pressure vessels. Much of the earlier work focused on idealized geometries or other materials, leaving room to explore the unique behaviour of HDPE under realistic imperfection scenarios. By systematically varying the amplitude of imperfections such as dimples, circular cut outs, flat patches, and eigenmode-affine shapes, this study examines their effect on buckling strength. The results reveal the significant influence of geometric flaws and material properties on structural stability. These findings help establish critical imperfection thresholds, guide manufacturing tolerances, and enhance the reliability of HDPE vessels under practical operating conditions.

Another significant innovation lies in the application of variable wall thickness designs. While most existing research has explored uniform wall thickness configurations, this study advances the field by focusing on variable wall thickness

in the two geometries that demonstrate superior performance in both stress and buckling analyses. By strategically increasing wall thickness in regions of high stress or vulnerability to buckling while reducing it in less critical areas, this approach achieves an optimal balance between material efficiency and structural strength. The investigation examines the effects of these adjustments on improving load distribution, reducing stress concentrations, and enhancing buckling resistance, particularly in complex head geometries such as tori-spherical and elliptical designs

This dual focus on imperfection sensitivity and wall thickness optimization represents a significant step forward in the design of HDPE pressure vessels. By addressing real-world challenges such as geometric imperfections and optimizing structural performance, the research not only fills existing gaps but also provides a robust foundation for the development of safer, more resilient, and lightweight pressure tanks for industrial applications.

# Chapter 3

# Integration of membrane and bending theory with HDPE pressure vessel

## 3.1 Methodology

In collaboration with a company specializing in washing service units, a lightweight plastic pressure tank was designed to serve as a storage and operational component within their system. The tank, assumed to be fabricated from high-density polyethylene (HDPE) using rotational molding, was designed to accommodate a specified internal volume of 500 liters, ensuring compatibility with the operational requirements of the service unit. Rotational molding was chosen as the assumed manufacturing process due to its suitability for producing large, seamless plastic vessels with complex geometries, such as the elliptical, torispherical, and hemispherical heads considered in this study. This process, however, can introduce geometric imperfections such as surface irregularities, which were accounted for in the numerical simulations of buckling analysis in chapter 4. In its actual application, the tank will be connected to a vacuum pump, creating a controlled internal pressure environment critical for its functionality.

The pressure tank model, as illustrated in Figure 35, was developed as a simplified numerical representation for stress analysis. The joints between the cylindrical shell and elliptical heads were simulated as continuous and rigid connections, assuming ideal conditions without manufacturing imperfections. The

model was created as a single, continuous geometry in the finite element analysis software, with no explicit separation between the cylinder and head regions. This approach simplifies the modeling process while ensuring accurate stress analysis, particularly in critical regions such as the boundary of elliptical heads and cylindrical sections. To address the limitations of prior research which often failed to account for bending internal forces like transverse shear and bending moment, this study adopts moment theory as a comprehensive framework. As described before, moment theory enables accurate stress analysis, particularly near critical regions such as the boundary of elliptical heads and cylindrical sections, where internal bending forces are most significant.

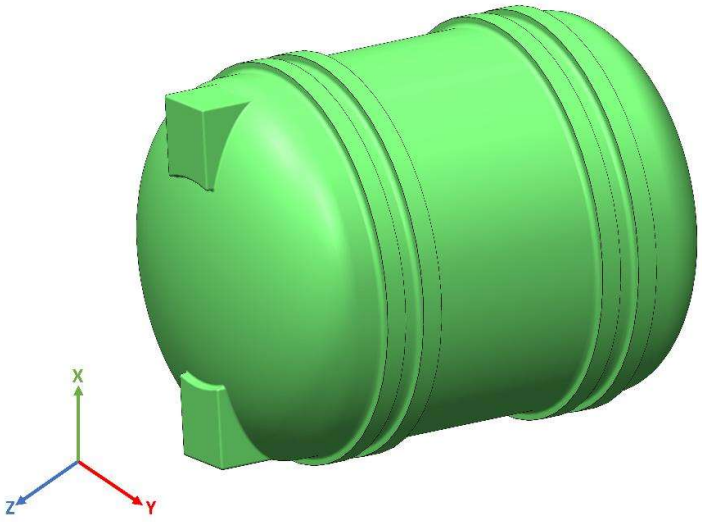


**Figure 35: Model of a Lightweight Tank**

Let's define the meridian of the dished head within the Cartesian coordinate system ($x$, y), where $x$ represents the abscissa corresponding to the axis of revolution for the shell, and y denotes the ordinate referring to the radius of the curve. Along these axes, two parameters can be defined describing the head: the depth $b$ and the radius $a$, which equals the radius of the cylindrical tank closed with the mentioned head. The flattening factor 'k' is defined as the ratio of major axis length 'a' to the minor axis length 'b'. The thickness of the head is described by the

parameter t. These parameters are illustrated in Figure 36. As the dished head serves as a shell of revolution, the main radii of curvature longitudinal $R_1$ and circumferential $R_2$ can be defined as follows:

$$R_1 = (a^4X^2 + b^4Y^2)^{\frac{3}{2}}/(a^4b^4)$$
$$R_2 = (a^4X^2 + b^4Y^2)^{\frac{1}{2}}/b^2 \quad (1)$$

The methodology involves developing an analytical model to derive a theoretical stress calculation formula based on the deformation continuity equation, specifically tailored for HDPE material properties. In particular, the influence of different parameters such as thickness and flattening factor of the ellipsoid head on the mechanical behavior and stress state is considered. This consideration will be examined by comparing the analytical results with those obtained from finite element models. Subsequent comparison and analysis of theoretical and FEA stress values in the discontinuous region between elliptical heads and cylinders will validate the proposed approach for HDPE pressure tank.

The HDPE material used in this study is assumed to be obtained through standard industrial polymerization processes, such as slurry or gas-phase polymerization, which are commonly used to produce HDPE for pressure vessel applications. The material properties, including Young's modulus, Poisson's ratio, and nonlinear stress-strain behavior, were sourced from literature and material databases to ensure accuracy in the numerical simulations. While the study does not explicitly investigate the polymerization process, the material properties used are representative of commercially available HDPE grades. The material and model properties used in analytical and FEA model are illustrated in Table 1.

**Table 1: Material and model properties** [72]

| Property | Value |
|---|---|
| Material | High Density Polyethylene (HDPE) |
| Modulus of Elasticity | 995 MPa |
| Poisson's ratio | 0.45 |
| Density | 954 kg/m$^3$ |
| Yield strength | 26.2 MPa |
| Inner diameter d/mm | 750 mm |
| Thickness t/mm | 10 mm |

### 3.1.1. Analytical Model

The boundary load diagram is illustrated in Figure 36, highlighting the various load components acting on the cylindrical and elliptical heads, as well as the geometric features of the pressure vessel considered in the analysis. The internal pressure generates membrane stress via the internal membrane force, while the edge force $T_0$ and edge moment $M_0$ produce bending stress through the internal bending force [73,74]. The combined stress results from the superposition of membrane and bending stresses.

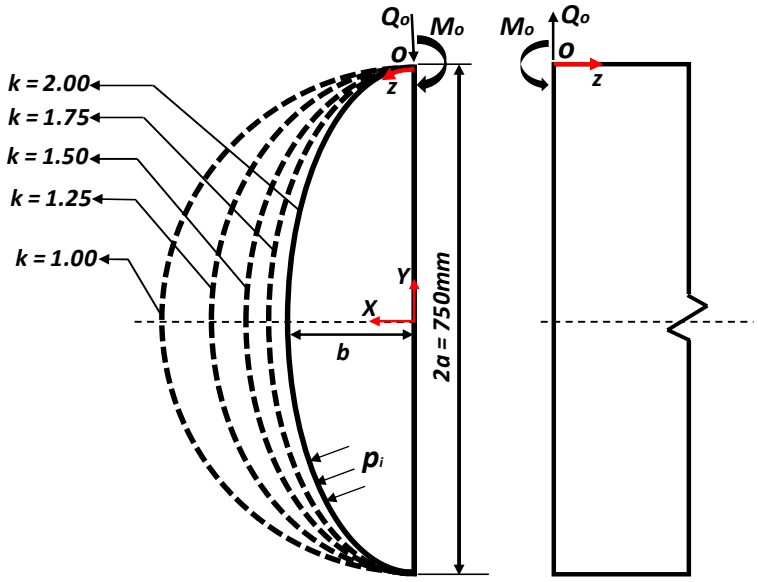


**Figure 36: Geometric features of the pressure vessel (a) elliptical shell (left) (b) cylindrical shell (right) used for the case study**

According to the literature [75], the total stress in the discontinuous region can be divided into the membrane stress and bending stress, and the theoretical stress equation of the elliptical head can be expressed as:

$$\sigma_x = \sigma_x^{\mathrm{P}} + N_x^{(\mathrm{T_0+M_0})}/c \pm 6M_x^{(\mathrm{T_0+M_0})}/c^2$$
$$\sigma_\theta = \sigma_\theta^{\mathrm{P}} + N_\theta^{(\mathrm{T_0+M_0})}/c \pm 6M_\theta^{(\mathrm{T_0+M_0})}/c^2 \quad (2)$$

Where,

- $\sigma_x$ is the total longitudinal stress
- $\sigma_\theta$ is the total transverse stress
- $\sigma_x^{\mathrm{P}}$ and $\sigma_\theta^{\mathrm{P}}$ are the longitudinal stress and the transverse stress under internal pressure P, respectively

- $N_x^{(T_0+M_0)}$, $N_\theta^{(T_0+M_0)}$ are the internal forces along the longitudinal and tangential under the action of the edge force $T_0$ and edge moment $M_0$ respectively
- $M_x^{(T_0+M_0)}$, $M_\theta^{(T_0+M_0)}$ are the internal torques along the longitudinal and tangential under the action of the edge force $T_0$ and edge moment $M_0$ respectively.

Figure 37 provides a detailed diagram showing the stress resultant components and their distribution in critical regions, such as the junctions between the cylindrical shell and elliptical heads, supporting the equations presented in this chapter.

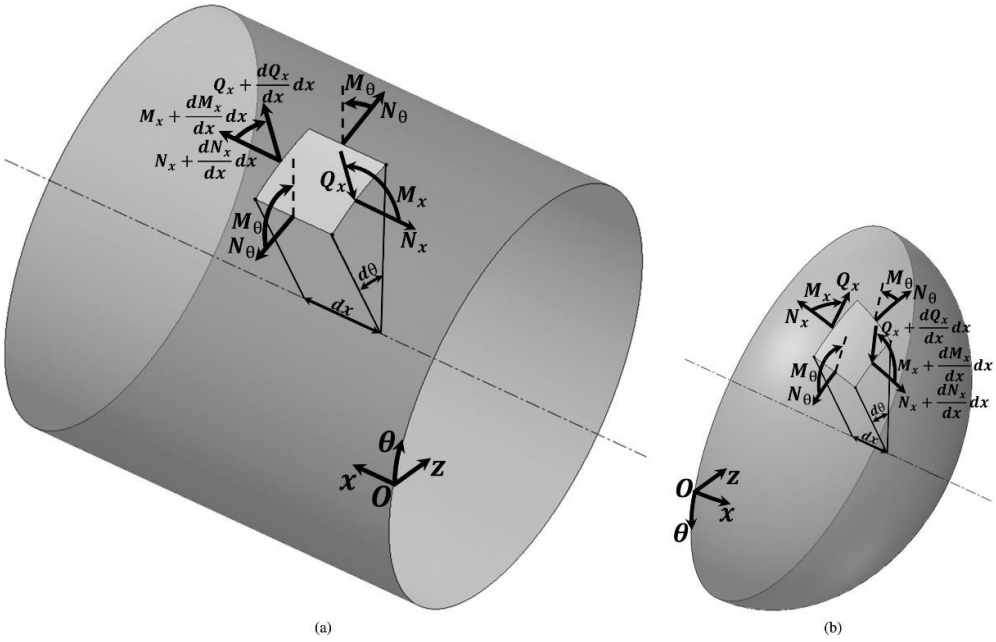


**Figure 37: (a) Cylindrical shell and (b) an elliptical head, showing the stress resultants on a fundamental element of structure [38].**

The internal force and internal torque equations of the elliptical head can be expressed as:

$$
\begin{aligned}
N_x^{(\mathrm{T_0+M_0})} &= N_x^{\mathrm{T_0}} = \tan\, xe^{-\beta_1 z}T_0(\cos\,\beta_1 x - \sin\,\beta_1 x)R/R_2 \\
N_\theta^{(\mathrm{T_0+M_0})} &= N_\theta^{\mathrm{T_0}} = 0.25P\mathrm{Re}^{-\beta_1 x}\cos\,\beta_1 x(\mathrm{a/b})^2\sqrt{R/R_2} \\
M_x^{(\mathrm{T_0+M_0})} &= M_x^{\mathrm{T_0}} = \frac{e^{-\beta_1 x}T_0 R}{\sqrt[4]{3(1-\mu^2)}}\sqrt{\frac{c}{R_2}}\sin\,\beta_1 x \\
M_\theta^{(\mathrm{T_0+M_0})} &= M_\theta^{\mathrm{T_0}} = \mu M_x^{\mathrm{T_0}} \\
\beta_1 &= \sqrt[4]{3(1-\mu^2)}R_1/\sqrt{R_2 c}
\end{aligned}
\tag{3}
$$

By replacing the equation presented in (3) into (2), the overall theoretical stress in the edge region of elliptical head is derived as indicated below:

$$
\begin{aligned}
\sigma_x &= \frac{PR_2}{2c} + \frac{P\tan\, xe^{-\beta_1 x}\sqrt{Rt}(\cos\,\beta_1 x - \sin\,\beta_1 x)(\frac{a}{b})^2 R}{8c\sqrt[4]{3(1-\mu^2)}R_2} \pm \frac{3P\mathrm{Re}^{-\beta_1 x}\,\sin\,\beta_1 x}{4c\sqrt{3(1-\mu^2)}}(\frac{a}{b})^2\sqrt{\frac{R}{R_2}} \\
\sigma_\theta &= \frac{PR_2}{2c}(2-\frac{R_2}{R_1}) + \frac{P\mathrm{Re}^{-\beta_1 x}\,\cos\,\beta_1 x}{4c}(\frac{a}{b})^2\sqrt{\frac{R}{R_2}} \pm \frac{6PRc\mu e^{-\beta_1 x}\sin\,\beta_1 x}{8c^2\sqrt{3(1-\mu^2)}}(\frac{a}{b})^2\sqrt{\frac{R}{R_2}}
\end{aligned}
\tag{4}
$$

The theoretical stress equation of the cylinder is expressed as:

$$
\begin{aligned}
\sigma_x &= \sigma_x^{\mathrm{P}} + N_x^{(\mathrm{T_0+M_0})}/c \pm 6M_x^{(\mathrm{T_0+M_0})}/c^2 \\
\sigma_\theta &= \sigma_\theta^{\mathrm{P}} + N_\theta^{(\mathrm{T_0+M_0})}/c \pm 6M_\theta^{(\mathrm{T_0+M_0})}/c^2
\end{aligned}
\tag{5}
$$

The internal force and internal torque equations of the cylinder can be expressed as:

$$
\begin{aligned}
N_x^{(\mathrm{T_0+M_0})} &= N_x^{\mathrm{T_0}} = 0 \\
N_\theta^{(\mathrm{T_0+M_0})} &= N_\theta^{\mathrm{T_0}} = -2\beta \mathrm{Re}^{-\beta x} T_0 \cos\, \beta x \\
M_{\mathrm{x}}^{(\mathrm{T_0+M_0})} &= -e^{-\beta x} T_0 \sin\, \beta x/\beta \\
M_\theta^{(\mathrm{T_0+M_0})} &= \mu M_x^{(\mathrm{T_0+M_0})} \\
\beta &= \sqrt[4]{3(1-\mu^2)}/\sqrt{Rc}
\end{aligned}
\tag{6}
$$

Substituting Eq. (6) into Eq. (5) yields the total theoretical stress in the edge region of the cylinder.

### 3.1.2. Finite element model

The stress distribution obtained through the analytical approach will be compared with the solution provided by the finite element model. A linear static structural analysis is conducted using ABAQUS, employing the solid element C3D8R, which features eight nodes with three degrees of freedom each (displacements in the X, Y, and Z directions) and a reduced integration scheme. To complete the pressure vessel model and optimize computational efficiency, symmetrical boundary conditions are applied on the X, Y, and Z edges. A dished head was modelled as part of a cylindrical tank with a diameter of 750 mm and a shell thickness of 10 mm, as illustrated in Figure 38.

The internal pressure of 0.2 MPa was chosen to replicate the maximum vacuum pressure generated by the MEC1600P vacuum pump, which will be attached to the pressure tank to create a controlled internal vacuum environment. This value represents the operating pressure of the system and ensures that the numerical simulations accurately reflect real-world conditions. The cylindrical portion and the dished head are analyzed under static conditions to determine the stress distribution. The mesh is designed to enhance accuracy near critical areas, ensuring a refined element distribution where needed. The mechanical properties of the material

correspond to high-density polyethylene (HDPE), with a Young's modulus (E) of 998 MPa and a Poisson's ratio (ν) of 0.4.

As a result of the static structural analysis, the transverse and longitudinal stresses along the meridian of the dished head and the cylindrical tank are evaluated. These results provide insight into the stress behaviour of the pressure vessel under the applied loading conditions. Additionally, load tests or burst tests can validate the stress analysis results, with strain gauges placed at critical locations such as the junctions of cylindrical shells and heads.

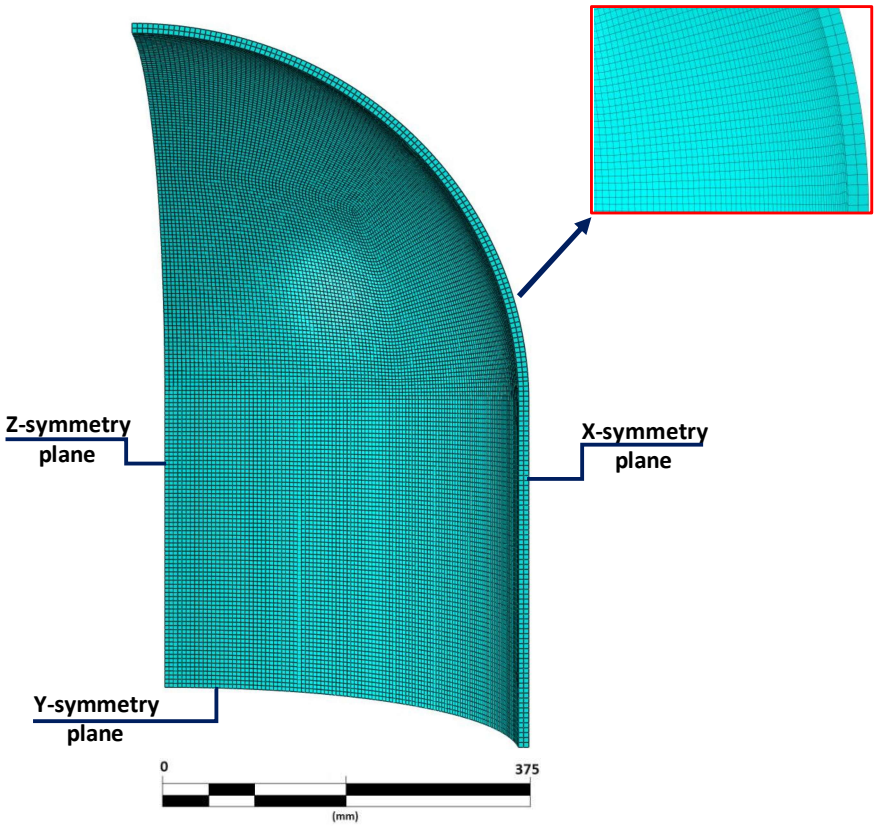


**Figure 38: FE symmetrical pressure vessel model**

## 3.2 Results and discussion

The stress distribution at the junction of the cylinder and dished head for various values of the flattening factor (k) is depicted in Figures 39 to 43. The flattening factor (k) ranges from 1 to 2, where the value 1 represents a perfectly hemispherical head and the value 2 indicates that the major axis is double the size of the minor axis of the ellipse. The transverse and longitudinal stresses in MPa are represented on the vertical axis, while the length z of the meridian is depicted on the horizontal axis.

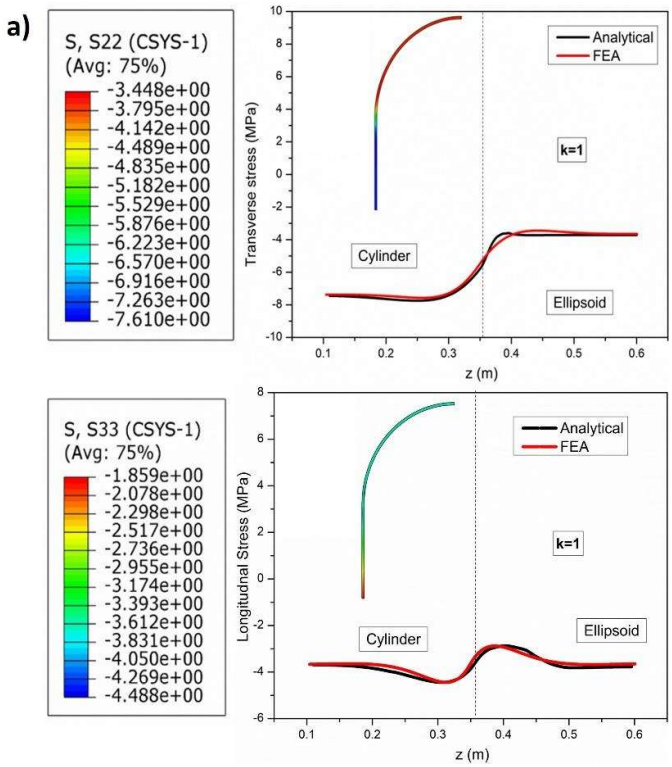


**Figure 39: Transverse and longitudinal stresses for k=1**

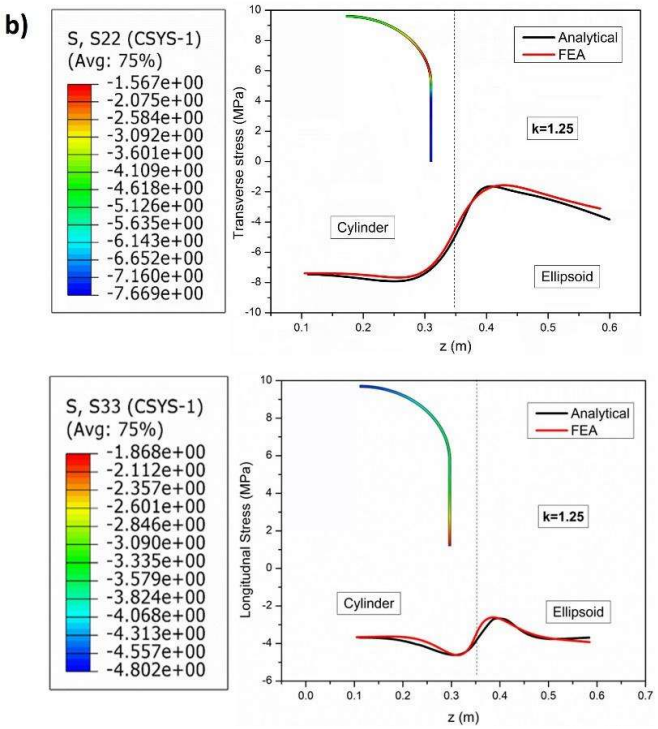


**Figure 40: Transverse and longitudinal stresses for k=1.25**

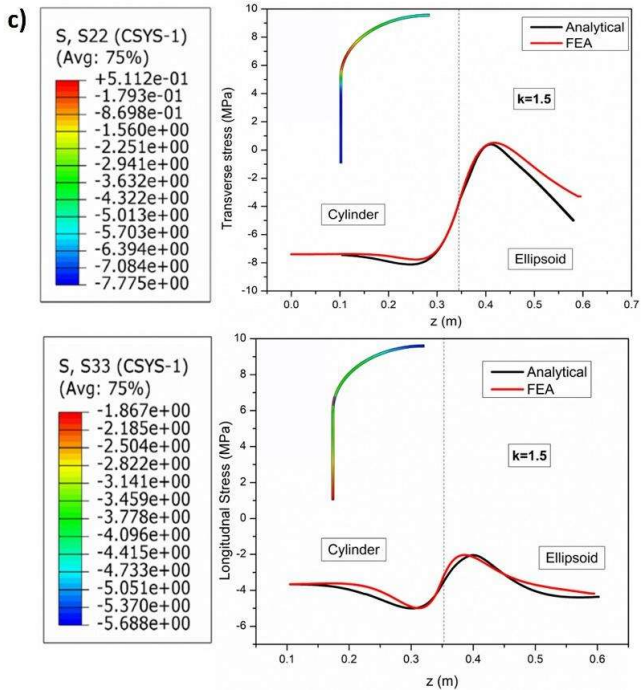


**Figure 41: Transverse and longitudinal stresses for k=1.5**

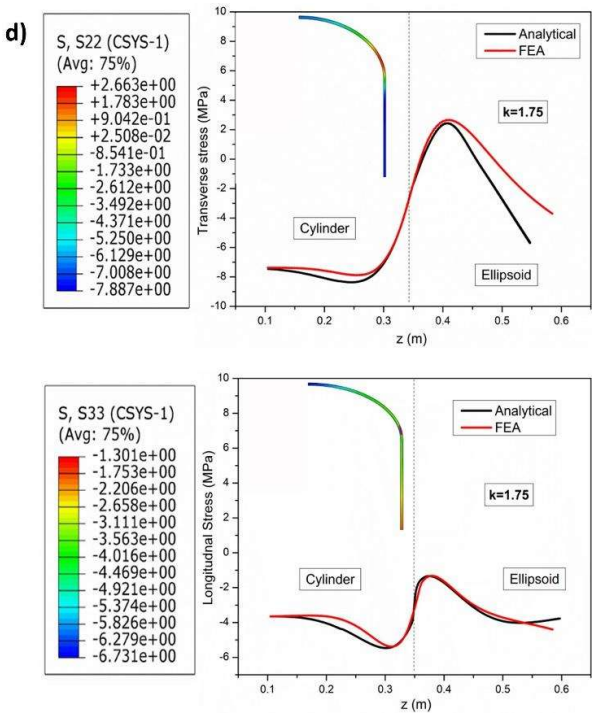


**Figure 42: Transverse and longitudinal stresses for k=1.75**

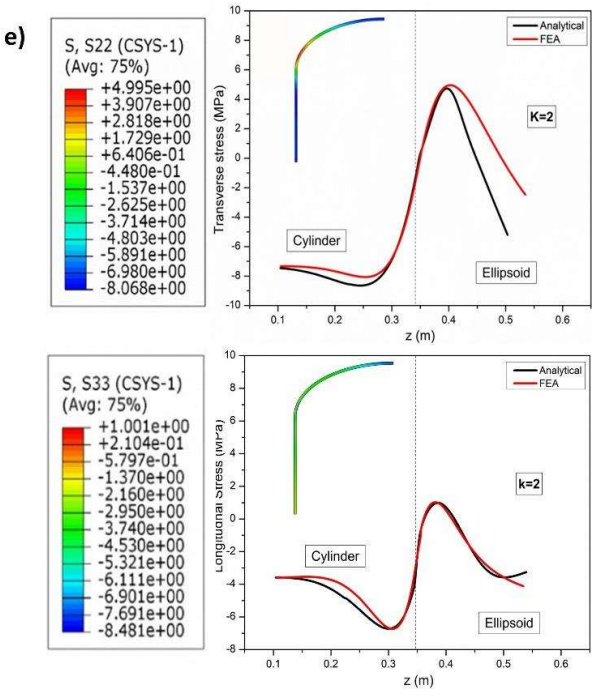


**Figure 43: Transverse and longitudinal stresses for k=2**

Both the FEA and the analytical approach are utilized, with results shown by solid red and black lines, respectively. The shape of the dished head is provided for reference in each plot. Observing the plots, it is evident that the solutions from both methods closely overlap near the junction of the cylinder and elliptical head. However, as one moves away from the junction, disparities between the FEA and analytical results become apparent, primarily due to the assumptions made in the analytical model, which hold validity near the junction of the cylinder and dished head. It is evident from the figures that there is a strong correspondence between the FEA and analytical results.

Figure 44 shows the comparison of transverse and longitudinal stress values for different k values. For k parameters ranging from 1 (hemispherical) to 1.5, the transverse stress remains consistently compressive, not transitioning to tensile stress. However, for k parameters of 1.75 and 2, which correspond to more ellipsoidal and flatter shapes, there is a notable peak in the transverse stress near the junction of the cylinder and the ellipsoid. At this junction, the stress transitions into the tensile range. As the distance from this junction increases, the transverse stress returns to a compressive state.

The reason for this behaviour is primarily due to the geometric changes and resulting stress concentrations in the vessel. For k ranging from 1 to 1.5, the smoother and more gradual curvature of the vessel does not create significant stress concentrations, so the transverse stress remains compressive. In contrast, at higher k parameters of 1.75 and 2, the vessel shape becomes more ellipsoidal and flatter, introducing sharper transitions in curvature at the junction of the cylinder and ellipsoid. This change in geometry causes localized stress concentrations, resulting in a peak in transverse stress that transitions into the tensile range. As the distance from this junction increases, the influence of geometric discontinuity diminishes, causing the stress to revert to a compressive state. The longitudinal stress plot illustrates that only the configuration with k=2 transitions into the tensile range. Shapes with smaller k values, indicating greater elongation, exhibit smoother

connections to the cylinder and result in less noticeable stress changes. Thus, the interplay between vessel shape and stress distribution is crucial, with more pronounced geometric transitions leading to temporary shifts from compressive to tensile stress. This phenomenon underscores the importance of vessel shape in determining the mechanical stresses experienced under load.

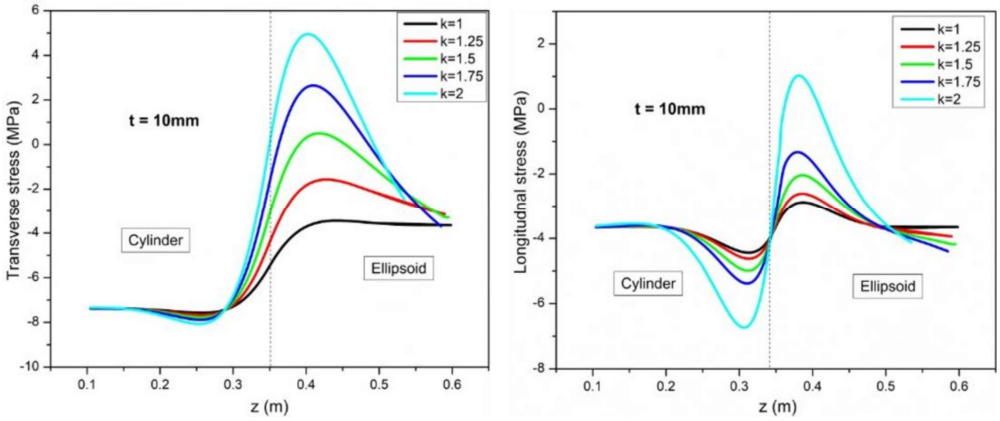


**Figure 44: Comparison of transverse and longitudinal stress for different flattening factor k with constant thickness of 10mm**

Figure 45 compares transverse and longitudinal stress values for different wall thicknesses (5 mm, 10 mm, and 15 mm) while keeping the 'k' value constant at 1.5. k=1.5 was chosen for its practical benefits, providing a reasonable stress level while also being more convenient in terms of fabrication and design, making it a suitable choice for optimized performance without compromising material integrity. The observed trends in transverse and longitudinal stress variation with different wall thicknesses can be intricately linked to the influence of wall thickness on both stress distribution and stress concentration phenomena within the pressure vessel. As wall thickness decreases, the vessel is subjected to higher stress concentrations, leading to more pronounced compressive transverse stresses. This is due to the thinner

walls' inability to evenly distribute the internal pressures, resulting in localized areas of high stress. Conversely, thicker walls facilitate a more uniform distribution of stresses, significantly mitigating the stress magnitudes experienced by the vessel. This uniform stress distribution in thicker walls is critical for enhancing the vessel's structural integrity and reducing the risk of material failure.

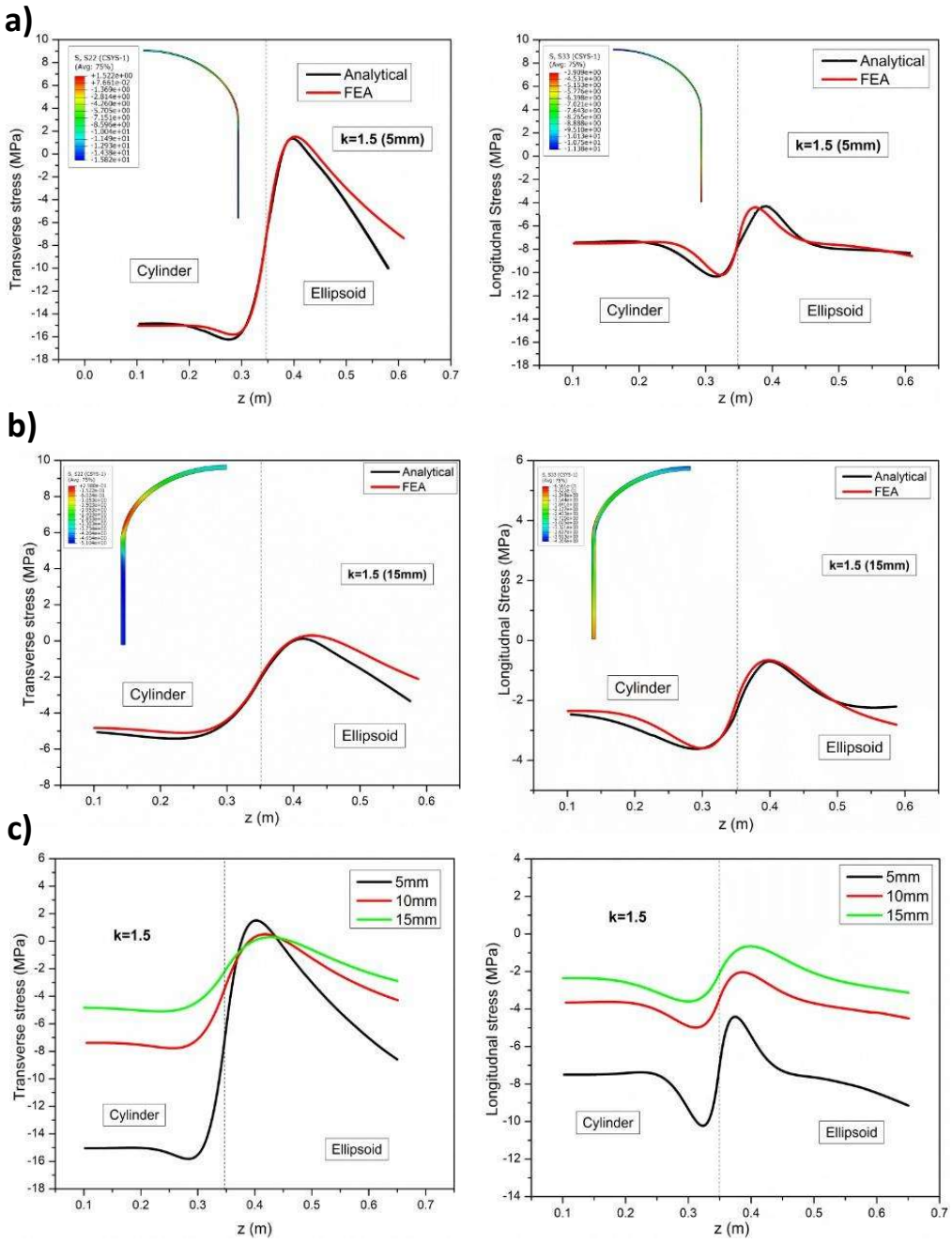


**Figure 45: Stress distribution with constant k=1.5 for a) c=5mm b) c=15mm c) Comparison of stress distribution for different thicknesses with constant k=1.5**

In the design of pressure vessels, employing variable wall thickness, as illustrated in Figure 46, offers significant advantages by strategically altering the wall thickness at critical junctions. For example, transitioning from a 5 mm to 8 mm thickness at specific points before reducing the thickness again, or shifting from 7 mm to 10 mm thickness, optimizes material distribution to address areas prone to stress concentrations. This method enhances the structural integrity of the vessel by ensuring that thicker sections are present where higher stress is anticipated, thereby mitigating the risk of failure. The gradual change in thickness helps in distributing the stresses more evenly across the vessel, reducing the likelihood of weak points and potential stress-related damage. Additionally, this approach leads to a reduction in overall material usage since material is only added where necessary, contributing to weight reduction and cost savings without compromising safety or performance. By efficiently managing the wall thickness, the pressure vessel not only becomes lighter but also demonstrates improved durability and reliability in operation, highlighting the dual benefits of enhanced mechanical performance and economic efficiency.

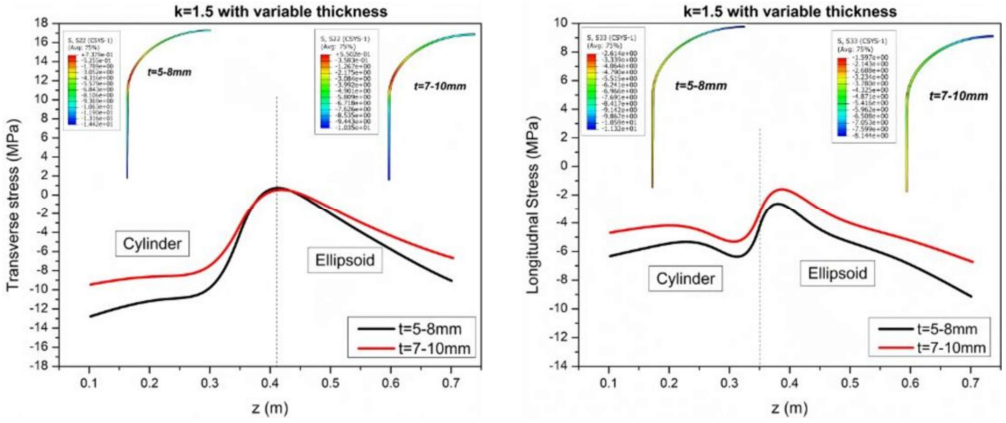


**Figure 46: Transverse and longitudinal stress for variable thickness from 5-8 mm and 7-10 mm**

In conclusion, this chapter highlights the crucial role of tank geometry and wall thickness in determining the structural integrity of pressure vessels. The transition from cylindrical to ellipsoidal shapes introduces significant stress concentrations, especially at junctions, which can be mitigated by careful consideration of wall thickness. The findings show the importance of optimizing wall thickness in pressure vessel design to balance material efficiency with structural strength, thereby improving both safety and longevity. Furthermore, the study emphasizes the need to account for localized bending effects, particularly at the transition zones, where traditional membrane theory fails to accurately predict stress behavior. Failing to consider these localized bending effects could result in pressure tanks that are unable to withstand the necessary pressure loads. By incorporating the influence of internal forces, such as transverse shear and bending moments, the study extends beyond conventional membrane theory, offering a more comprehensive understanding of pressure tank behavior and ensuring the development of safer, more efficient designs.

# Chapter 4

# Numerical Analysis of Buckling Behavior in Tori-spherical and Elliptical Pressure Vessel Heads

## 4.1 Numerical Modelling Description

Building on the knowledge established in Chapter 2, this chapter discusses the detailed numerical analysis of tori-spherical and elliptical pressure vessel heads. A key focus is placed on the influence of aspect ratio variations, represented by the k factor (the ratio of the major axis to the minor axis), on the buckling behavior of these heads under internal pressure. Variations in the k factor, as shown in Figure 47, alter the geometric configuration of the heads, thereby affecting their mechanical performance and stability underload. These changes have significant implications for the structural integrity and safety of pressure vessels.

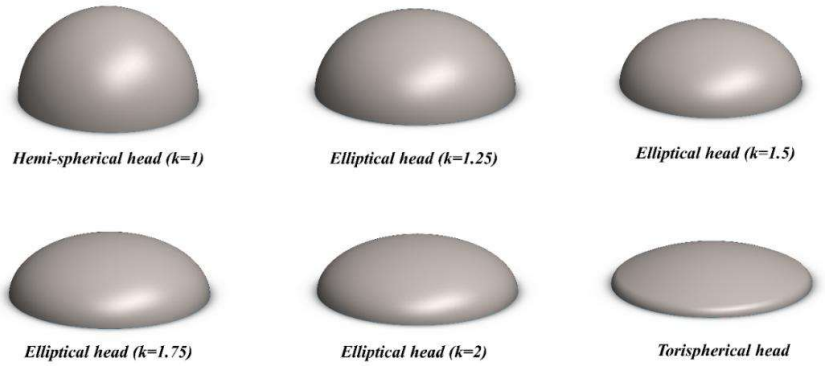


**Figure 47: Different pressure vessel head configurations**

The buckling behavior of pressure vessel heads is particularly critical, as failure due to buckling can lead to catastrophic consequences in high pressure applications. Therefore, accurate prediction of buckling capacity is essential for the reliable design and safety assessment of such structures. This chapter investigates the structural response of pressure tank heads made of HDPE (material properties in Table 1) using finite element analysis (FEA) conducted in Abaqus. The analysis incorporates variations in the k factor and the introduction of geometric imperfections to simulate realistic deviations from ideal geometries.

The numerical approach consists of both linear and nonlinear buckling analyses to evaluate stability under internal pressure. Linear buckling analysis provides ideal critical buckling pressure while nonlinear techniques, such as the Riks method, are used to study post-buckling behavior and assess critical failure pressures, incorporating geometric nonlinearities for enhanced accuracy. The Riks method has been effectively employed by Yang et al. [76] to analyze post-buckling phenomena. Boundary conditions are applied to replicate real-world constraints, while the introduction of localized indentations, flat patch, cutouts and eigenmode affine imperfections provides details of the structural sensitivity of the heads. These imperfections are intended to mimic potential manufacturing flaws or operational damage and are integral to understanding the buckling response of the pressure tank heads.

The shell structures are modeled using S4R elements, a four-node, reduced-integration type of shell element which are well-suited for capturing the thin-walled behavior of these pressure vessels. These elements are particularly advantageous for such analyses due to their ability to capture bending, membrane, and shear effects, while minimizing computational costs. A structured quad-dominated mesh is used to ensure uniformity and precision in the discretization of the model. This type of mesh, shown in Figure 48, helps maintain a balance between accuracy and computational efficiency. To ensure that the mesh size does not adversely affect the

results, a mesh sensitivity analysis is conducted. This analysis involves systematically refining the mesh to identify the optimal element size that provides accurate results while minimizing computational resources.

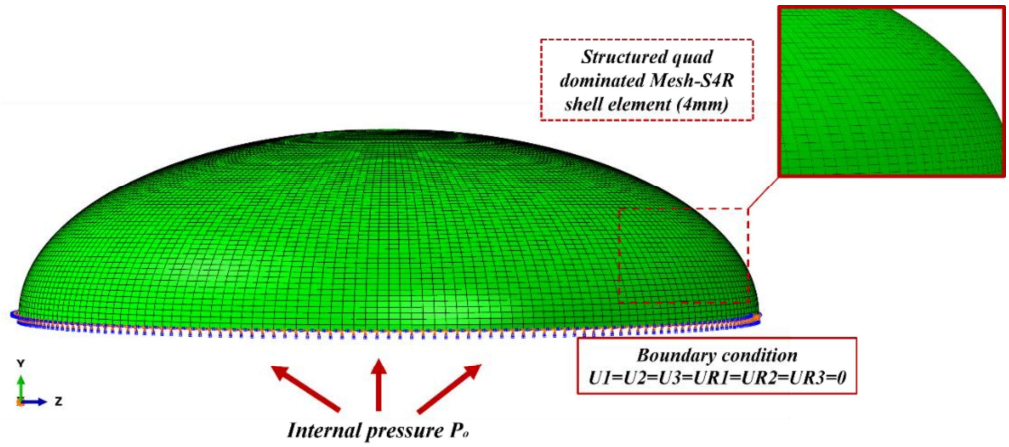


**Figure 48: Numerical model of vessel head with loading, boundary conditions and mesh type**

The boundary conditions are fully clamped (all degrees of freedom i.e. displacement and rotation are restricted) at the edges of the shell. These constraints mimic the real-world scenario where pressure vessel heads are typically welded or rigidly connected to cylindrical shells. In such configurations, the clamped edges effectively prevent movement, replicating the physical conditions of many industrial applications. This realistic boundary setup ensures that the model captures the behavior of the structure under practical operating conditions, providing deep understanding that can directly inform design decisions.

The analysis begins with a linear buckling analysis (LBA), which is used to determine the critical buckling pressure and to identify potential failure modes. LBA provides insights into the elastic instability of the shell structure by calculating eigenvalues associated with different buckling modes. These eigenvalues are crucial as they indicate the pressure levels at which the structure might lose stability

under ideal geometric conditions. The uniform pressure load value of 1 MPa in a linear buckling analysis (LBA) is typically chosen for convenience and does not inherently affect the calculation of the critical buckling load ($P_{cr}$). In LBA, the eigenvalue derived from the analysis represents a scaling factor that, when multiplied by the applied reference load, determines the actual buckling load. Thus, as long as the applied pressure load is nonzero and uniform, the eigenvalue multiplier will appropriately scale the load to predict buckling, meaning the magnitude of the reference pressure load (e.g. 1 MPa) is not fundamentally significant.

Following the LBA, a nonlinear buckling analysis is performed to gain a deeper understanding of the post-buckling behavior of the tori-spherical and elliptical heads. Unlike linear analysis, this method incorporates both material and geometric nonlinearities, which are essential for accurately capturing the complex behavior of pressure vessel heads under realistic loading conditions. The material properties of High-Density Polyethylene (HDPE), detailed in Table 2, are modeled using an elastic-plastic material law. This law accounts for key characteristics of HDPE, such as its yield stress, elastic modulus and Poisson's ratio, enabling the simulation of its mechanical response under increasing pressure. The analysis combines the Newton-Raphson method with the Riks method to thoroughly examine the buckling behavior of pressure vessel heads. The Newton-Raphson method is first used to calculate the load-deflection response, giving an understanding of the shell's stability and deformation as pressure increases. Building on this, the Riks method is applied to follow the full loading path, capturing both the nonlinear and post-buckling behavior up to the point of failure [77,78]. This integrated approach provides a comprehensive view of the shell's performance, from initial stability to complex responses under high internal pressure. The Riks method is especially effective for capturing large deformations and snap-through buckling [79,80], which are critical phenomena often observed in thin-walled structures such as pressure vessel heads.

The Riks method uses the arc length technique to effectively trace the equilibrium path through nonlinear regions, even in cases of severe instability. The parameters for the Riks model are described in Table 2, where the analysis is controlled using up to 300 increments to ensure adequate resolution. The initial arc length increment is set to 0.01, with a minimum increment size of $1\times10^{-50}$ and a maximum increment size of 0.01, ensuring numerical stability and preventing divergence during highly sensitive post-buckling scenarios.

**Table 2: Step settings for non-linear buckling analysis in Abaqus**

| **Riks model parameters for non-linear buckling analysis** | |
|---|---|
| Maximum load proportionality factor | 1 |
| Incrementation type | Automatic |
| Nlgeom setting | ON |
| Maximum Number of increments | 300 |
| Minimum Increment size | 1E-50 |
| Initial increment size | 0.01 |
| Maximum increment size | 0.01 |
| Estimated total arc length | 1 |

The analysis also evaluates the impact of geometric imperfections on the buckling strength of tori-spherical and elliptical heads under internal pressure. Since real-world structures rarely satisfy ideal geometries due to manufacturing flaws or operational damage, these imperfections must be considered. A Geometric Nonlinear Imperfection Analysis (GNIA) approach is adopted to assess the effects of such geometric imperfections on structural/buckling stability. As shown in figure 49, this analysis introduces four types of imperfections namely single dimple indentation, circular cutout, flat patch, and eigen affine imperfection, to the shell structure. These imperfections are separately applied to the geometrically perfect model, with their effects on the buckling pressure assessed through detailed GNIA simulations.

Numerical simulations, while powerful, have inherent limitations. These include assumptions in material properties, simplifications in boundary conditions, and challenges in accurately modeling geometric imperfections and material nonlinearities. Mesh sensitivity and convergence issues can also affect the accuracy of results. Therefore, experimental validation is crucial to ensure the reliability of numerical predictions. Experimental tests, such as buckling tests and load tests, provide real-world data that can be used to refine numerical models and verify their accuracy. Experimental buckling tests can be conducted using a pressure test rig to validate the numerical results obtained from linear buckling analysis. The critical buckling load and mode shapes predicted numerically can be compared with experimental observations. For nonlinear buckling analysis, full-scale pressure tests incorporating geometric imperfections (e.g., dimples or cutouts) can be employed to validate the results. Strain gauges and displacement sensors can be used to measure deformation and stress distribution.

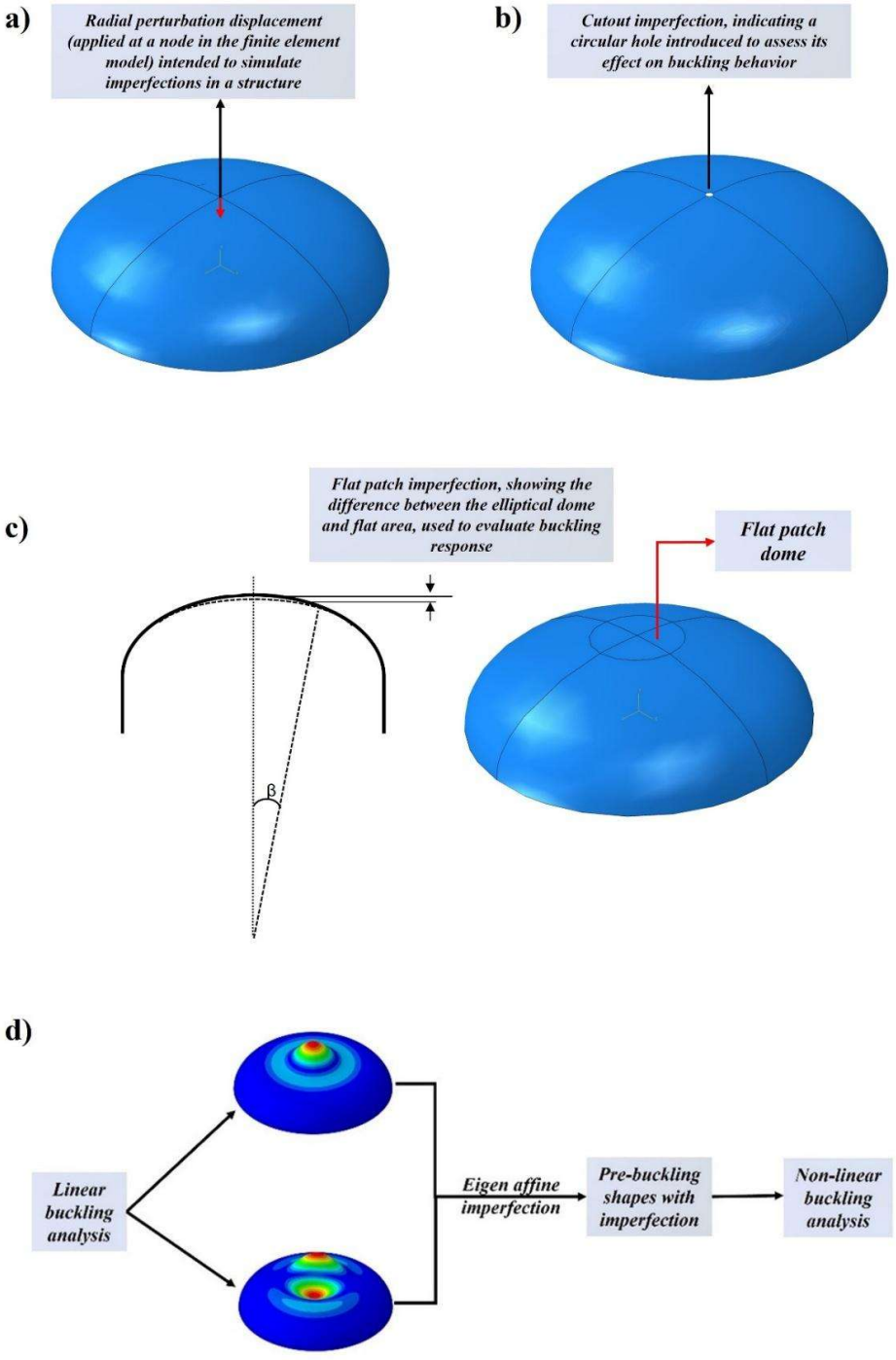


**Figure 49: Representation of a) Geometric dimple imperfection b) Circular cut-out imperfection c) Flat patch imperfection d) Eigenmode affine imperfection in an elliptical shell**

## 4.2 Geometric imperfections

Geometric imperfections critically influence the stability and mechanical performance of thin-walled structures [81–85]. These imperfections, though introduced intentionally in numerical models to simulate real-world conditions, are typically a result of manufacturing processes, mishandling, or operational requirements in actual applications [86–89]. This section explores four types of geometric imperfections: Single Dimple Indentation (SDI), Circular Cutout Imperfections (CCI), Eigenmode Affine Imperfections, and Flat Dome Imperfections, each with distinct characteristics and implications for buckling behavior.

Single dimple indentation (SDI) imperfections involve localized dimpling of the shell structure caused by applying a concentrated load, while circular cutout imperfections (CCI) entail the removal of a circular section from the shell, creating a structural weakness [90–93]. These imperfections are strategically applied at critical locations identified through eigenmode analysis [94]. Specifically, for elliptical and tori-spherical heads, both imperfections are positioned at the apex, while for hemispherical heads, they are applied between the apex and equator. This targeting of critical locations highlights the significant influence of stress concentrations on buckling modes. This SDI method allows for direct control of the dimple shape through indentation displacement, providing a more realistic representation of imperfection sensitivity compared to eigenmode-based perturbations [95]. Small dents or localized deformations, such as those caused by accidental impact, mishandling, or external forces during transportation or installation, can introduce dimple imperfections in pressure vessels or storage tanks [96,97]. For instance, a tool drop or collision with equipment can create a small dent, weakening the structure. Internal pressure equal to that obtained from the first eigenmode for each configuration is applied to carry out the nonlinear analysis. As the imperfection amplitude is increased, the corresponding buckling pressures were evaluated for each shell geometry.

In circular cutout imperfection approach, the radius of the cutout is gradually increased, and finite element analyses (FEA) are conducted for each variation. Circular cutouts are often necessitated by operational requirements, including pipe connections, valves, manholes, and inspection ports. However, during fabrication or as a result of corrosion and wear over time, these cutouts can introduce stress risers that significantly affect structural integrity. In buckling analysis, cutout imperfections effectively replicate the presence of such holes or weakened regions, which disrupt load distribution and increase the susceptibility of structures to buckling. This approach captures the vessel's response to imperfections as the cutout radius increases, providing detailed insights into the effect of the presence and size of these imperfections on the buckling behavior of the shells.

Eigenmode affine imperfections incorporates the geometric deviations derived from the buckling modes obtained through linear eigenvalue analysis. This type of imperfection represents generalized deformations that follow the structure’s natural buckling mode shapes. It could arise due to uneven material properties, uneven loading, or residual stresses from manufacturing processes such as welding or thermal expansion. Eigenmode affine imperfection amplifies the natural tendencies of a structure to buckle in a specific mode. These imperfections aim to simulate realistic deviations in the shell geometry, which are critical in evaluating the buckling behavior of thin-walled structures, such as pressure vessels. This method scales predefined imperfection amplitudes according to the first and second buckling modes, reflecting potential manufacturing flaws and enhancing structural realism [98].

Flat dome imperfections, also known as increased radius of curvature imperfections (IRCI), are introduced in tori-spherical and elliptical HDPE heads. These localized imperfections simulate regions with an increased radius of curvature, which can significantly influence the buckling pressure. Flat spots can occur due to manufacturing errors, poor forming processes, or repairs. For instance, during welding or repair work, a pressure vessel surface may be flattened, creating

an irregular area in an otherwise curved surface. The imperfection width, denoted as β, is gradually increased in the analysis to observe its effect on the stability of the shells. As the imperfection width increases, the dome becomes increasingly flattened, causing a greater deviation from the original geometry. In line with previous studies, the imperfection width is varied to a certain extent to avoid unrealistic alterations in the shell's shape [99]. Multiple finite element analyses (FEA) are conducted on different head configurations to determine the buckling pressure, for each variation of imperfection width.

## 4.3 Results and Discussion

The results obtained from the linear buckling analysis (LBA) in Abaqus reveal important insights into the critical buckling pressures and corresponding eigenvalue mode shapes for various pressure vessel head configurations, as shown in Figure 50. The hemispherical head (k=1) exhibits the highest resistance to buckling. The first eigenvalue mode for this shape shows a highly symmetric buckling pattern, and the critical buckling pressure ($P_{cr}$) is 0.84878 MPa. In the second eigenvalue mode, the buckling deformation is more localized in several regions, yet the critical pressure remains very similar at 0.84882 MPa. This high buckling pressure can be attributed to the spherical shape's uniform curvature, which evenly distributes the load and significantly improves its stability under pressure.

As the ellipticity increases, moving from hemispherical (k=1) to elliptical heads with varying aspect ratios, the critical buckling pressures gradually decrease. For an elliptical head with k=1.25, the first eigenvalue mode results in a $P_{cr}$ of 0.58539 MPa, while the second mode shows a slightly higher $P_{cr}$ of 0.59202 MPa. Similarly, for k=1.5, the critical pressure for the first mode drops to 0.42126 MPa, with the second mode yielding a $P_{cr}$ of 0.43028 MPa. The gradual reduction in critical pressures as the shape becomes flatter suggests that the stability of elliptical heads is compromised with increasing ellipticity, making them more prone to buckling at lower pressures compared to hemispherical heads.

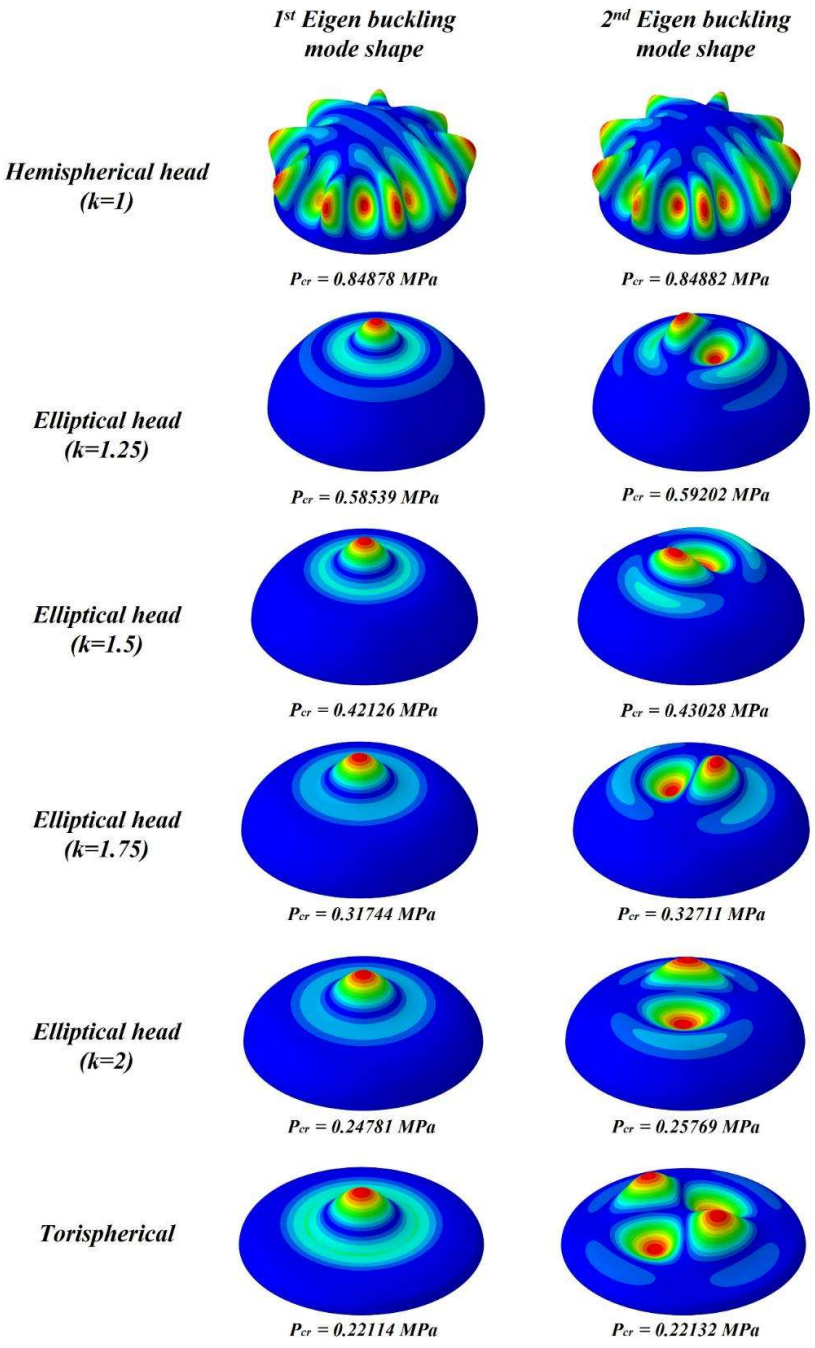


**Figure 50: Eigen mode shapes and corresponding critical buckling pressure obtained from FE Linear Buckling analysis for various head configurations**

For even flatter elliptical configurations, the trend continues. An elliptical head with k=1.75 has a $P_{cr}$ of 0.31744 MPa for the first mode, while the second mode

results in a critical pressure of 0.32711 MPa. For k=2, the first eigenmode yields a buckling pressure of 0.24781 MPa, and the second mode shows a slightly higher $P_{cr}$ of 0.25769 MPa. These findings emphasize the sharp decline in buckling pressures for flatter elliptical heads, which correlates with their increased susceptibility to failure under applied internal pressure.

At the lowest tier, the tori-spherical head, which combines both spherical and toroidal sections, exhibits the lowest critical buckling pressures among all configurations analyzed. The first eigenvalue mode for this head produces a $P_{cr}$ of 0.22114 MPa, and the second mode, while showing a more complex buckling shape with multiple localized deformations, results in a critical pressure of 0.22132 MPa. The minimal difference between these two modes indicates that tori-spherical heads are highly sensitive to small imperfections, making them more likely to experience buckling even under relatively low pressures.

Then the effects of geometric imperfections were analyzed, across different ellipticities of elliptical heads and a tori-spherical head by performing geometric nonlinear imperfection analysis (GNIA). Figure 51a shows the variation in the intensity of the geometric dimple imperfection, measured by the amplitude of the applied dimple, and its effect on buckling pressure for heads with varying shapes, offering insight into the sensitivity of each configuration to imperfections. The x-axis of the graph represents the dimple amplitude (in millimeters), which is a localized geometric perturbation applied at the apex of the heads, ranging from 0.01 mm to 10 mm. The y-axis represents the corresponding buckling pressure in MPa, and numerical values were interpolated using spline. A dimple amplitude of 0.01 mm represents a near-perfect surface, reflecting minimal manufacturing imperfections, while an amplitude of 10 mm indicates a severe dent, akin to noticeable damage or deformation from handling or external impact.

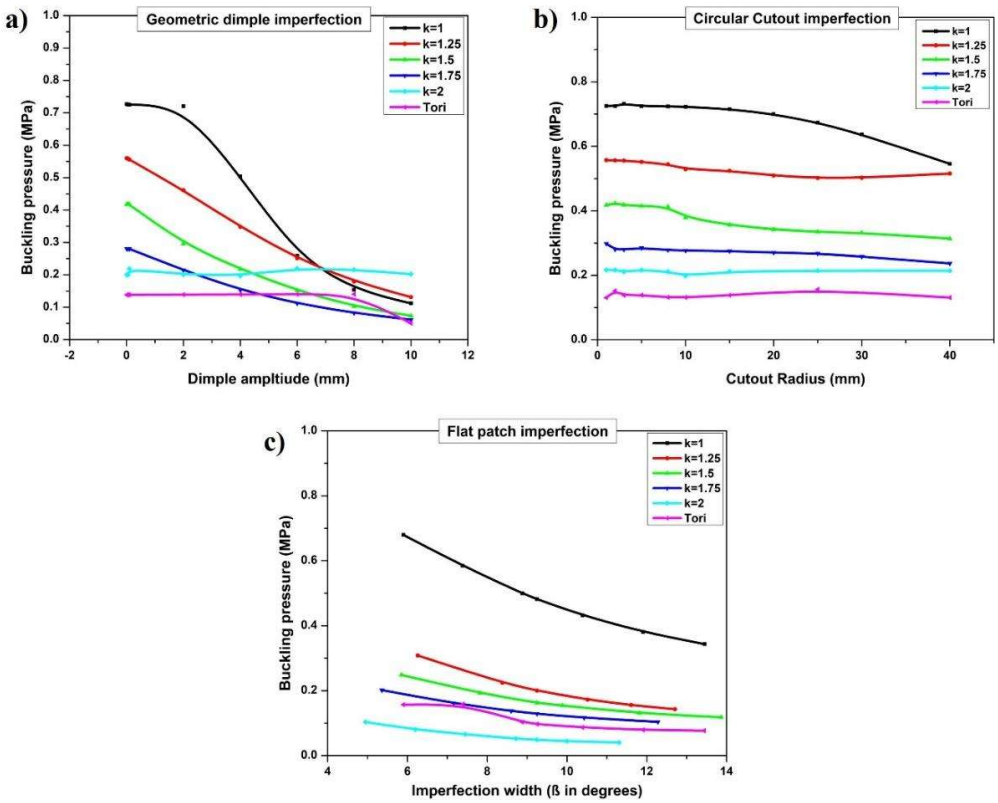


**Figure 51: Effect of increasing a) dimple amplitude (Geometric dimple imperfection) b) cutout radius (Circular cutout imperfection) c) imperfection width (Flat patch imperfection) on buckling pressure for various head configurations**

From the plot, it is evident that initially, under ideal conditions (for a dimple amplitude of 0 mm), the hemispherical head (k=1) has the highest buckling pressure, followed sequentially by the heads with increasing ellipticities: k=1.25, k=1.5, k=1.75, k=2 and finally the tori-spherical head, which has the lowest buckling pressure. This ordering reflects the general structural stiffness of these shapes, where more curved configurations, such as the hemispherical head, can withstand higher internal pressure before buckling due to their geometric rigidity.

However, as the dimple amplitude increases, the buckling pressure for all configurations decreases. Notably, the rate of decrease is much more pronounced for the hemispherical head (k=1), which shows the steepest decline in buckling pressure. This indicates that although it starts with the highest buckling pressure, it

is also the most sensitive to imperfections. The rapid decline suggests that small imperfections can significantly reduce the stability of highly curved shapes like hemispherical heads.

As the ellipticity (k) increases from 1.5 to 1.75, the sensitivity to dimple amplitude decreases. The buckling pressure still reduces with increasing imperfection amplitude, but the rate of decline is less severe compared to the hemispherical head. This trend can be explained by the fact that as the heads become more elliptical (flatter in the direction perpendicular to the major axis), the structural configuration becomes less reliant on perfect curvature for stability. Thus, it becomes marginally more resilient to localized geometric imperfections.

Interestingly, the k=2 and tori-spherical heads demonstrate minimal variation in buckling pressure with increasing dimple amplitude. For these flatter configurations, the effect of the imperfection is less pronounced, especially for dimple amplitudes below 8 mm. At higher amplitudes, the tori-spherical head does show a slight decline in buckling pressure, but it remains significantly less affected than the more curved heads. This suggests that the structural behavior of flatter heads is dominated more by global deformation modes, and they are therefore less sensitive to small-scale local imperfections like dimples.

The lower sensitivity of the flatter heads and tori-spherical configuration can be attributed to the redistribution of stresses in these shapes, which are naturally less dependent on the localized geometric precision that governs the stability of more spherical shapes. As the head becomes flatter, the curvature effect diminishes, reducing the vulnerability to local imperfections.

Figure 51b focuses on the effects of circular cutout imperfections on buckling behavior across heads with varying ellipticities, including a tori-spherical head. It demonstrates the effect of cutout radius which is increased from 0 mm to 40 mm on the buckling pressure of different head shapes. The selection of cutout sizes ranging from 0 mm to 40 mm in this study simulates these real-world conditions

and enables the evaluation of their influence on the structural integrity and buckling behavior of pressure vessel heads. A cutout size of 0 mm represents an idealized, unperturbed surface, serving as a baseline for maximum structural strength. As the cutout size increases, smaller openings (e.g., up to 20 mm) simulate standard connections for process nozzles, which are common in industrial vessels. These configurations introduce minor geometric imperfections but are typically within acceptable design thresholds. Larger cutouts, up to 40 mm, represent extreme cases such as manholes or access ports, which are necessary for maintenance but significantly reduce the structure's buckling resistance. The circular cutout, unlike localized imperfections, affects a larger surface area of the dome, potentially influencing its overall structural performance. Despite this, the results show that the effect of this imperfection on buckling pressure is generally minimal for most configurations.

In the case of the hemispherical head (k=1), a steady decline in buckling pressure is observed as the cutout radius increases. This decline is the most pronounced among all the configurations, highlighting the sensitivity of this geometric shape to imperfections that disturb its structural symmetry. Hemispherical domes, while highly rigid in their ideal form, rely heavily on geometric perfection for maintaining stability. The introduction of a circular cutout disrupts the stress distribution and reduces the dome's capacity to resist internal pressure, leading to a consistent drop in buckling pressure as the cutout size grows.

The impact of the cutout imperfection is less significant for heads with higher ellipticities (ranging from k=1.25 to 1.75). While the buckling pressure does decrease with an increase in cutout size, the reduction is much smaller compared to the hemispherical head. These more elliptical shapes are less reliant on perfect curvature for stability, allowing them to tolerate the introduction of imperfections without a substantial loss of strength. The broader, flatter surface of these heads distributes stress more uniformly around the cutout, enhancing the structure's resistance to localized weakening caused by the cutout. For the flatter

configurations, such as k=2 and the tori-spherical head, the circular cutout has an even smaller effect on buckling pressure. The nearly flat shape of these configurations means that the stress distribution is less affected by the presence of a cutout, even as its size increases. The buckling pressure remains relatively constant, indicating that these shapes are inherently more robust against imperfections. This stability can be attributed to their geometry, which, by reducing curvature, lessens the concentration of stresses around the cutout area and reduces the overall imperfections sensitivity.

Figure 51c illustrates the effect of flat patch imperfections, quantified by the width β (in degrees), on the buckling pressure for heads with different ellipticities. The x-axis represents the imperfection width, where increasing β corresponds to a progressively flatter upper dome. The y-axis shows the corresponding buckling pressure in MPa. This analysis highlights the impact of increasing the flatness of the dome's upper region on its structural integrity across a range of geometries. For the hemispherical head (k=1), the buckling pressure is initially the highest among all configurations when the imperfection width is smallest but steadily and significantly declines as β increases. The hemispherical dome exhibits greater sensitivity to flat patch imperfections compared to flatter configurations due to its reliance on uniform curvature for structural stability. The introduction of a flat patch significantly disturbs this curvature, leading to a marked reduction in structural stiffness and promoting localized stress concentrations

The other elliptical heads (k=1.25, k=1.5, k=1.75, k=2) follow a similar trend, with buckling pressure decreasing as the imperfection width increases. However, these configurations start at lower buckling pressure values compared to the hemispherical dome and exhibit a slower rate of decline. As the ellipticity increases, the structural reliance on perfect curvature decreases, making these domes slightly more resilient to the introduction of flat patches. In the case of k=1.25 and k=1.5, the buckling pressure steadily decreases but at a much less dramatic rate than the hemispherical dome. These shapes, while still affected by imperfection, are more

capable of redistributing stresses around the flat patch due to their less curved geometry.

The flatter configurations, particularly k=2, demonstrate a more gradual decline in buckling pressure. The flatter the dome, the less significant the effect of the flat patch imperfection becomes. This is because flatter domes already have a lower curvature, so the introduction of additional flatness through an imperfection does not significantly alter the stress distribution across the dome. As a result, the buckling pressure remains relatively stable even as the imperfection width increases, though it does show a mild decline overall.

The tori-spherical head exhibits an interesting behavior, particularly at smaller values of β. Initially, the buckling pressure remains nearly constant despite an increase in imperfection width, indicating a unique resilience to flat patch imperfections in this early range. This could be attributed to the inherent geometry of the tori-spherical head, which combines a spherical cap with a cylindrical portion. The initial flatness in this configuration may not significantly affect its structural integrity due to the way stresses are distributed along its curved and cylindrical sections. However, beyond a certain threshold of flatness, the buckling pressure begins to decrease similarly to the other configurations, suggesting that even the tori-spherical head is eventually affected by the increasing imperfection width.

In Figure 52, the influence of the first and second eigenmode affine imperfections on the buckling behavior of HDPE domes with varying ellipticities is presented. The eigenmodes, derived from linear buckling analysis, represent the most critical deformation patterns that the domes exhibit prior to buckling. By applying these modes as geometric imperfections to the original model, the sensitivity of each configuration to these imperfection patterns can be observed.

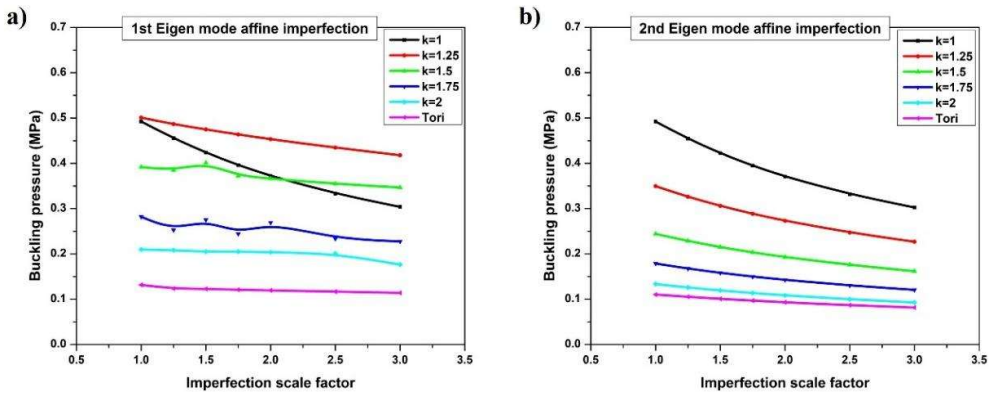


**Figure 52: Effect of increasing imperfections scale factor on the buckling pressure for different head shapes using a) first eigenmode affine imperfection and b) Second eigenmode affine imperfection**

Figure 52a demonstrates the buckling behavior when the first eigenmode affine imperfection is applied to domes of varying ellipticities (represented by different k values). As shown, for k=1 (the hemispherical dome), the buckling pressure significantly decreases as the imperfection scale factor increases, especially beyond the scale factor of 2. Initially, the hemispherical dome holds the highest buckling pressure, but its sharp decline causes its buckling pressure to drop below that of the k=1.5 dome after a scale factor of 2. This rapid decrease can be attributed to the hemispherical dome's high symmetry, which makes it particularly sensitive to the first eigen mode. As the imperfection scale factor increases, the symmetry is progressively disturbed, causing a significant reduction in load-carrying capacity. Beyond a scale factor of 2, these symmetry-breaking effects intensify, causing a steep decline in buckling pressure

For k = 1.25, although it starts with nearly the same buckling pressure as k = 1, its decline is more gradual, and it maintains the highest buckling pressure across the range of scale factors. This suggests that, despite being less curved than the hemispherical dome, the k=1.25 dome remains more resilient to the first eigenmode imperfection, likely due to the more balanced distribution of stresses across its surface.

As the ellipticity increases further (i.e., k=1.5, k=1.75, k=2, and the tori-spherical dome), the trend becomes flatter. In particular, for k=1.5, there is a slight decrease in buckling pressure with increasing imperfection scale factor, but the rate of decline is not as steep as for k=1. For the tori-spherical and k=2 domes, the buckling pressure remains almost constant, indicating that flatter configurations are less affected by the first eigenmode imperfection. This behavior can be linked to the fact that flatter domes are dominated by global deformation modes rather than local curvature effects, making them less sensitive to the first eigenmode imperfection.

In contrast, Figure 52b illustrates the effect of applying the second eigenmode affine imperfection. In this case, the overall trend is more consistent across the ellipticities. For the hemispherical dome (k=1), the buckling pressure starts higher, but decreases steadily as the imperfection scale factor increases. The rate of decline is more moderate compared to the first eigenmode, but still more pronounced than for the other shapes. This implies that the second eigenmode imperfection, while impactful, does not destabilize the hemispherical shape as drastically as the first eigenmode.

For the k=1.25 dome, the trend mirrors that of k=1, with a steady decrease in buckling pressure. However, k=1.25 retains a lower rate of decrease compared to k=1, further confirming its higher stability under eigenmode imperfections. For the flatter configurations (k=1.5, k=1.75, k=2, and the tori-spherical dome), the decrease in buckling pressure is more gradual, and the trends are nearly linear. This indicates that as the dome becomes flatter, its sensitivity to the second eigenmode imperfection reduces, similar to the first eigenmode case. However, the overall magnitude of buckling pressure remains lower, consistent with the structural behavior of flatter domes, which are less able to resist buckling loads due to their reduced geometric rigidity.

For both k = 1.25 and k = 1.5, as shown in Figure 53 and 54 respectively, the comparison of imperfection types reveals distinctive trends in buckling pressure

and highlights the structural vulnerability introduced by each type. These two k values are selected for detailed analysis because they perform better in buckling behavior compared to other geometries. Specifically, k = 1 (hemispherical) exhibits higher buckling pressure but is much more sensitive to geometric imperfections, with a significant drop in buckling pressure as imperfection amplitude changes. In contrast, k = 1.75, k = 2 and tori-spherical shapes have lower buckling pressures and less structural stability. Therefore, focusing on k = 1.25 and k = 1.5, which provide a balance between structural stiffness and sensitivity to geometric imperfections, enables a clearer comparison of the effect of imperfections on the dome's internal buckling performance.

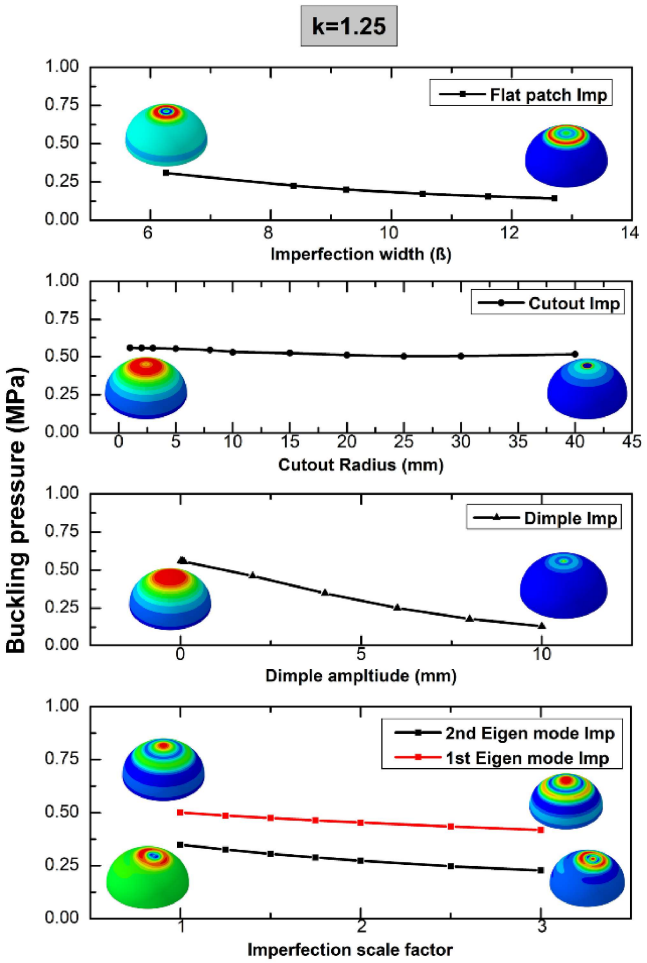


**Figure 53: Comparison of critical buckling pressure for different types of imperfections for k=1.25**

In both cases, flat patch imperfections consistently lead to the lowest buckling pressures as the imperfection width (β) increases. As the flatness at the dome's apex expands, the structure becomes less capable of withstanding external loads due to the reduction in curvature, which weakens its ability to distribute stresses. This effect is especially noticeable in k = 1.25, where the buckling pressure starts lower and steadily decreases, but it is similarly significant for k = 1.5, showing that flat patches severely compromise structural integrity regardless of the dome's initial curvature.

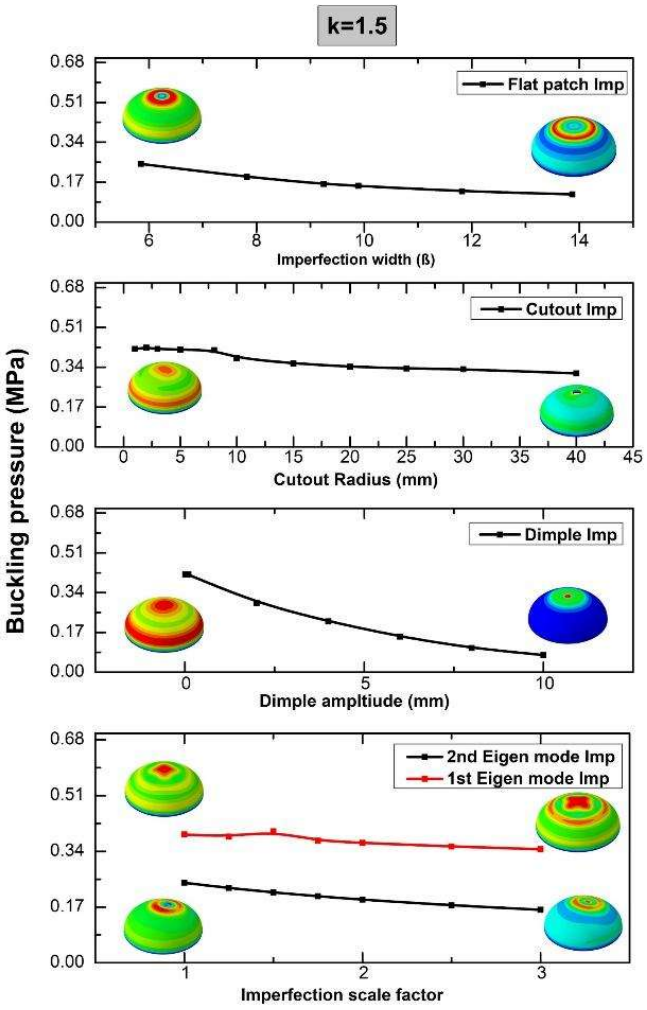


**Figure 54: Comparison of critical buckling pressure for different types of imperfections for k=1.5**

Similarly, 2nd eigenmode-affine imperfections result in notably low buckling pressures for both k = 1.25 and k = 1.5. The 2nd eigenmode introduces more localized deformation patterns, which disrupt the dome's stress distribution more drastically compared to the 1st eigenmode. As the imperfection scale factor increases, the buckling pressure declines sharply, especially in k = 1.5 domes. This shows that for slender structures, localized stress concentrations caused by higher order eigenmodes are particularly damaging.

In contrast, dimple imperfections start with relatively high buckling pressures but experience the steepest decline as the dimple amplitude increases. Initially, the domes show resilience to small dimples, but as the amplitude grows, the concentrated stresses around the dimples weaken the structure significantly. This effect is more pronounced in k = 1.5 domes, where the initial high buckling pressure sharply decreases, whereas in k = 1.25 domes, the decline is more gradual but still significant. Dimples, although initially less severe than flat patches or eigenmodes, ultimately lead to the greatest reduction in buckling capacity, making them the most detrimental imperfection at larger amplitudes.

Cutout imperfections, on the other hand, exhibit the most stable behavior across both k values. Despite the increasing cutout radius, the buckling pressure remains nearly constant, showing minimal impact on the dome's overall structural performance. This consistency indicates that removing material in this form does not significantly affect the global load distribution of the dome. The cutout's minimal influence contrasts sharply with the other imperfections, particularly dimples and flat patches, which severely weaken the structure. Finally, 1st eigenmode-affine imperfections maintain higher buckling pressures compared to the 2nd eigenmode. The 1st mode's global deformation pattern is less disruptive to the dome's structural behavior, especially for k = 1.5, where it remains relatively stable across the scale factor.

Although hemispherical heads exhibit the highest buckling pressure, their fabrication is complex and challenging. Among the elliptical configurations, the

shapes with aspect ratios of k = 1.25 and k = 1.5 demonstrated superior performance in the buckling analysis compared to other geometries. Consequently, the subsequent investigation will focus on analyzing the effect of variable wall thickness on these two configurations.

### 4.3.1. Combined Eigenmode Imperfection Analysis

In practical engineering applications, pressure vessel heads rarely exhibit imperfections that perfectly align with a single eigenmode. Instead, the imperfections present in these structures are caused by a variety of factors, including manufacturing tolerances, material inconsistencies, welding residual stresses, and operational wear and tear. These imperfections typically manifest as a combination of multiple eigenmodes, creating complex deviation patterns that influence the structural performance under loading. To address this reality, a combined eigenmode imperfection approach was used in this study, wherein both the first and second eigenmodes were superimposed and applied to the pressure vessel head models. This combined imperfection scenario represents a significant step beyond analyzing individual eigenmodes in isolation, as it demonstrates the realistic nature of imperfections observed in real-world structures.

The combined eigenmode imperfection analysis is essential for several reasons. First, it introduces a more comprehensive understanding of imperfection patterns and their interactions under loading conditions. While individual eigenmode analyses are good for isolating specific failure mechanisms associated with each mode, they may oversimplify the actual structural response. In contrast, the superposition of multiple eigenmodes allows for the investigation of nonlinear interaction effects, which can significantly influence buckling behavior. These interactions can either amplify or counteract the structural sensitivity to imperfections, depending on the way the shapes of the eigenmodes combine. For instance, the first eigenmode often represents a global buckling shape, while the second eigenmode may capture localized deformation characteristics. When combined, these modes may create a more complex deformation pattern that affects

the overall stability of the structure in ways that single-mode analyses cannot predict.

From a practical standpoint, the combined mode approach is particularly relevant for the ellipsoidal and tori-spherical pressure vessel heads studied here, as these geometries are inherently sensitive to imperfections due to their non-uniform curvature and stress distribution. The application of combined eigenmode imperfections provides a more realistic representation of the challenges faced by these components under internal pressure or external loads. Real-world deviations in geometry, such as those introduced during the fabrication process, are unlikely to conform according to the shape of a single eigenmode. By incorporating a combined mode analysis, this study aligns more closely with actual physical conditions, providing a robust assessment of the buckling resistance of pressure vessel heads.

Moreover, the combined mode analysis holds significant implications for the design and safety of pressure vessels. The interaction of imperfections captured in this approach can reveal critical failure paths that may remain undetected when analyzing individual modes. This is especially important for ensuring that the vessel design includes adequate safety margins to account for the compounded effects of multiple imperfections. In practical terms, understanding from combined mode analyses can guide engineers in refining manufacturing tolerances, improving quality control processes, and optimizing structural designs to minimize vulnerability to buckling.

The trends observed in the combined eigenmode curves vary across different head geometries, reflecting the influence of their unique characteristics. In this section, the behavior of the combined eigenmode imperfection is compared with the individual eigenmode results for ellipsoidal heads ($k$ = 1.25 to $k$ = 2), hemispherical heads ($k$ = 1), and tori-spherical heads. The relationship between imperfection amplitude and buckling pressure was analyzed for ellipsoidal pressure vessel heads with varying aspect ratios ($k$) ranging from $k$ = 1 (hemispherical) to $k$

= 2 (most flat elliptical), along with a tori-spherical head. For each geometry, separate plots were generated for the first eigenmode and second eigenmode imperfections, as well as a combined mode imperfection that superimposes both. These plots reveal critical trends in buckling pressure ($y$-axis) as a function of imperfection amplitude ($x$-axis), providing understanding of the structural stability under different imperfection scenarios.

For **ellipsoidal heads** with aspect ratios ($k$) ranging from 1.25 to 2 (figure 55 to 58), the combined eigenmode imperfection curve lies between the individual first and second eigenmode curves. In most cases, the combined curve is slightly closer to the second eigenmode curve. This behavior can be attributed to the dominant influence of localized deformation patterns introduced by the second eigenmode.

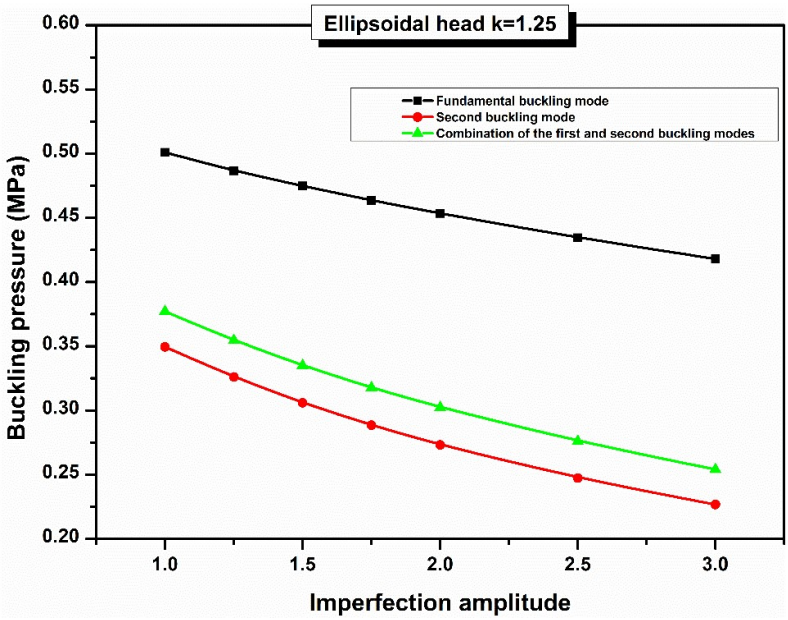


**Figure 55: Effect of increase in imperfection amplitude considering first, second and combined eigenmode affine imperfection on the buckling pressure for aspect ratio of k=1.25**

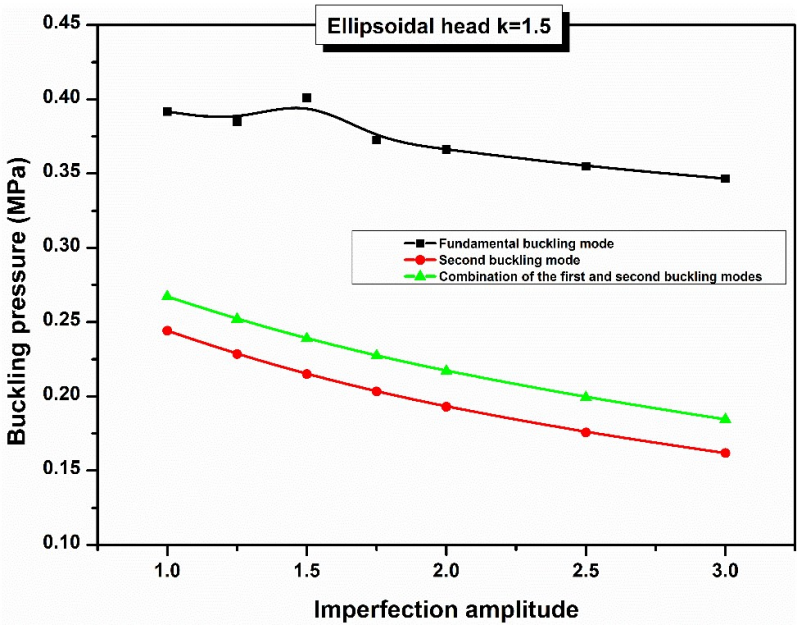


**Figure 56: Effect of increase in imperfection amplitude considering first, second and combined eigenmode affine imperfection on the buckling pressure for aspect ratio of k=1.5**

The first eigenmode represents a global deformation shape, spreading the imperfection effect over a larger area, which tends to stabilize the structure and maintain higher buckling pressures. On the other hand, the second eigenmode corresponds to localized deformations, introducing regions of higher stress concentration that significantly reduce the buckling pressure. When these modes are combined, their interaction creates a deformation pattern that retains the destabilizing effects of the 2nd eigenmode, particularly for flatter ellipsoidal heads ($k$=2). Consequently, the combined eigenmode imperfection curve reflects a compromise between the global and localized effects, with the localized characteristics often dominating at different imperfection amplitudes.

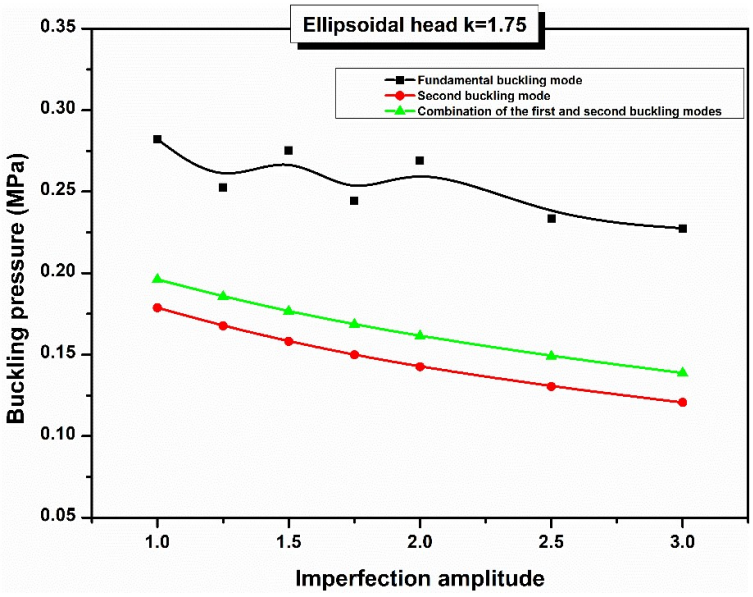


**Figure 57: Effect of increase in imperfection amplitude considering first, second and combined eigenmode affine imperfection on the buckling pressure for aspect ratio of k=1.75**

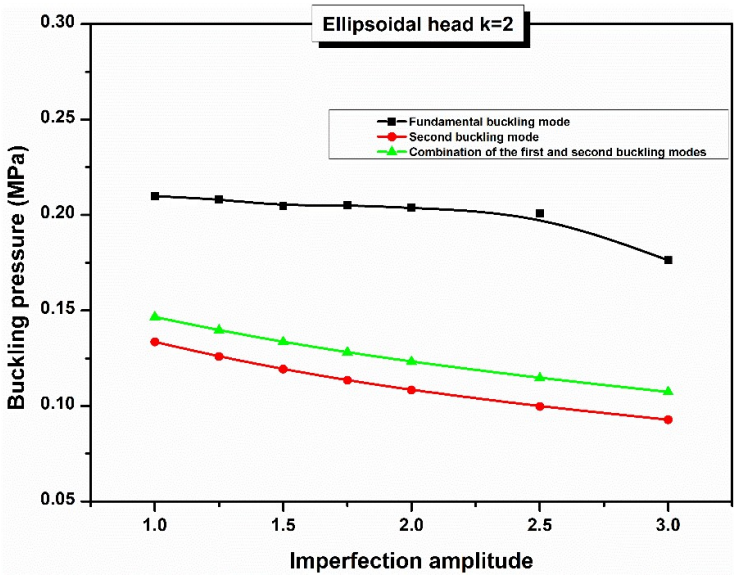


**Figure 58: Effect of increase in imperfection amplitude considering first, second and combined eigenmode affine imperfection on the buckling pressure for aspect ratio of k=2**

For the **hemispherical head** ($k$=1), a different and unique trend is observed as shown in figure 59. The curves for the first and second eigenmode imperfections overlap, indicating that these modes contribute similarly to the buckling behavior. This is primarily due to the symmetry and robustness of the hemispherical geometry, which distributes stresses uniformly and minimizes localized stress concentrations.

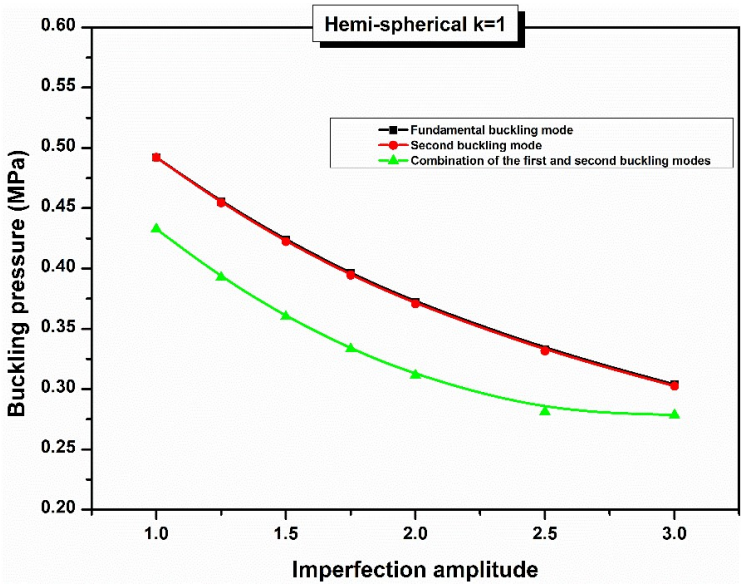


**Figure 59 Effect of increase in imperfection amplitude considering first, second and combined eigenmode affine imperfection on the buckling pressure for aspect ratio of k=1**

However, the combined eigenmode imperfection curve for the hemispherical head lies below both the first and second eigenmode curves. This deviation arises because the superposition of the two modes introduces subtle asymmetries in the imperfection pattern. These asymmetries, absent in the individual modes, create new stress concentration zones that reduce the buckling pressure further. This trend shows the combined influence of imperfections in a structure that is typically characterized by high inherent stability.

The **tori-spherical** head exhibits another unique trend where the combined eigenmode imperfection curve falls below both the first and second eigenmode

curves. This behavior, as shown in figure 60, is significantly different from that of the ellipsoidal heads and can be attributed to the complex geometry of the tori-spherical head.

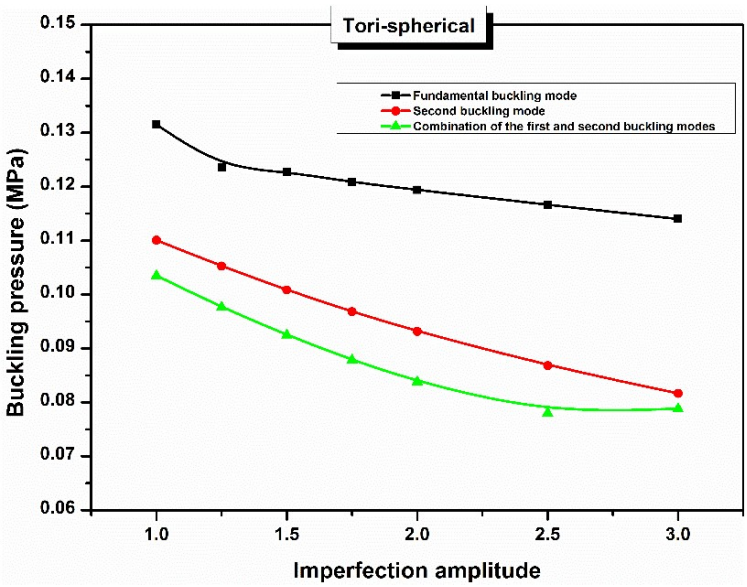


**Figure 60: Effect of increase in imperfection amplitude considering first, second and combined eigenmode affine imperfection on the buckling pressure for tori-spherical head**

Unlike the more uniform geometries of ellipsoidal, the tori-spherical head has distinct transitions between the crown, knuckle, and straight regions. These geometric transitions inherently create stress concentration zones that are highly sensitive to imperfections. When the global (1st eigenmode) and localized (2nd eigenmode) imperfection patterns are combined, their interaction increases these stress concentrations, leading to a greater reduction in buckling pressure. The nonlinear behavior of the tori-spherical head further amplifies this effect, resulting in the combined curve being lower than both individual mode curves.

In the case of the tori-spherical head, as the imperfection amplitude increases, the combined eigenmode curve gradually starts to approach the second eigenmode curve, and the difference between the combined and second mode curves keeps decreasing. Actually, at higher imperfection amplitudes, the

contribution of the 1st eigenmode (global imperfections) becomes relatively smaller because the localized imperfections from the 2nd eigenmode have a more significant impact on the overall structural stability. The increased amplitude amplifies the localized deformations, and the structure's response is increasingly governed by the localized effects, making the combined imperfection curve behave more similarly to the second eigenmode. As a result, the difference between the combined and second eigenmode curves decreases as the imperfection amplitude continues to grow.

### 4.3.2. Combined Effects of Dimple and Eigenmode Imperfections on Pressure Vessel Heads

Numerical analysis was performed to study the structural stability of pressure vessel heads by incorporating two distinct types of imperfections which are localized dimples and global eigenmode affine imperfections. Dimple imperfections, representing localized geometric deviations, mimic realistic defects such as small dents caused by manufacturing errors or handling. In contrast, eigenmode affine imperfections, derived from linear buckling analysis (LBA), simulate global deviations that align with the structure's critical buckling modes.

The interaction between these imperfections reflects real-world conditions where localized and global flaws coexist, and it potentially amplifies their impact on structural performance. Dimples create stress concentrations in specific regions, while eigenmode imperfections redistribute stresses across the entire structure, reducing its overall stiffness.

In the first part of this analysis, the dimple imperfection amplitude was fixed at 2 mm, while the eigenmode imperfection amplitude scale factor varied from 1 to 3. This variation was analyzed individually for the first eigenmode, the second eigenmode, and a combination of the first and second eigenmodes. The analysis was performed for two different aspect ratios (k=1.25 and k=1.5) of the ellipsoidal

head, allowing for a comparative evaluation of the geometric influence on buckling performance.

In the second part of this study, the eigenmode imperfection amplitude scale factor was held constant at 1.5, and the dimple imperfection amplitude was incrementally varied from 0.1 mm to 6 mm. The corresponding buckling pressures were recorded to evaluate the sensitivity of the structure to localized imperfections of varying magnitudes. This dual approach provides understanding of the collective influence of global and localized imperfections on the critical buckling pressure of pressure vessel heads.

In the first case (Figure 61), a constant dimple of 2 mm was applied to a pressure vessel head with an aspect ratio of 1.5 (k = 1.5). The analysis considered three conditions which are the dimple combined with the first eigenmode, the dimple combined with the second eigenmode, and the dimple combined with both eigenmodes simultaneously. The buckling pressure was recorded at 0.29 MPa when only the 2mm dimple imperfection was applied without eigenmode affine imperfection in the last section. When the dimple was combined with the first eigenmode, the buckling pressure increased, reaching a higher value than when only the dimple imperfection was applied. This increase indicates a stabilizing effect of the first eigenmode, which redistributes the structural stresses in such a way that it partially offsets the destabilizing effect introduced by the dimple imperfection. The results revealed that the lowest buckling pressure occurred when the dimple was combined with the second eigenmode. The combined eigenmode case produced a buckling pressure that was intermediate, falling between the values observed for the first eigenmode and the second eigenmode. The first eigenmode alone exhibited the highest buckling pressure, suggesting that its deformation pattern introduces less severe destabilization compared to the second eigenmode, which introduces higher asymmetry and localized deformation.

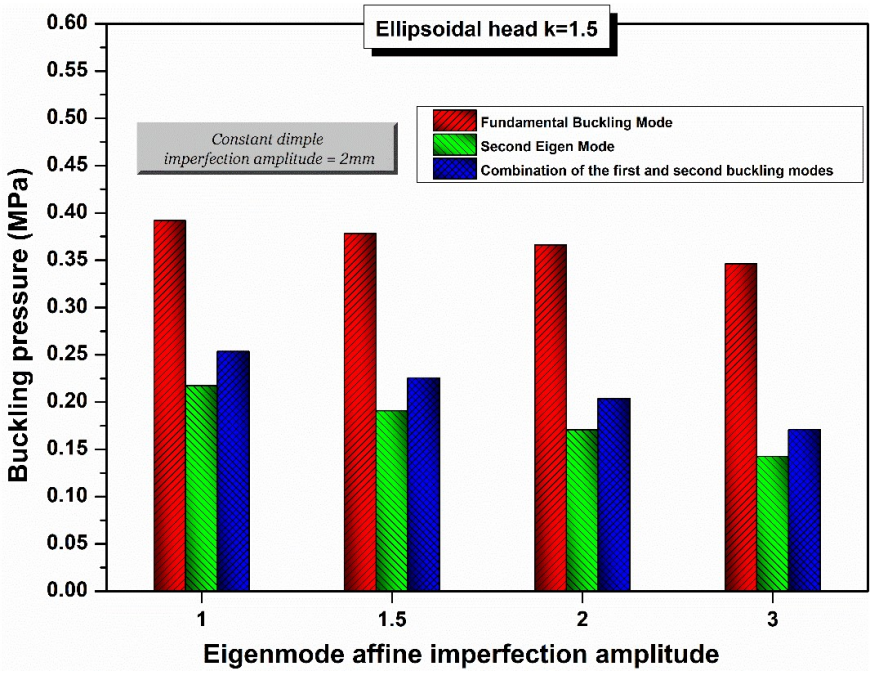


**Figure 61: Effect of change in eigenmode affine imperfection amplitude on buckling pressure for elliptical head k=1.5 along with the application of constant dimple imperfection of 2mm**

A similar trend was observed in the second case (Figure 62), where the aspect ratio was reduced to 1.25 (k = 1.25) while maintaining a constant dimple amplitude of 2 mm. Here too, the lowest buckling pressure was observed when the dimple was combined with the second eigenmode, demonstrating its dominant destabilizing influence. The buckling pressure for the combined eigenmode case remained between the first and second eigenmodes, confirming that while the interaction of multiple modes amplifies imperfections, it does not reduce the buckling pressure as significantly as the second eigenmode acting alone.

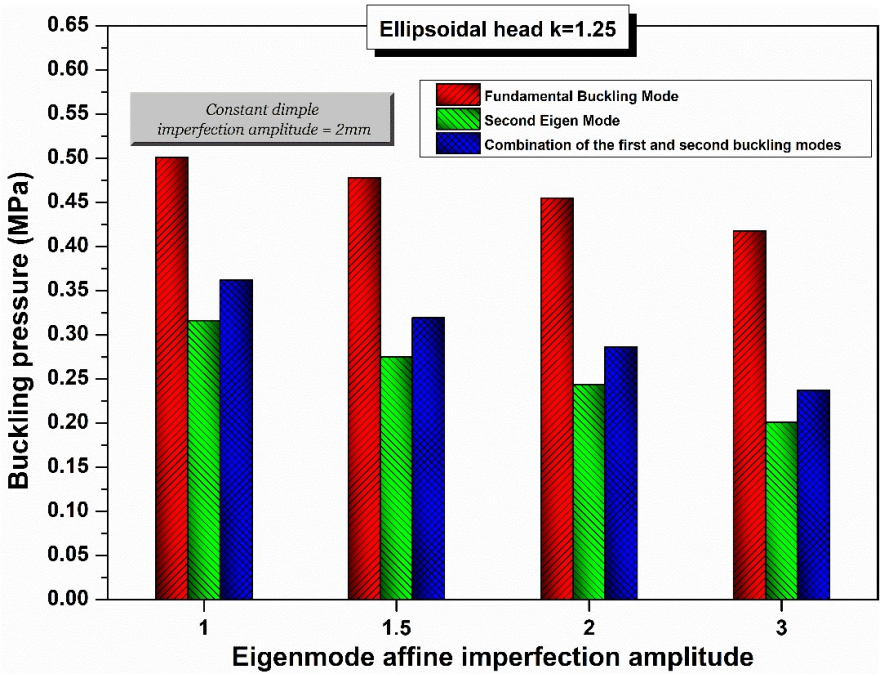


**Figure 62: Effect of change in eigenmode affine imperfection amplitude on buckling pressure for elliptical head k=1.25 along with the application of constant dimple imperfection of 2mm**

In the third case (Figure 63), a constant eigenmode imperfection amplitude of 1.5 was applied to the pressure vessel head with an aspect ratio of 1.5 (k = 1.5), and the dimple amplitude was varied. The first eigenmode deformation pattern has a stabilizing effect when combined with the dimple at this aspect ratio and amplitude. The first eigenmode redistributes stress in such a way that it offsets the destabilizing influence of the dimple. This partial stabilization arises from the eigenmode's shape aligning with the structure's natural buckling response, delaying the onset of buckling. However, as the dimple amplitude increases further, the imperfection becomes dominant, and the stabilizing effect diminishes, leading to reduced buckling pressures.

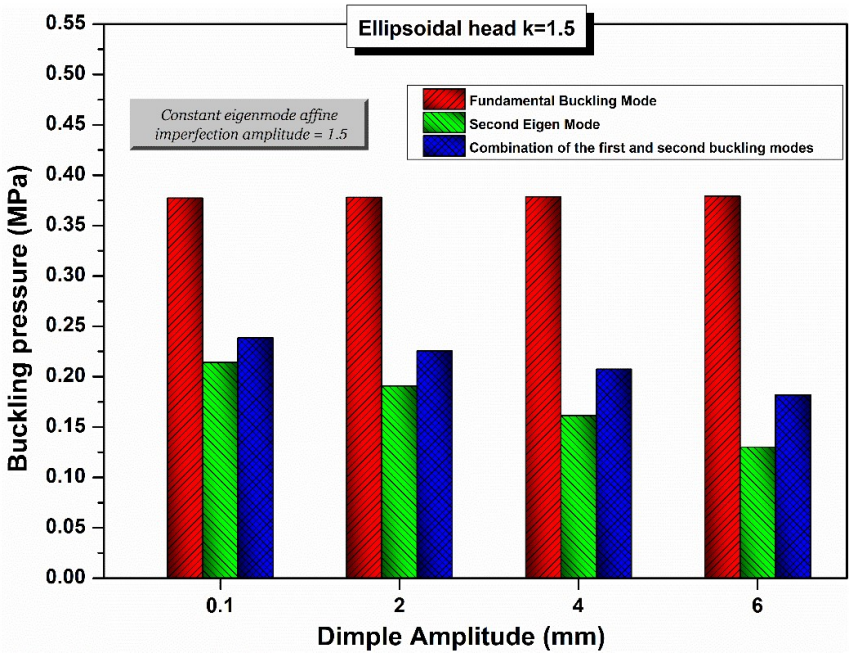


**Figure 63: Effect of change in dimple amplitude on buckling pressure for elliptical head k=1.5 along with the application of constant eigenmode affine imperfection amplitude of 1.5**

In the fourth case (Figure 64), the same analysis was repeated for an aspect ratio of 1.25 (k = 1.25). Similar to the behavior observed in Figure 3, the buckling pressure for the first eigenmode combined with the dimple remained constant across varying dimple amplitudes, indicating a consistent stabilizing effect of the first eigenmode at this amplitude. Meanwhile, the second eigenmode consistently produced the lowest buckling pressures, reaffirming its strong destabilizing influence. The second eigenmode and combined eigenmode continue to decrease with increasing dimple amplitude at constant eigenmode affine imperfection amplitude but the overall buckling pressure is lower when these imperfections are considered alone.

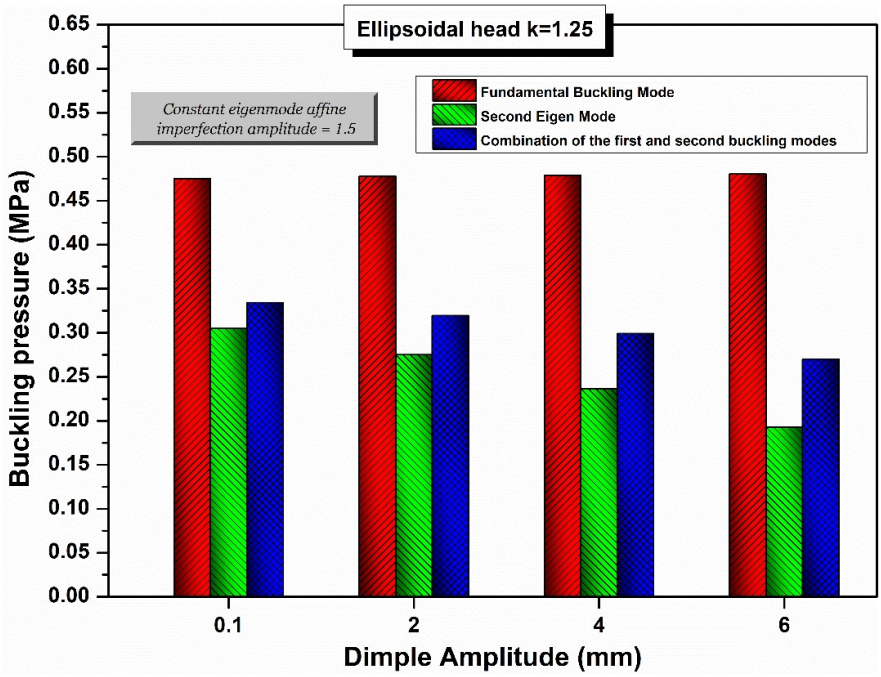


**Figure 64: Effect of change in dimple amplitude on buckling pressure for elliptical head k=1.25 along with the application of constant eigenmode affine imperfection amplitude of 1.5**

The analysis of the pressure vessel head highlights the significant influence of eigenmode shapes, amplitudes, and geometric imperfections on buckling behavior. For both aspect ratios (k = 1.5 and k = 1.25), the second eigenmode produced the lowest buckling pressures, emphasizing its destabilizing nature due to its asymmetric deformation pattern. The combined eigenmode case resulted in intermediate buckling pressures, while the first eigenmode exhibited the highest resistance to buckling.

A key observation is the behavior of the buckling pressure when eigenmode imperfections are combined with increasing dimple amplitudes at a constant eigenmode affine imperfection amplitude. The second eigenmode and combined eigenmode show a continuous decrease in buckling pressure as the dimple amplitude increases. However, it is important to note that the overall buckling pressure remains lower than the buckling pressure when the dimple and eigenmode affine imperfections are considered individually.

This behavior arises due to the interaction effects between the two imperfections. The eigenmode affine imperfection introduces a global structural deformation that inherently reduces the buckling resistance. When the dimple imperfection is applied simultaneously, it localizes stress concentrations within the structure. As the dimple amplitude increases, these localized imperfections aggravate the existing deformation caused by the eigenmode affine imperfection, further destabilizing the structure and reducing its buckling pressure.

Thus, the continuous decrease in buckling pressure with increasing dimple amplitude reflects the cumulative destabilizing impact of combining imperfections, especially for imperfections with strong asymmetry (like the second eigenmode). When considered alone, each imperfection imposes a less severe destabilization, allowing the structure to maintain a slightly higher buckling pressure.

The results emphasize the importance of accounting for both localized and global imperfections in pressure vessel design and analysis. Localized dimples can act as initiators of premature buckling, particularly when they coincide with high-stress regions predicted by eigenmodes. This combined approach provides a realistic assessment of imperfection sensitivity and offers valuable insights for improving safety margins and reliability in pressure vessel construction.

### 4.3.3. Effect of Indentation Angle on Buckling Pressure of Ellipsoidal Heads

Among the various factors influencing buckling behavior, the location of imperfections, represented here by the angle of indentation, has a direct impact on the buckling pressure. These imperfections, such as dimples and cutouts, often result from manufacturing or operational processes and create localized stress concentrations that can compromise the performance, stability, and safety of pressure tanks. By systematically varying the angle of these imperfections, it becomes possible to analyze their effects on stress distribution, buckling resistance,

and failure initiation. This understanding is essential for designing tanks that are resilient to imperfections and capable of withstanding complex real-world conditions. Addressing these factors ensures the accurate identification of potential failure zones and supports the reliable design and analysis of ellipsoidal heads.

In this study, the angular position of both dimple and cutout imperfections varied between 15° to 90° from the apex of the ellipsoidal head, and the resulting buckling pressures were measured. The apex (90°) corresponds to the topmost region of the ellipsoidal head, while smaller angles progressively move the imperfection location toward the equator. The results demonstrate that as the indentation angle increases and imperfections move closer to the apex, the buckling pressure decreases significantly for both k=1.25 and k=1.5 aspect ratio heads. This behavior highlights a critical finding: imperfections at the apex cause the most significant reduction in buckling pressure, making this region the most sensitive to instability.

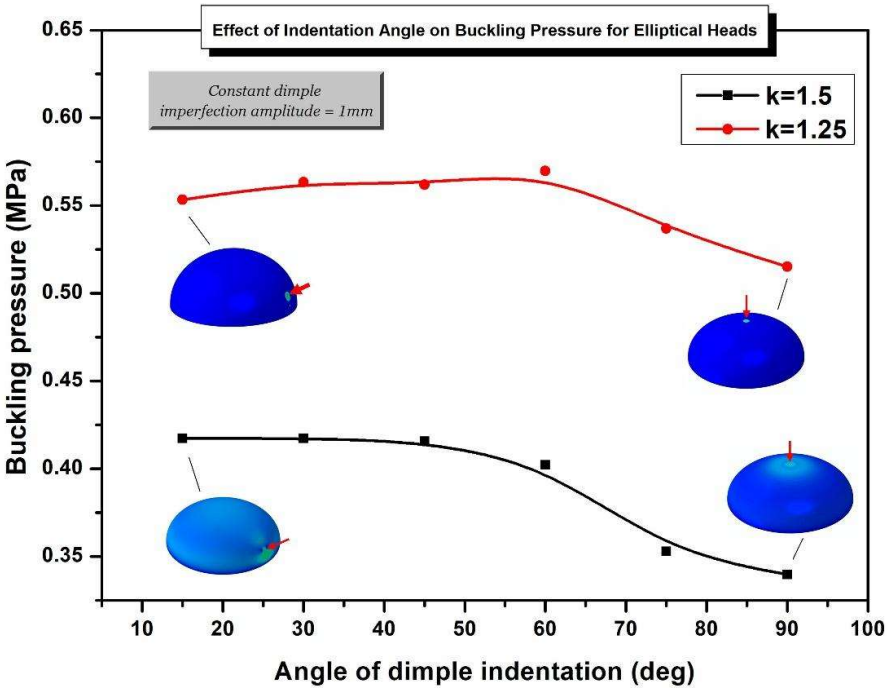


**Figure 65: Effect of change in indentation angle for geometric dimple imperfection on buckling pressure of elliptical head with aspect ratio of k=1.25 and k=1.5**

For the k=1.25 aspect ratio, the behavior of buckling pressure differs noticeably between dimple and cutout imperfections. In the case of dimple imperfections (Figure 65), the buckling pressure remains relatively high as the indentation angle increases initially, but it experiences a more intense drop near the apex (90°). This sharp decline shows that even for shallower heads, dimple imperfections positioned closer to the apex can significantly reduce buckling resistance. On the other hand, for circular cutout imperfections (Figure 66), the buckling pressure decreases more gradually, from approximately 0.6 MPa to 0.55 MPa, as the angle increases toward the apex. This slower decline indicates that the angle of the cutout imperfection has a less severe impact on buckling pressure for shallower heads compared to dimples.

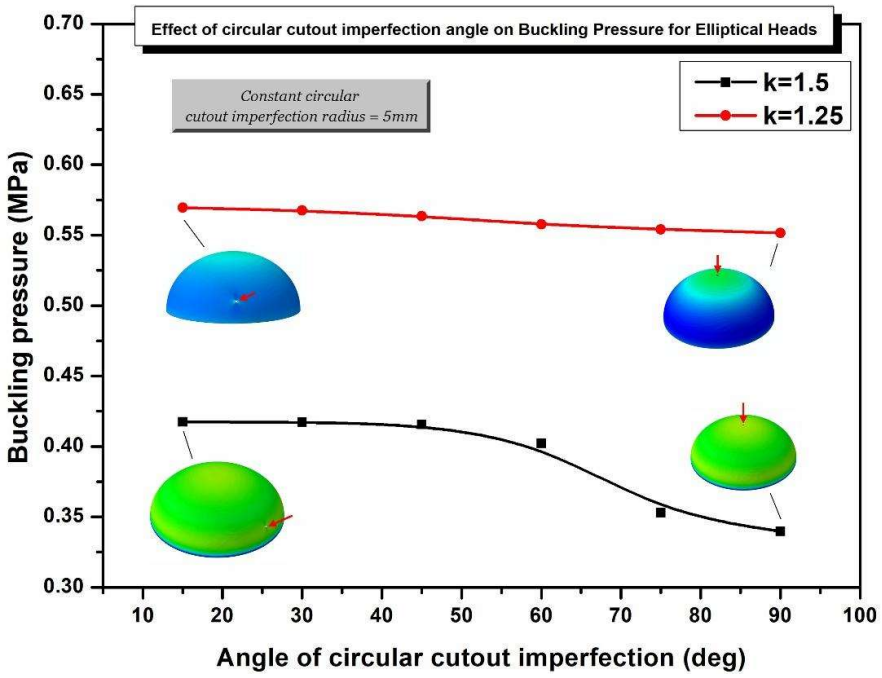


**Figure 66: Effect of change in indentation angle for circular cutout imperfection on buckling pressure of elliptical head with aspect ratio of k=1.25 and k=1.5**

The contrasting behavior can be attributed to the nature of these imperfections. Dimples create localized stress concentrations and deform the structure more significantly, leading to a sharper drop in buckling pressure when positioned at critical locations like the apex. In contrast, cutout imperfections, while still

weakening the structure, distribute stress more evenly around the edges of the cutout, resulting in a more gradual reduction in buckling pressure. This finding demonstrates that for shallower heads, the position (angle) of cutout imperfections has a less severe impact on structural stability compared to dimples, further reinforcing the need to consider both the type and location of imperfections in the analysis of buckling behavior.

For the k=1.5 aspect ratio, which represents a deeper ellipsoidal head, both dimple and cutout imperfections exhibit a similar trend in buckling pressure as the indentation angle increases. In both cases, the buckling pressure decreases progressively as the angle moves toward the apex (90°), where the reduction becomes more pronounced. This behavior highlights that deeper ellipsoidal heads are significantly more sensitive to imperfections located near the apex, regardless of whether the imperfection is a dimple or a cutout.

For dimple imperfections (Figure 65), the buckling pressure decreases steadily as the indentation angle increases, dropping from around 0.42 MPa to approximately 0.35 MPa at the apex. A similar trend is observed for cutout imperfections (Figure 66), where the buckling pressure follows a comparable decline. This indicates that, for k=1.5, the influence of indentation angle on buckling pressure is similarly severe for both types of imperfections.

The practical significance of these findings is substantial, particularly for industries relying on the safe operation of pressure vessels. First, the results validate the assumption made in previous studies that the apex (90°) is the most critical location for imperfections. By confirming this, the study ensures that structural analyses, numerical simulations, and physical testing focus on the most vulnerable point of the ellipsoidal head, leading to more accurate assessments of failure risk. Engineers can now prioritize inspection and reinforcement at the apex, where imperfections are most detrimental to stability.

Second, these findings emphasize the importance of precision in the fabrication and handling of pressure vessels. During manufacturing, imperfections such as dimples or cutouts are often unavoidable due to material defects, welding processes, or machining errors. However, this study shows that imperfections at specific angular positions, particularly near the apex, pose a far greater risk than imperfections located closer to the equator. Manufacturers can use this knowledge to implement stricter quality control measures, especially for regions near the apex.

### 4.3.4. Variable wall thickness Model with Eigenmode affine imperfections

In this section, buckling behavior was analyzed for an ellipsoidal pressure head with variable wall thickness, focusing on the impact of wall thickness variation on structural stability. The thickness of the model varied from 11.6 mm at the apex to 8.4 mm near the equator, in contrast to prior analyses that utilized a uniform thickness of 10 mm throughout. As depicted in Figure 67 and Table 3, the thickness decreases from the apex (0°) to the equator (90°), with the apex retaining the maximum thickness due to its increased sensitivity to buckling. This distribution is crucial to optimize the structural integrity of the pressure head, where buckling resistance is most critical. The design adheres to recommendations from existing literature, including the requirement that the minimum wall thickness should be no less than 68% of the maximum thickness to ensure sufficient strength under pressure conditions [76]. This criterion ensures that the structural design is both efficient and capable of withstanding external pressures. By introducing variable thickness based on the isostrength principle, the pressure head achieves an optimized balance between material usage and load-bearing capacity.

**Table 3: Wall thickness distribution at different angles of elliptical heads with aspect ratio of 1.25 and 1.5**

| Variable wall thickness at different angles of ellipsoidal heads k=1.25 and k=1.5 | | | | | | | | |
|---|---|---|---|---|---|---|---|---|
| Angle (rad) | | 0 | $\frac{\pi}{12}$ | $\frac{\pi}{6}$ | $\frac{\pi}{4}$ | $\frac{\pi}{3}$ | $\frac{5\pi}{12}$ | $\frac{\pi}{2}$ |
| Thickness t (mm) | k=1.25 | 11.6 | 11.57 | 11.18 | 10.5 | 9.6 | 8.71 | 8.4 |
| | k =1.5 | 11.6 | 11.51 | 11.23 | 10.7 | 9.87 | 8.9 | 8.4 |

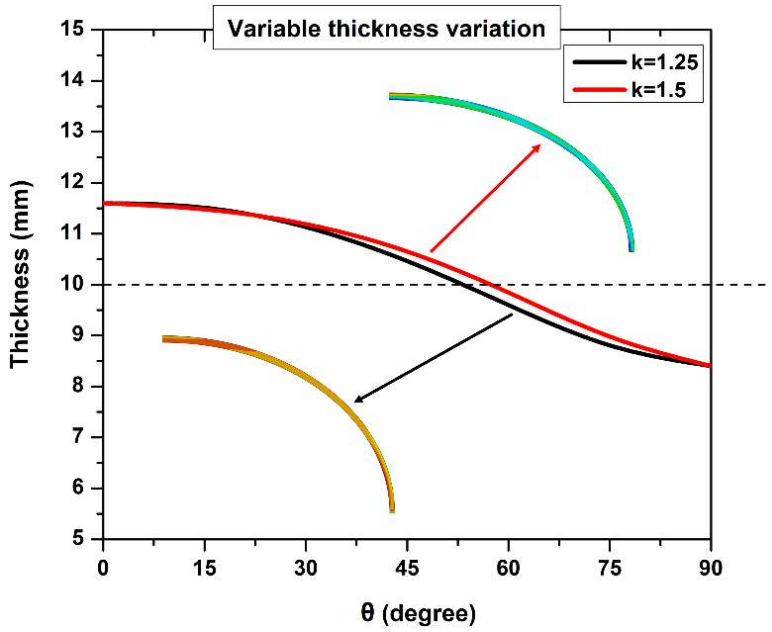


**Figure 67: Wall thickness distribution for elliptical head aspect ratios of 1.25 and 1.5**

The analysis was performed for two different ellipticities (k=1.25 and k=1.5), which correspond to different geometrical shapes of the ellipsoidal pressure head. Initially, a linear buckling analysis was conducted to determine the critical buckling pressure and the associated eigenmodes. Subsequently geometrically nonlinear analysis (GNA) was conducted, using the static Riks model in the Abaqus, with the analysis parameters consistent with those detailed earlier. To simulate the effects of manufacturing imperfections, both first and second eigenmode imperfections were incorporated into the initial model, followed by nonlinear buckling analysis. The

analysis methodology adopted is the same as that used for constant-thickness head shapes. This comprehensive approach, as highlighted in earlier sections, offers a more robust and realistic representation of structural behavior under operational conditions, facilitating a detailed comparison between the buckling performance of variable-thickness and constant-thickness models.

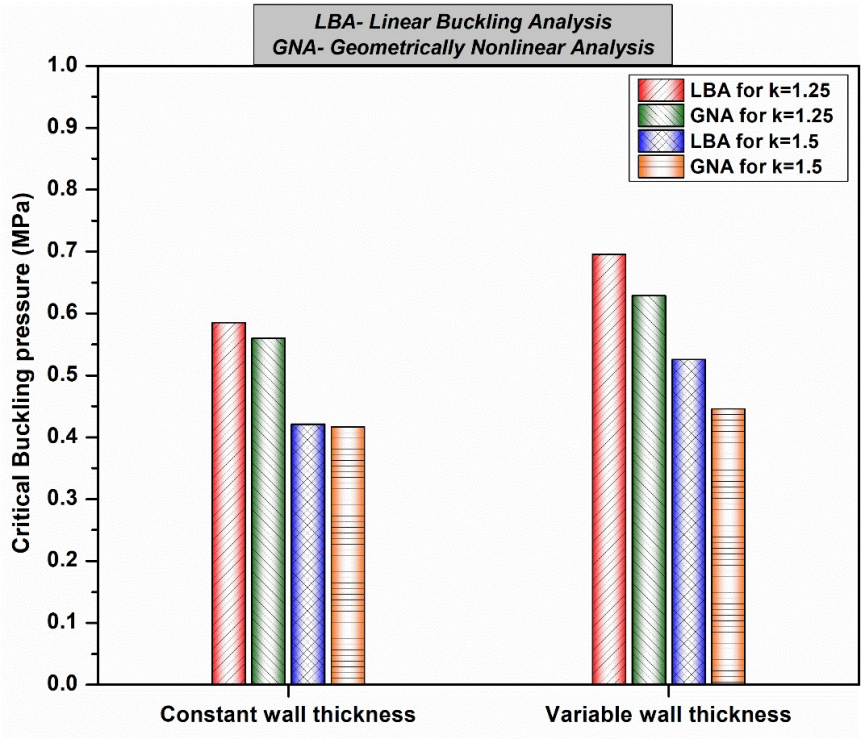


**Figure 68: Comparison of critical buckling pressure of elliptical heads with constant and variable wall thickness for aspect ratios of 1.25 and 1.5 corresponding to linear and non-linear buckling analysis without imperfections**

In Figure 68, the critical buckling pressure for both Linear Buckling Analysis (LBA) and Geometrically Nonlinear Analysis (GNA) is illustrated for models with constant and variable wall thicknesses at two different ellipticity ratios, specifically k=1.25 and k=1.5. The results reveal that the variable thickness model consistently exhibits higher buckling resistance compared to the constant thickness model. This is evidenced by the significantly high critical buckling pressures for the variable

thickness model in both LBA and GNA analyses, indicating that the introduction of variable thickness effectively enhances structural stability against buckling loads.

The observed differences in buckling performance can be attributed to the geometric advantages provided by variable wall thickness, particularly at the apex of the structure where buckling tends to initiate. By incorporating greater thickness in this region, the variable thickness model is able to redistribute stresses more effectively, enabling it to better withstand applied loads. The enhanced thickness at the apex, where heads typically experience buckling, contributes significantly to the observed higher critical buckling pressures. This design feature helps to mitigate the risk of buckling and underscores the effectiveness of variable wall thickness in improving structural stability.

The ellipticity ratio also plays a crucial role in influencing buckling performance. Consistent with earlier analyses, the results show that a lower ellipticity ratio (k=1.25) correlates with higher critical buckling pressures compared to a higher ellipticity ratio (k=1.5). This further proves that shapes closer to spherical configurations offer greater resistance to buckling due to their favorable geometric properties.

The analysis presented in Figures 69 and 70 investigates the critical buckling pressures for two ellipticity ratios ($k$=1.25 and $k$=1.5) while incorporating eigenmode-affine imperfections through Geometric Nonlinear Analysis (GNA). These figures compare cases with constant thickness and variable thickness. In all instances, the introduction of variable thickness results in an increase in the critical buckling pressure, indicating the beneficial effect of the thickness variation on structural stability. This effect is consistent for both ellipticity ratios, demonstrating a uniform stiffening response across different geometries.

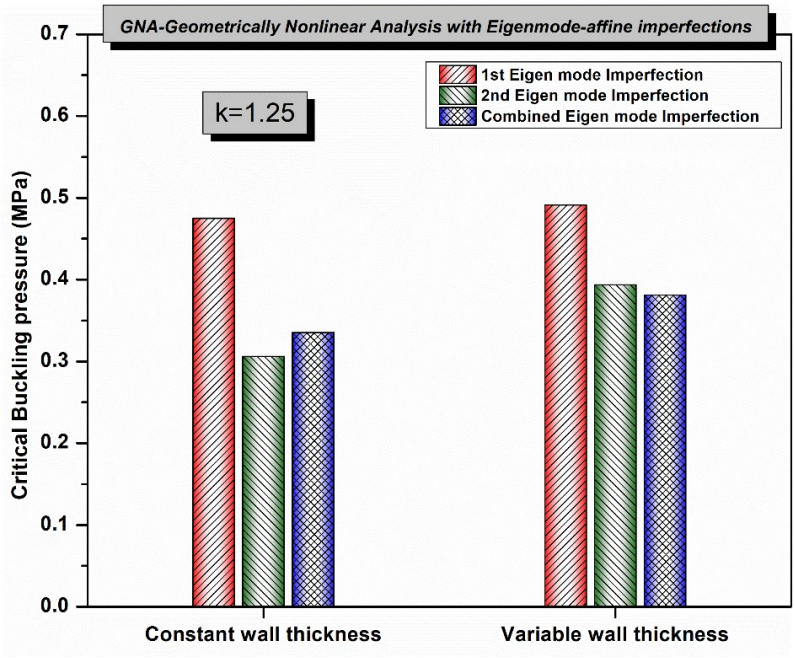


**Figure 69: Comparison of critical buckling pressure of elliptical heads with constant and variable wall thickness for aspect ratio of 1.25 corresponding to Non-linear buckling analysis with 1st, 2nd and combined eigenmode affine imperfection**

For $k$=1.5, with constant thickness, the second eigenmode consistently yields the lowest critical buckling pressure. This is attributed to the specific destabilizing nature of the second eigenmode, which governs the structure's response more dominantly than the first eigenmode or the combined eigenmode-affine imperfections. With variable thickness, the critical pressures for all cases (first eigenmode, second eigenmode, and combined eigenmode-affine imperfections) are uniformly increased due to the stiffening effect of the variable thickness. The hierarchy of responses remains the same, with the second eigenmode continuing to exhibit the lowest critical pressure.

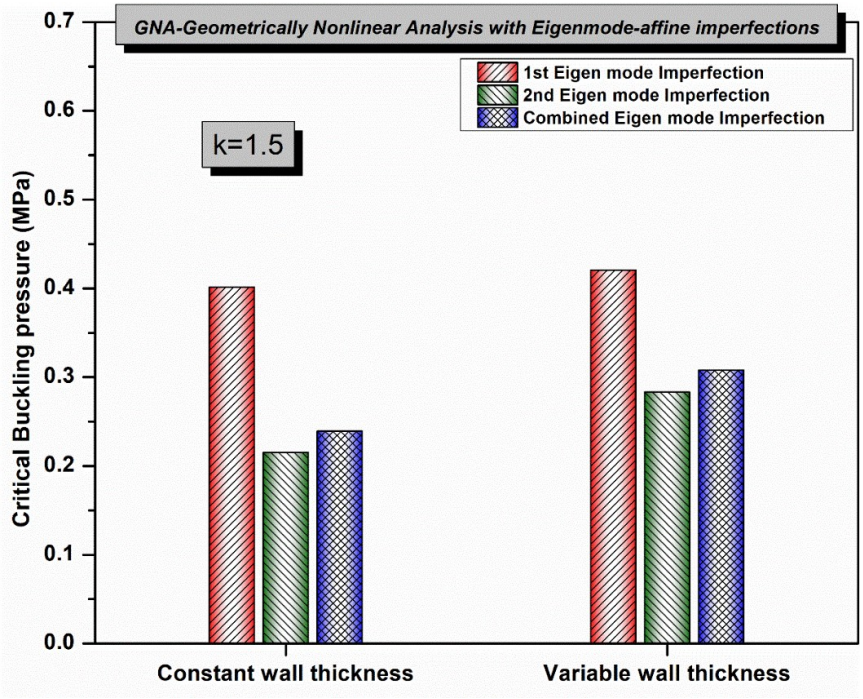


**Figure 70: Comparison of critical buckling pressure of elliptical heads with constant and variable wall thickness for aspect ratio of 1.5 corresponding to Non-linear buckling analysis with 1st, 2nd and combined eigenmode affine imperfection**

For $k$=1.25, the behavior differs notably. While the second eigenmode still results in the lowest critical pressure for the constant thickness case, the introduction of variable thickness alters this hierarchy. The second eigenmode shows a significant increase in critical pressure, to the extent that its peak surpasses the combined eigenmode-affine imperfections. This indicates that the variable thickness interacts more favorably with the second eigenmode configuration in the $k$=1.25 geometry, enhancing the structure's resistance to buckling beyond the combined eigenmode-affine imperfections. However, in the combined eigenmode case, the critical pressure remains lower than that of the second eigenmode, reaffirming the unique sensitivity of the second mode to variable thickness in this aspect ratio.

The differences in response between the two aspect ratios can be attributed to the geometrical characteristics of the elliptical heads. The more elongated shape at $k$=1.25 appears to amplify the influence of the combined eigenmode imperfection under variable thickness, whereas the less elongated geometry at $k$=1.5 results in a more uniform response across all imperfection types. These findings show the complex interplay between geometry, imperfection patterns, and material distribution in determining the buckling behavior of elliptical heads.

# Conclusion

## I. Summary

This study has been designed to explore various factors influencing the structural performance and buckling behaviour of HDPE pressure vessels. By focusing on the impact of geometric imperfections, applying an advanced moment theory approach, and investigating the optimization of geometry and wall thickness, the research aimed to establish a deeper understanding of these elements' interaction and their effect on the overall integrity and stability of the pressure vessels. The following conclusions present a summary of the key findings derived from the systematic analysis of these objectives, which contribute to the development of more efficient and durable HDPE pressure tank designs:

- The stress distribution in pressure vessels is closely tied to their shape, wall thickness, and overall geometry. For smoother, more hemispherical shapes (flattening factor (k = 1) to (k = 1.5), the transverse stress stays compressive throughout. However, as the vessel becomes flatter and more elliptical (k = 1.75) and (k = 2), sharp curvature transitions cause stress peaks near the junction of the cylinder and head, briefly shifting the transverse stress into a tensile state before returning to compressive farther away. Wall thickness also plays a crucial role as thinner walls (like 5 mm) face challenges in achieving uniform pressure distribution, leading to higher stress concentrations, while thicker walls (like 10 mm or 15 mm) distribute stresses more uniformly, improving the vessel's structural integrity and reducing failure risk. Using variable wall thickness offers further advantages by strategically adding material only where needed, strengthening critical areas, and balancing durability with material efficiency. Together, these factors highlight the importance of careful design to create pressure vessels that are both reliable and cost-effective.

- The hemispherical head (k=1) demonstrates the highest critical buckling pressures under ideal conditions, highlighting its robust structural stability. However, its performance is highly sensitive to imperfections such as dimples or flat patches. Even minor geometric disturbances can significantly reduce its buckling resistance, emphasizing the importance of precise manufacturing standards when applying hemispherical heads in practical applications.
- As geometry transitions from hemispherical to more elliptical shapes, with increasing k values, critical buckling pressures decrease progressively. For elliptical heads with k=1.25 and k=1.5, a balance is observed between structural stiffness and tolerance to imperfections. These geometries exhibit a reduced reliance on perfect curvature, allowing them to better withstand localized imperfections like dimples, cutouts, and flat patches, although their overall buckling pressures remain lower compared to the hemispherical shape. This makes them a suitable option for applications requiring moderate buckling resistance along with improved durability to imperfections.
- The trend of decreasing buckling pressures continues as the ellipticity increases, with configurations such as k=1.75 and k=2. These flatter profiles exhibit even lower critical buckling pressures, but they are less sensitive to localized imperfections, showing a more gradual decline in buckling pressure as imperfections increase in severity. This diminished sensitivity is due to the geometry's ability to distribute stresses more uniformly and its reduced dependence on localized curvature. Similarly, the tori-spherical head, with its combination of spherical and toroidal sections, demonstrates the lowest critical buckling pressures under ideal conditions. However, it is notably more resilient to larger imperfections, making it suitable for applications where such imperfections are more likely.
- The type of imperfection significantly influences the buckling behavior of these geometries. Flat patch imperfections consistently lead to the greatest

reduction in buckling pressure, especially as the width of the imperfection increases. This effect is particularly pronounced in hemispherical and moderately elliptical heads. Dimples, although initially less severe, cause the steepest decline in buckling pressure at larger amplitudes, showing their potential to induce catastrophic failures in domes with high initial buckling pressures. In contrast, cutout imperfections have the least impact on structural performance, as they cause minimal disruption to the global stress distribution, even for larger cutout sizes.

- The buckling behavior of domes with varying ellipticities under affine imperfections reveals crucial insights into their structural performance. The hemispherical dome (k=1) exhibits high sensitivity to the first eigenmode imperfection, causing a steep decline in buckling pressure. However, the second eigenmode imperfections prove to be even more damaging, as they result in notably lower buckling pressures for all configurations, especially for domes with intermediate ellipticities like k=1.25 and k=1.5. The second eigenmode introduces more localized deformation, disrupting the dome's stress distribution more drastically than the first eigenmode, making it a more dangerous factor in terms of buckling stability. Flatter domes (k=1.5 and beyond) show greater durability to both eigenmode imperfections, with their buckling pressures remaining more stable due to their reduced curvature
- The comparative analysis of imperfection types across different geometries underscores the trade-offs between structural stiffness, buckling resistance, and sensitivity to imperfections. Hemispherical domes, while offering the highest resistance to buckling under ideal conditions, are highly susceptible to imperfections. Moderately elliptical shapes provide a balanced compromise between resistance to buckling and imperfection resilience, while flatter configurations, such as k=2 and tori-spherical heads, though structurally weaker, exhibit superior tolerance to geometric disturbances. These findings emphasize the critical role of geometric design and

imperfection consideration in optimizing the performance of pressure vessel heads in practical applications.

- The combined eigenmode imperfection analysis provides a more realistic representation of the structural performance of pressure vessel heads, accounting for the fact that imperfections in real-world structures often result from a combination of multiple eigenmodes. By superimposing the first and second eigenmode imperfections, this approach provides a more comprehensive understanding of the interaction between different imperfection patterns under loading conditions. Unlike single eigenmode analyses, which may oversimplify the structural response, the combined mode analysis captures the nonlinear interactions between global and localized deformation patterns, providing a more accurate prediction of buckling behaviour. The trends observed in the combined eigenmode analysis show that for ellipsoidal heads, the combined imperfection curve reflects a balance between the stabilizing effects of the first eigenmode and the destabilizing influence of the second eigenmode, especially for flatter geometries. In contrast, for hemispherical and tori-spherical heads, the combined mode leads to a reduction in buckling pressure, illustrating the complex interaction of imperfections. These findings emphasize the importance of considering multiple eigenmode-affine imperfections in the design and safety evaluation of pressure vessels, ensuring more accurate assessments and more reliable structural designs.
- The combined effects of localized dimple imperfections and global eigenmode imperfections significantly influence the buckling behaviour of pressure vessel heads, with the second eigenmode (with dimple imperfection) producing the lowest buckling pressures. It causes the greatest destabilization which results in the lowest buckling pressures. The first eigenmode has a stabilizing effect resulting in higher buckling pressure when combined with the dimple. As the dimple amplitude increases, the combined effect of both imperfections further reduces the buckling

resistance, especially with the second eigenmode. The interaction between these imperfections can intensify the overall structural instability, particularly when dimple amplitudes are large. Hence, the combining imperfections lead to significantly lower buckling pressures compared to considering each imperfection independently.

- The angular position of imperfections, particularly near the apex (90°), plays a decisive role in determining the buckling pressure of ellipsoidal heads. For both k=1.25 and k=1.5 aspect ratios, dimples positioned near the apex result in a sharp decline in buckling resistance, while cutouts exhibit a more gradual effect. Imperfections closer to the equator have comparatively less influence on buckling. These results highlight the apex as the most vulnerable region, showing the importance for targeted inspection and reinforcement during design and fabrication.
- The introduction of variable wall thickness in ellipsoidal pressure tank heads substantially improves buckling resistance compared to constant thickness designs. Specifically, by increasing the thickness at the apex, where buckling is most likely to occur, and gradually reducing it toward the equator, the variable thickness model optimizes stress distribution, achieving higher critical buckling pressures. For both ellipticity ratios (k=1.25 and k=1.5), variable thickness consistently outperforms constant thickness across all buckling analyses, including Linear Buckling Analysis (LBA) and Geometric Nonlinear Analysis (GNA). The k=1.25 model, with its more spherical geometry, shows higher increase in buckling resistance, especially under second eigenmode imperfections, where critical pressures surpass those observed for combined eigenmode-affine imperfections. This finding shows the effectiveness of variable wall thickness in mitigating buckling risks, especially for geometries with lower ellipticity ratios, while providing a uniform stiffening response across imperfection scenarios for higher ellipticity ratios (k=1.5).

Based on the results of this study, several strategies can be implemented to prevent sudden failure events and repair damage induced by stress concentrations caused by geometric imperfections. To prevent failure, the design of HDPE pressure tanks should incorporate stiffeners or reinforcements in high-stress regions, such as the junctions between the cylindrical shell and elliptical heads, to enhance structural rigidity and reduce stress concentrations. Regular non-destructive testing (NDT) techniques, such as ultrasonic testing or strain monitoring, can be employed to detect early signs of damage or stress accumulation. In the event of damage, localized repair techniques, such as patching with compatible HDPE materials or applying composite overlays, can be used to restore structural integrity. These proactive and reactive measures, informed by the stress and buckling analyses conducted in this study, can significantly improve the safety and longevity of HDPE pressure tanks in real-world applications.

## II. Perspectives for future research

Building upon the findings of this study, future research could focus on extending the numerical models developed in this study by fabricating and testing pressure tank heads prototypes with varying geometries, wall thickness distributions, and controlled imperfections. Such efforts would provide practical insights into real-world applications and demonstrate the robustness of the proposed designs. Additionally, exploring the incorporation of composite materials or modified HDPE blends could enhance mechanical properties, offering improved resistance to buckling and stress concentrations. Advanced computational methods, including machine learning-based optimization techniques, could be applied to identify ideal design configurations that efficiently balance factors such as cost, weight, and structural integrity. Additionally, developing and implementing advanced manufacturing processes, such as those enabling precise variable wall thickness designs, would allow for improved buckling resistance and material efficiency. These avenues of research will contribute to creating safer, more

efficient, and cost-effective HDPE pressure vessel designs, ensuring their suitability for a wide range of practical applications.

# References

[1] Wanhill RJH, Byrnes RT, Smith CL. Stress corrosion cracking (SCC) in aerospace vehicles. Stress corrosion cracking: Theory and practice, Elsevier Ltd; 2011, p. 608–50. https://doi.org/10.1533/9780857093769.4.608.

[2] Bouvier M, Guiheneuf V, Jean-Marie A. Modeling and simulation of a composite high-pressure vessel made of sustainable and renewable alternative fibers. Int J Hydrogen Energy 2019;44. https://doi.org/10.1016/j.ijhydene.2019.03.088.

[3] Fouad H, Elleithy R, Al-Zahrani SM, Ali MA haj. Characterization and processing of High Density Polyethylene/carbon nano-composites. Mater Des 2011;32:1974–80. https://doi.org/10.1016/j.matdes.2010.11.066.

[4] Pressure Vessels in Oil & Gas Industry | Sherwood Design & Engineering n.d. https://www.sherwoodengineering.com.au/pressure-vessels-oil-gas-industry/ (accessed January 6, 2025).

[5] Triotank - T BLUSTAR. Https://WwwTblustarCom/Triotank/?Lang=de n.d.

[6] Wang Z, Zhang Z, Chen J, Bai J. Stress analysis and applicability analysis of the elliptical head. Sci Rep 2021;11. https://doi.org/10.1038/s41598-021-02397-7.

[7] Wang H, Ding S, Li L, Sang Z, Krakauer BW. Buckling of thin-walled torispherical heads in water heater tanks. Thin-Walled Structures 2014;85:156–64. https://doi.org/10.1016/J.TWS.2014.08.007.

[8] Tripathi SM, Anup S, Muthukumar R. Effect of geometrical parameters on mode shape and critical buckling load of dished shells under external pressure. Thin-Walled Structures 2016;106:218–27. https://doi.org/10.1016/J.TWS.2016.02.011.

[9] Jasion P. Stability analysis of shells of revolution under pressure conditions. Thin-Walled Structures 2009;47:311–7. https://doi.org/10.1016/J.TWS.2008.07.005.

[10] Sobhani E, Arbabian A, Civalek Ö, Avcar M. The free vibration analysis of hybrid porous nanocomposite joined hemispherical–cylindrical–conical shells. Eng Comput 2022;38:3125–52. https://doi.org/10.1007/S00366-021-01453-0.

[11] Liu L, Li J. Dynamic Deformation and Perforation of Ellipsoidal Thin Shell Impacted by Flat-Nose Projectile. Materials 2022, Vol 15, Page 4124 2022;15:4124. https://doi.org/10.3390/MA15124124.

[12] Mackenzie D, Camilleri D, Hamilton R. Design by Analysis of Ductile Failure and Buckling in Torispherical Pressure Vessel Heads n.d.

[13] Li K, Zheng J, Liu S, Ge H, Sun G, Zhang Z, et al. Buckling behavior of large-scale thin-walled ellipsoidal head under internal pressure. Thin-Walled Structures 2019;141:260–74. https://doi.org/10.1016/J.TWS.2019.04.031.

[14] Fazlalipour N, Showkati H. Geometric properties and imperfections influence on buckling behavior of Variable-Thickness steel cylindrical shells subjected to combined Loading: Experimental and numerical study. Structures 2023;55:834–52. https://doi.org/10.1016/J.ISTRUC.2023.06.064.

[15] Lo Frano R, Forasassi G. Experimental evidence of imperfection influence on the buckling of thin cylindrical shell under uniform external pressure. Nuclear Engineering and Design 2009;239:193–200. https://doi.org/10.1016/J.NUCENGDES.2008.09.004.

[16] Korentz J. Influence of Geometric Imperfections on Buckling Resistance of Reinforcing Bars during Inelastic Deformation. Materials 2020, Vol 13, Page 3473 2020;13:3473. https://doi.org/10.3390/MA13163473.

[17] Lo Frano R, Forasassi G. Experimental evidence of imperfection influence on the buckling of thin cylindrical shell under uniform external pressure. Nuclear Engineering and Design 2009;239:193–200. https://doi.org/10.1016/J.NUCENGDES.2008.09.004.

[18] Wan L, Tao WM, Wu XX, He SY. The influence of initial geometric imperfection on the localized buckling of pressure vessel under internal pressure. Proceedings of the International Conference on Nuclear Engineering (ICONE12) 2004;2:329–34. https://doi.org/10.1115/ICONE12-49397.

[19] Sadovský Z, Kriváček J. Influential geometric imperfections in buckling of axially compressed cylindrical shells – A novel approach. Eng Struct 2020;223:111170. https://doi.org/10.1016/J.ENGSTRUCT.2020.111170.

[20] Tsouvalis NG, Zafeiratou AA, Papazoglou VJ. The effect of geometric imperfections on the buckling behaviour of composite laminated cylinders under external hydrostatic pressure. Compos B Eng 2003;34:217–26. https://doi.org/10.1016/S1359-8368(02)00106-3.

[21] Possidente L, Freddi F, Tondini N. Dynamic increase factors for progressive collapse analysis of steel structures considering column buckling. Eng Fail Anal 2024;160:108209. https://doi.org/10.1016/J.ENGFAILANAL.2024.108209.

[22] Schau H, Mkrtchyan L, Geier M. The influence of imperfections and nonlinearities on the failure and B2 stress index of thin-walled pipes. Journal of Pressure Vessel Technology, Transactions of the ASME 2015;137. https://doi.org/10.1115/1.4030366.

[23] NASA STI Program Report Series. Buckling of Thin-Walled Circular Cylinders. 2020.

[24] Yang L, Zhu Y, Yu J, Yin B, Zhang J. Design of externally pressurized ellipsoidal heads with variable wall thicknesses. International Journal of Pressure Vessels and Piping 2021;191. https://doi.org/10.1016/j.ijpvp.2021.104330.

[25] Prasittisopin L, Ferdous W, Kamchoom V. Microplastics in construction and built environment. Developments in the Built Environment 2023;15:100188. https://doi.org/10.1016/J.DIBE.2023.100188.

[26] The Concept of Non-Metallic Piping: Explained - MFG Shop n.d. http://shop.machinemfg.com/the-concept-of-non-metallic-piping-explained/ (accessed January 10, 2025).

[27] HDPE : The Complete Buyer's Guide - Provident Procurement n.d. https://provprocure.com/hdpe-high-density-polyethylene/ (accessed January 10, 2025).

[28] The advantages and applications of HDPE n.d. https://blogue.polyalto.com/en/the-advantages-and-applications-of-hdpe (accessed January 10, 2025).

[29] Kumar A, Gupta RK. Fundamentals of Polymer Engineering. CRC Press; 2018. https://doi.org/10.1201/9780429398506.

[30] Brinson HF, Brinson LC. Polymer engineering science and viscoelasticity: An introduction, Second edition. Springer US; 2015. https://doi.org/10.1007/978-1-4899-7485-3.

[31] Chanda M, Roy SK. Plastics fundamentals, properties, and testing. CRC Press; 2008. https://doi.org/10.1201/9781420080612.

[32] Mahl M, Jelich C, Baier H. Thermo-mechanical behavior of polyethylene under mechanical loads at cryogenic and elevated temperatures.

International Journal of Pressure Vessels and Piping 2017;150:11–8. https://doi.org/10.1016/j.ijpvp.2016.12.007.

[33] Fatima M, Mohamed S, Mohamed E. Burst behavior of CPVC compared to HDPE thermoplastic polymer under a controlled internal pressure. Procedia Structural Integrity, vol. 3, Elsevier B.V.; 2017, p. 380–6. https://doi.org/10.1016/j.prostr.2017.04.041.

[34] Rondinella A, Capurso G, Zanocco M, Basso F, Calligaro C, Menotti D, et al. Study of the Failure Mechanism of a High-Density Polyethylene Liner in a Type IV High-Pressure Storage Tank. Polymers (Basel) 2024;16. https://doi.org/10.3390/polym16060779.

[35] Jasion P, Magnucki K. Strength and elastic buckling of a sandwich cylindrical pressure vessel with dished heads. International Journal of Pressure Vessels and Piping 2023;205:105002. https://doi.org/10.1016/J.IJPVP.2023.105002.

[36] Magnucki K, Jasion P. Strength of a cylindrical pressure vessel with individual ellipsoidal dished heads. International Journal of Pressure Vessels and Piping 2022;199. https://doi.org/10.1016/j.ijpvp.2022.104751.

[37] Sowiński K, Magnucki K. Shaping of dished heads of the cylindrical pressure vessel for diminishing of the edge effect. Thin-Walled Structures 2018;131:746–54. https://doi.org/10.1016/j.tws.2018.07.018.

[38] Belardi VG, Ottaviano M, Vivio F. Bending theory of composite pressure vessels: A closed-form analytical approach. Compos Struct 2024;329. https://doi.org/10.1016/j.compstruct.2023.117799.

[39] KARMAN TH VON, TSIEN H-S. The Buckling of Spherical Shells by External Pressure. Https://DoiOrg/102514/81019 2012;7:43–50. https://doi.org/10.2514/8.1019.

[40] Thompson J. The rotationally-symmetric branching behaviour of a complete spherical shell. 1964.

[41] Sanders JLJr. Nonlinear theories for thin shells. Q Appl Math 1963;21:21–36. https://doi.org/10.1090/QAM/147023.

[42] MacKerle J. Finite elements in the analysis of pressure vessels and piping, an addendum (1996–1998). International Journal of Pressure Vessels and Piping 1999;76:461–85. https://doi.org/10.1016/S0308-0161(99)00012-5.

[43] Gavrilenko GD, Matsner VI. Effect of localized imperfections on the critical loads of ribbed shells. International Applied Mechanics 2010;46:771–5. https://doi.org/10.1007/S10778-010-0366-5/METRICS.

[44] Bazhenov VA, Luk'yanchenko OO, Kostina O V., Gerashchenko O V. Nonlinear Bending Stability of a Long Flexible Cylindrical Shell with Geometrical Imperfections. Strength of Materials 2016;48:308–14. https://doi.org/10.1007/S11223-016-9766-Z/FIGURES/6.

[45] Bushnell D. Buckling of Shells-Pitfall for Designers. Https://DoiOrg/102514/360058 2012;19:1183–226. https://doi.org/10.2514/3.60058.

[46] Gotsulyak EO, Luk'yanchenko OO, Kostina O V., Garan IG. Stability of supported cylindrical shell with geometric imperfections under combined loading. Strength of Materials 2012;44:556–61. https://doi.org/10.1007/S11223-012-9408-Z/FIGURES/4.

[47] Grigorenko YM, Gulyaev VI. Nonlinear problems of shell theory and their solution methods (review). Soviet Applied Mechanics 1991;27:929–47. https://doi.org/10.1007/BF00887499.

[48] Di Pasqua MF, Khakimova R, Castro SGP, Arbelo MA, Riccio A, Raimondo A, et al. Investigation on the Geometric Imperfections driven Local Buckling

Onset in Composite Conical Shells. Applied Composite Materials 2016;23:879–97. https://doi.org/10.1007/S10443-016-9490-7.

[49] Błachut J. Buckling of externally pressurized steel toriconical shells. International Journal of Pressure Vessels and Piping 2016;144:25–34. https://doi.org/10.1016/J.IJPVP.2016.05.002.

[50] Błachut J. Buckling of multilayered metal domes. Thin-Walled Structures 2009;47:1429–38. https://doi.org/10.1016/J.TWS.2009.07.011.

[51] Błachut J. Elastic buckling of stringer reinforced torispheres under external pressure. International Journal of Pressure Vessels and Piping 2019;175. https://doi.org/10.1016/J.IJPVP.2019.103921.

[52] Evkin A, Krasovsky V, Lykhachova O, Marchenko V. Local buckling of axially compressed cylindrical shells with different boundary conditions. Thin-Walled Structures 2019;141:374–88. https://doi.org/10.1016/J.TWS.2019.04.039.

[53] Evkin A. Analytical model of local buckling of axially compressed cylindrical shells. Thin-Walled Structures 2021;168:108261. https://doi.org/10.1016/j.tws.2021.108261.

[54] Kriegesmann B, Jansen EL, Rolfes R. Design of cylindrical shells using the Single Perturbation Load Approach – Potentials and application limits. Thin-Walled Structures 2016;108:369–80. https://doi.org/10.1016/J.TWS.2016.09.005.

[55] Evkin A. Properties of local buckling of spherical shell under external pressure. Thin-Walled Structures 2023;185:110629. https://doi.org/10.1016/j.tws.2023.110629.

[56] Evkin A. Sensitivity and uncertainty propagation in buckling of spherical shells under external pressure. Thin-Walled Structures 2023;190:110978. https://doi.org/10.1016/j.tws.2023.110978.

[57] Yang FJ, Liu YL, Wang J, Wang BJ, Guo J. Deep-sea implosion of spherical pressure shell considering geometric imperfection. Ocean Engineering 2024;307:118162. https://doi.org/10.1016/J.OCEANENG.2024.118162.

[58] Enoma N, Zingoni A. Buckling of an externally pressurised toroidal shell of revolution with a doubly-symmetric parabolic-ogival cross-section. International Journal of Pressure Vessels and Piping 2020;183:104106. https://doi.org/10.1016/J.IJPVP.2020.104106.

[59] Jasion P, Magnucki K. Strength and elastic buckling of a sandwich cylindrical pressure vessel with an individual functionally graded core. International Journal of Pressure Vessels and Piping 2024;210:105238. https://doi.org/10.1016/J.IJPVP.2024.105238.

[60] Magnucki K, Jasion P, Rodak M. Strength and buckling of an untypical dished head of a cylindrical pressure vessel. International Journal of Pressure Vessels and Piping 2018;161:17–21. https://doi.org/10.1016/j.ijpvp.2018.02.003.

[61] Li K, Zheng J, Zhang Z, Gu C, Zhang X, Liu S, et al. Experimental Investigation on Buckling of Ellipsoidal Head of Steel Nuclear Containment. Journal of Pressure Vessel Technology, Transactions of the ASME 2017;139:061206. https://doi.org/10.1115/1.4038013.

[62] Ismail MS, Muhammad al-Attas SM, Mahmud J. Buckling behaviour of steel dome cap design under external pressure. International Journal of Pressure Vessels and Piping 2024;208:105135. https://doi.org/10.1016/j.ijpvp.2024.105135.

[63] Zhang J, Wang Y, Wang F, Tang W. Buckling of stainless steel spherical caps subjected to uniform external pressure. Ships and Offshore Structures 2018;13:779–85. https://doi.org/10.1080/17445302.2018.1459358.

[64] Zhu Y, Zhang Y, Zhao X, Zhang J, Xu X. Elastic–plastic buckling of externally pressurised hemispherical heads. Ships and Offshore Structures 2019;14:829–38. https://doi.org/10.1080/17445302.2018.1564541.

[65] Zoelly R. Ueber ein Knickungsproblem an der Kugelschale 1915. https://doi.org/10.3929/ETHZ-A-000091951.

[66] Cho SR, Muttaqie T, Lee SH, Paek J, Sohn JM. Ultimate Strength Assessment of Steel-Welded Hemispheres under External Hydrostatic Pressure. Journal of Marine Science and Application 2020;19:615–33. https://doi.org/10.1007/S11804-020-00178-8/FIGURES/18.

[67] Wagner HNR, Hühne C, Zhang J, Tang W. On the imperfection sensitivity and design of spherical domes under external pressure. International Journal of Pressure Vessels and Piping 2020;179:104015. https://doi.org/10.1016/J.IJPVP.2019.104015.

[68] Wagner HNR, Niewöhner G, Pototzky A, Hühne C. On the imperfection sensitivity and design of tori-spherical shells under external pressure. International Journal of Pressure Vessels and Piping 2021;191:104321. https://doi.org/10.1016/J.IJPVP.2021.104321.

[69] Xin R, Le VT, Goo NS. Buckling identification in composite cylindrical shells with measured imperfections using a Multi-DIC method and finite element analysis. Thin-Walled Structures 2022;177:109436. https://doi.org/10.1016/J.TWS.2022.109436.

[70] Zhang J, Hua Z, Tang W, Wang F, Wang S. Buckling of externally pressurised egg-shaped shells with variable and constant wall thicknesses.

Thin-Walled Structures 2018;132:111–9. https://doi.org/10.1016/j.tws.2018.08.013.

[71] Abdalla HMA, Casagrande D, De Bona F, De Monte T, Sortino M, Totis G. An optimized pressure vessel obtained by metal additive manufacturing: Preliminary results. International Journal of Pressure Vessels and Piping 2021;192. https://doi.org/10.1016/j.ijpvp.2021.104434.

[72] Overview of materials for High Density Polyethylene (HDPE), Injection Molded n.d. https://www.matweb.com/search/datasheet.aspx?MatGUID=fce23f90005d4fbe8e12a1bce53ebdc8&ckck=1 (accessed October 9, 2024).

[73] Nevin Nelson. An Assessment on the Effect of Membrane and Bending Stress on an Edge Crack in a Finite Width Plate. NATIONAL CONFERENCE ON RECENT ADVANCEMENTS IN ENGINERING & TECHNOLOGY, Kerala, India: 2021.

[74] Gwara M. Application of discrete mathematics in the real world. Michael Owuor Gwara 2019.

[75] Zheng J, Li K. New Theory and Design of Ellipsoidal Heads for Pressure Vessels. New Theory and Design of Ellipsoidal Heads for Pressure Vessels 2021:1–190. https://doi.org/10.1007/978-981-16-0467-6/COVER.

[76] Yang L, Zhu Y, Yu J, Yin B, Zhang J. Design of externally pressurized ellipsoidal heads with variable wall thicknesses. International Journal of Pressure Vessels and Piping 2021;191:104330. https://doi.org/10.1016/J.IJPVP.2021.104330.

[77] Azarniya O, Forooghi A, Bidhendi M V., Zangoei A, Naskar S. Exploring buckling and post-buckling behavior of incompressible hyperelastic beams through innovative experimental and computational approaches. Mechanics

Based Design of Structures and Machines 2024;52:4791–810. https://doi.org/10.1080/15397734.2023.2242473.

[78] Paulo RMF, Carlone P, Valente RAF, Teixeira-Dias F, Rubino F. Numerical simulation of the buckling behaviour of stiffened panels: Benchmarks for assessment of distinct modelling strategies. Int J Mech Sci 2019;157–158:439–45. https://doi.org/10.1016/J.IJMECSCI.2019.04.042.

[79] Barbieri E, Ongaro F, Pugno NM. A J-integral-based arc-length solver for brittle and ductile crack propagation in finite deformation-finite strain hyperelastic solids with an application to graphene kirigami. Comput Methods Appl Mech Eng 2017;315:713–43. https://doi.org/10.1016/J.CMA.2016.10.043.

[80] Abbasi A, Sano TG, Yan D, Reis PM. Snap buckling of bistable beams under combined mechanical and magnetic loading. Philosophical Transactions of the Royal Society A 2023;381. https://doi.org/10.1098/RSTA.2022.0029.

[81] Alaedini S, Kabir MZ, Al-Mahaidi R. Stability performance of thin-walled pultruded beams with geometric web-flange junction imperfections. Journal of Building Engineering 2021;33:101549. https://doi.org/10.1016/J.JOBE.2020.101549.

[82] Heinen AH, Büllesbach J. On the influence of geometric imperfections on the stability and vibration of thin-walled shell structures. Int J Non Linear Mech 2002;37:921–35. https://doi.org/10.1016/S0020-7462(01)00106-8.

[83] Lopes SRX, Gonçalves PB, Pamplona DC. Influence of initial geometric imperfections on the stability of thick cylindrical shells under internal pressure. Commun Numer Methods Eng 2007;23:577–97. https://doi.org/10.1002/CNM.916.

[84] Vu QA, Pham NH. Review on Impacts of Geometric Imperfections on Behavior of Cold-Formed Structural Members. Lecture Notes in Civil

Engineering 2024;526 LNCE:630–9. https://doi.org/10.1007/978-981-97-4355-1_61/FIGURES/8.

[85] Rzeszut K, Garstecki A. MODELING OF INITIAL GEOMETRICAL IMPERFECTIONS IN STABILITY ANALYSIS OF THIN-WALLED STRUCTURES. JOURNAL OF THEORETICAL AND APPLIED MECHANICS 2009;47:667–84.

[86] Cyrus J. R. Kosztowny. Implementing Geometric Surface Imperfections into Sandwich Composite Cylinder Finite Element Method Models . 2021.

[87] Glaesener RN, Kumar S, Lestringant C, Butruille T, Portela CM, Kochmann DM. Predicting the influence of geometric imperfections on the mechanical response of 2D and 3D periodic trusses. Acta Mater 2023;254:118918. https://doi.org/10.1016/J.ACTAMAT.2023.118918.

[88] Wagner HNR, Hühne C. On the imperfection sensitivity and design of buckling critical wind turbine towers. Thin-Walled Structures 2025;206:112577. https://doi.org/10.1016/J.TWS.2024.112577.

[89] SONNA DONKO Maël. IMPERFECTION TOLERANCES DURING THE ERECTION OF STEEL PLATE GIRDERS AND GEOMETRICAL NONLINEARITIES. University of Padua, 2020.

[90] Wullschleger L, Meyer-Piening HR. Buckling of geometrically imperfect cylindrical shells - Definition of a buckling load. Int J Non Linear Mech 2002;37:645–57. https://doi.org/10.1016/S0020-7462(01)00089-0.

[91] Ifayefunmi O, Mahidan FM. Collapse of conical shells having single dimple imperfection under axial compression. Journal of Pressure Vessel Technology, Transactions of the ASME 2021;143. https://doi.org/10.1115/1.4047681.

[92] Schiller A;, Bisagni C, Schiller A, Bisagni C. Buckling of Composite Cylindrical Shells with Circular Cutouts 2022. https://doi.org/10.2514/6.2022-1492.

[93] Çelebi M, Gürdal Z, Tatting BF, Blom-Schieber A, Rassaian M, Wanthal S. Effects of size and location of a circular cutouton buckling and failure of a cylindrical shell in bending. 58th AIAA/ASCE/AHS/ASC Structures, Structural Dynamics, and Materials Conference, 2017 2017. https://doi.org/10.2514/6.2017-0433.

[94] Hao P, Wang B, Li G, Meng Z, Tian K, Zeng D, et al. Worst Multiple Perturbation Load Approach of stiffened shells with and without cutouts for improved knockdown factors. Thin-Walled Structures 2014;82:321–30. https://doi.org/10.1016/J.TWS.2014.05.004.

[95] Tafreshi A. Buckling and post-buckling analysis of composite cylindrical shells with cutouts subjected to internal pressure and axial compression loads. International Journal of Pressure Vessels and Piping 2002;79:351–9. https://doi.org/10.1016/S0308-0161(02)00026-1.

[96] Pin-Hsuan Wu. Effects of Hydrostatic Pressure on the Stability of Liquid Storage Tanks Subjected to Wind Loading. Purdue University, 2018.

[97] Zhang J, Huang C, Wagner HNR, Cui W, Tang W. Study on dented hemispheres under external hydrostatic pressure. Marine Structures 2020;74:102819. https://doi.org/10.1016/J.MARSTRUC.2020.102819.

[98] Orifici AC, Bisagni C. Perturbation-based imperfection analysis for composite cylindrical shells buckling in compression. Compos Struct 2013;106:520–8. https://doi.org/10.1016/J.COMPSTRUCT.2013.06.028.

[99] Wang H, Yao X, Li L, Sang Z, Krakauer BW. Imperfection sensitivity of externally-pressurized, thin-walled, torispherical-head buckling. Thin-

Walled Structures 2017;113:104–10. https://doi.org/10.1016/J.TWS.2017.01.018.